The Dissertation Committee for Scott Allen Striepe certifies that this is the approved version of the following dissertation:

Huygens Probe Entry, Descent, and Landing Trajectory Reconstruction Using the Program to Optimize Simulated Trajectories II

Committee:

Wallace T. Fowler, Supervisor

David G. Hull

Robert H. Bishop

Mary Kae Lockwood

Eric M. Queen

Huygens Probe Entry, Descent, and Landing Trajectory Reconstruction Using the Program to Optimize Simulated Trajectories II

by

Scott Allen Striepe, B.A.E., M.S.

Dissertation

Presented to the Faculty of the Graduate School of

The University of Texas at Austin

in Partial Fulfillment

of the Requirements

for the Degree of

Doctor of Philosophy

The University of Texas at Austin

December 2007

Dedication

I dedicate this dissertation to my family, for without their support this dissertation would not have been completed, and in memory of my father, Allen Neumann Striepe.

Acknowledgements

I would like to extend my thanks and appreciation to my advisor Dr. Wallace Fowler for his patience and guidance. Thanks are also extended to my dissertation committee. I would like to acknowledge several people whose technical discussions on topics addressed in this dissertation were much appreciated: Robert Blanchard, Michael Kirsch, and Richard Powell of the National Institute for Aerospace; David Way, Eric Queen, Jody Fisher, and Juan Cruz of NASA Langley Research Center. My thanks also go to George Allison of the NASA Langley Graduate Study Program.

The author would also like to thank the following groups and individuals: NASA Engineering Safety Center for funding this effort; the Huygens project scientists for sharing their data; Jean-Pierre Lebreton of ESA for his leadership of the Huygens mission and allowing my involvement; Carlo Bettanini of University of Padova, Italy, David Atkinson of the University of Idaho, and Bobby Kazeminejad of the German Space Operations Center (DLR) for their data and discussions regarding their reconstruction of the Huygens probe trajectory.

Finally, I extend thanks to my family (Lisa, Stephen, and Susanne Striepe) and extended family (Lynda Striepe, Steve and Sue Burton) for their support, patience, and encouragement throughout this entire process. Without them I would not have made it this far.

Huygens Probe Entry, Descent, and Landing Trajectory Reconstruction Using the Program to Optimize Simulated Trajectories II

Publication No._____

Scott Allen Striepe, Ph.D.

The University of Texas at Austin, 2007

Supervisor: Wallace T. Fowler

The objectives of this research were to develop a reconstruction capability using the Program to Optimize Simulated Trajectories II (POST2), apply this capability to reconstruct the Huygens Titan probe entry, descent, and landing (EDL) trajectory, evaluate the newly developed POST2 reconstruction module, analyze the reconstructed trajectory, and assess the pre-flight simulation models used for Huygens EDL simulation. An extended Kalman filter (EKF) module was developed and integrated into POST2 to enable trajectory reconstruction (especially when using POST2-based mission specific simulations). Several validation cases, ranging from a single, constant parameter estimate to multivariable estimation cases similar to an actual mission flight, were executed to test the POST2 reconstruction module. Trajectory reconstruction of the Huygens entry probe at Titan was accomplished using accelerometer measurements taken during flight to adjust an estimated state (e.g., position, velocity, parachute drag, wind velocity, etc.) in a POST2-based simulation developed to support EDL analyses and design prior to entry. Although the main emphasis of the trajectory reconstruction was to evaluate models used

in the NASA pre-entry trajectory simulation, the resulting reconstructed trajectory was also assessed to provide an independent evaluation of the ESA result. Major findings from this analysis include: Altitude profiles from this analysis agree well with other NASA and ESA results but not with Radar data, whereas a scale factor of about 0.93 would bring the radar measurements into compliance with these results; entry capsule aerodynamics predictions (axial component only) were well within 3-σ bounds established pre-flight for most of the entry when compared to reconstructed values; Main parachute drag of 9% to 19% above ESA model was determined from the reconstructed trajectory; based on the tilt sensor and accelerometer data, the conclusion from this assessment was that the probe was tilted about 10 degrees during the Drogue parachute phase.

Table of Contents

List of Tables

List of Figures

Nomenclature

Symbol	Definition
A	Matrix of state derivative with respect to time sensitivity to the state
AIAA	American Institute of Aeronautics and Astronautics
a_x	Acceleration in body-X direction, m/s^2
C_A	Aerodynamic axial force coefficient
CASU	Central Accelerometer Sensor Unit
C_D	Aerodynamic drag force coefficient
C_f	Atmospheric compression factor
CG	Center of Gravity
DAWG	Data Analysis Working Group
DCSS	Descent Control Subsystem
DGB	Disk-Gap-Band
DI	Descent Imager
DISR	Descent Imager Spectral Radiometer
DOF	Degree-Of-Freedom
DTWG	Descent Trajectory Working Group
DWE	Doppler Wind Experiment
EDL	Entry, Descent And Landing
EKF	Extended Kalman Filter
ESA	European Space Agency
ESTEC	European Space Research and Technology Centre
F	Total sensed force acting on probe, N
G	Calculated observation matrix
g	gravity acceleration, m/s^2
h	Huygens probe height, m
$\dot{h}$	Altitude rate of change, m/s
H	Sensitivity matrix of calculated observation to estimated state
HASI	Huygens Atmospheric Structure Instrument
HN	High noise case
HQ	NASA Headquarters
HRA	Huygens Radar Altimeters
HSWT	Huygens Science Working Team
I	Identity matrix
ITA	Independent Technical Assessment
J2	Zonal harmonic gravity term
JPL	Jet Propulsion Laboratory
JSC	NASA Johnson Space Center
K	Kalman filter
LaRC	NASA Langley Research Center
LN	Low noise case

Symbol	Definition
m	Huygens probe mass, kg
MER	Mars Exploration Rovers
MSL	Mars Science Laboratory
NASA	National Aeronautics and Space Administration
NESC	NASA Engineering and Safety Center
O	Observation matrix
p	Atmospheric pressure, Pa
$\hat{P}$	Updated covariance matrix
$\overline{P}$	Propagated covariance matrix
$\dot{\overline{P}}$	Time derivative of propagated covariance matrix
$\dot{p}$	Time rate of change in atmospheric pressure, Pa/s
P_0	Initial covariance matrix
POST2	Program to Optimize Simulated Trajectories II
Q	System noise covariance matrix
R	Universal gas constant, N-m/kmole-K
R	Measurement noise covariance
RMS	Root mean square
S	Aerodynamic reference area, m^2
SOI	Saturn Orbital Insertion
SSP	Surface Science Package
T	Atmospheric temperature, K
t	Time, s
T0	Pilot parachute mortar firing event
TILX	Tilt sensor about X-axis
TILY	Tilt sensor about Y-axis
Titan-GRAM	Titan Global Reference Atmospheric Model
vr	Probe atmospheric relative velocity, m/s
W	Measurement weighting matrix
W_{MM}	Atmospheric mean molecular weight, kg/kmole
X_0	Initial estimated state values
$\hat{X}$	Estimated state
$\overline{X}$	Propagated state
$\dot{\overline{X}}$	Time derivative of propagated state
Y	Residual difference between the observation measurement and calculated value
θ_x	Angle about Tilt sensor X-axis, deg
θ_y	Angle about Tilt sensor Y-axis, deg
μ	Gravitational constant, m^3/s^2
ρ	Atmospheric density, kg/m^3
σ	Standard deviation

Chapter 1: Introduction

1.1 RESEARCH OBJECTIVES

The objectives of the current research are to develop a reconstruction capability using the Program to Optimize Simulated Trajectories II (POST2), evaluate the newly developed POST2 reconstruction module, apply this capability to reconstruct the Huygens Titan probe entry, descent, and landing (EDL) trajectory, analyze the reconstructed trajectory, and assess the pre-flight simulation models used in NASA's simulation of the Huygens EDL. This POST2 reconstruction module will be similar to the existing optimization module and will allow for reconstructing a trajectory using a previously developed, detailed, mission-specific POST2 simulation. This capability will also provide the ability to rapidly estimate flight trajectory results and assess parameters used on that mission as well as those affecting other near-term missions.

1.2 RATIONALE FOR OBJECTIVES

Over the past decade, NASA has led planetary exploration missions that involve atmospheric flight either through EDL or aerobraking. As an internationally recognized center of excellence for atmospheric flight, NASA Langley Research Center has been involved in the design, development, and operation of these flight systems. A major challenge in this process is the limited amount of testing, and the total lack of end-to-end testing, in a relevant flight environment. Such tests would be very difficult (if not impossible) to perform and would be very expensive. Thus, a key component of the design of these systems and an integral part of the EDL system validation and verification has been detailed, end-to-end trajectory and flight simulations using models specific to

the system being developed (such as vehicle aerodynamics, sensors, propulsion systems, guidance, navigation, and control).[1,2]

As missions have become increasingly dependent upon trajectory simulation from design through operations, validation and verification of the simulations and system models have taken on greater importance, not only to confirm accuracy of current models, but also to ensure their applicability for future missions.[3] One method to provide this verification and validation in any flight environment is post-flight trajectory reconstruction and comparison with the pre-flight simulation. At NASA, models developed prior to mission completion (landing or final orbit acquisition) are validated against flight data via trajectory reconstruction and comparison. Traditionally, the pre-flight simulation (which includes these models and has completed many years of development, checkout, and validation) is not used in the trajectory reconstruction, requiring additional time and effort to validate the reconstruction models.

Increasingly, missions occur in sets, with one mission being followed quickly by a second similar mission. The Viking missions and the Mars Exploration Rovers (MER) were characterized by two systems performing EDL within weeks of each other following similar mission plans. To increase the chances of success on the second mission, these mission types require trajectory reconstruction of the first EDL to adjust parameters and models prior to the second entry (usually within weeks of the first entry).[4,5] Thus, a procedure that integrates the reconstruction process with the pre-flight, detailed, end-to-end trajectory simulation would not only reduce time and resources required to prepare for trajectory reconstruction and subsequent model validation but also provide a capability for rapid trajectory reconstruction to support multiple entries (a la Viking and MER).

At NASA Langley Research Center, the Program to Optimize Simulated Trajectories II (POST2) is the primary trajectory simulation tool. POST2 has been successfully used to support the atmospheric entry phase design, operations, trajectory determination/optimization and Monte-Carlo analyses of many recent missions. These missions include the Mars Pathfinder EDL [6,7], Mars Polar Lander EDL [8], Odyssey Orbiter aerobraking [9,10], proposed 2001 Lander EDL [11,12], 2003 MER Lander EDL [13], Genesis [14] and Stardust [15] Earth entry and descent, as well as the Huygens probe EDL at Titan [16,17]. Detailed POST2 simulations were developed to support the planning and operations of these missions. Additionally, POST2-based simulations are being used for Mars Phoenix lander[18] and Mars Science Laboratory (MSL) EDL[19] development as well as Lunar Lander studies.[20] Thus, POST2 was selected for the integration of a reconstruction capability.

NASA Langley was involved in Huygens Titan probe pre-entry EDL analyses conducted under the auspices of a NASA Engineering Safety Center's (NESC) Independent Technical Assessment (ITA).[16] A POST2-based trajectory simulation was developed that included models of the probe aerodynamics, parachute trigger logic and drag models for the Pilot, Main, and Drogue parachutes. As part of an agreement with the European Space Agency (ESA), the flight data was provided to NASA for trajectory reconstruction and model assessment. This application was selected to demonstrate and apply the POST2 reconstruction capability since trajectory reconstructions completed by ESA and NASA using different approaches would be available for comparison.

The chapters below provide details on the current research. General information on the POST2 software and trajectory reconstruction are discussed next. The following chapter describes the reconstruction module, its integration into POST2, and the test case results. Next, the Huygens probe EDL trajectory reconstruction problem and the data

available from the flight at Titan are addressed. After that, results of the application of the POST2 reconstruction capability to the Huygens EDL trajectory are presented. Finally, observations are made regarding the results presented and potential future work.

Chapter 2: Background

2.1 PROGRAM TO OPTIMIZE SIMULATED TRAJECTORIES II

2.1.1 POST2 History

The Program to Optimize Simulated Trajectories II (POST2) is a generalized point mass, rigid body, event driven, discrete parameter targeting and optimization trajectory simulation program. POST2 was developed from the original Program to Optimize Simulated Trajectories (POST) software starting in 1996. POST development began in the early 1970's in partnership with the Martin Marietta Co. as a space shuttle simulation program.[21] Throughout the years, many models and capabilities have been added to POST; the program has been significantly improved with additional capabilities added in the area of vehicle modeling, trajectory simulation, and targeting and optimization. Using these upgrades and modifications, support of a large variety of aerospace vehicle development and operations via trajectory simulation, analyses, and system performance assessments was possible. Three degree-of-freedom, or 3-DOF (integrating translational equations of motion only), and six degree-of-freedom, or 6-DOF (integrating rotational equations of motion also), versions of POST capable of optimizing and targeting ascent, entry, and orbital trajectories have been available since the early 1980's. POST has become an industry standard trajectory simulation and optimization tool that has been transferred to hundreds of organizations in government, industry, and academia. Since 2004, POST2 has also been made available and transferred to entities in the government, industry, and academia. As was the case with the original POST, enhancements and capabilities continue to be added to POST2.

2.1.2 General POST2 models and capabilities

POST2 increases the trajectory simulation capability of the original POST computer code and provides a state-of-the-art simulation tool for endo- and exo-atmospheric flight about a planetary body to support launch, orbital, and entry vehicle design, development, testing, assessment, and operations. POST2 provides the capability to target and optimize trajectories for multiple powered or unpowered vehicles near an arbitrary rotating, oblate planet. [22] The generality of the original POST program is retained in POST2 through its multiple phase input capability. This flexible capability is augmented by a discrete parameter optimization capability that includes equality and inequality constraints. Both 3-DOF and 6-DOF trajectory simulations can be executed using POST2. As such, POST2 has been used successfully to solve a wide variety of atmospheric ascent and reentry problems, as well as exoatmospheric orbital transfer problems.

POST2 contains many basic models (such as atmosphere, gravity, propulsion and navigation system models) that are used to simulate a wide variety of launch, orbital, and entry missions. POST2 can support 3-DOF and 6-DOF trajectories within the same simulation; that is, not only can each vehicle trajectory support different degrees-of-freedom, but also each trajectory segment within a given vehicle simulation can be either 3-DOF or 6-DOF. POST2 is coded in a combination of C and FORTRAN programming languages. [22]

POST2 maintains and increases the user's ability to modify certain subroutines for specific applications. The software is constructed such that user supplied code can be included to provide vehicle aerodynamic data, atmosphere model, and even optimization capability. While POST2 has very adequate models for including these data and functions, the user has substantial flexibility to include mission specific models and/or

company proprietary representations and functionality. Additionally, support for statistical analysis approaches (such as Monte Carlo dispersion analyses) is provided.

2.1.3 POST2 for Specific Mission Support

Exploiting the modular nature of the POST2 program by adding mission specific models to the existing POST2 architecture allows for the development of higher fidelity, mission specific simulations. These simulations support design, development, testing, and operations of vehicles for particular missions. The level of complexity for mission specific POST2 simulations varies from first-order trades (e.g. parachute size and deployment conditions, terminal descent engine size, etc.) to end-to-end Monte-Carlo simulations to day-of-entry operations. Traditionally, POST2-based simulations have not been an integral part of the trajectory reconstruction; this research provides the capability necessary to facilitate integrating these detailed, mission-specific POST2 simulations into the reconstruction process.

The models required for these mission-specific simulations depend on the desired fidelity of the analysis. In the initial phases of mission definition and vehicle conceptual design, basic models already available in POST2 are used without modification to provide a tool for top-level trades and conceptual level design. As the mission and systems get better defined and higher fidelity models become available, they are incorporated into the POST2 simulation to perform more mission specific trades and analyses of the updated systems. Eventually, three and six degree-of-freedom (3- and 6-DOF) simulations which span an entire phase of a mission (such as entry, descent and landing at Mars from the final exoatmospheric trajectory correction maneuver to lander touchdown) using the latest engineering models of onboard systems are available for detailed mission trades, system analyses, system testing, and mission operations. This

approach has been and is being applied to the Mars Science Laboratory mission for the Entry, Descent, and Landing high fidelity engineering simulation using POST2 as the main simulation engine. [19]

The POST2-based simulation tools have been used to support all elements of the design life cycle for a wide variety of missions. Early conceptual studies have been conducted using models in the basic production version of POST2. [6,14,23,24] Higher fidelity simulations have included many mission specific models and data including aerodynamic parameters from wind tunnel testing and Computational Fluid Dynamics (CFD) runs, vehicle mass properties, parachute, control systems, and onboard propulsion systems as these data and models became available.[11-13, 25-27] POST2-based simulations have been exercised for extensive Monte-Carlo runs including those for "stress tests" that determine the limits of system capability.[7,9,13,16,27,28] The technical capabilities of POST2 have already been validated against other Mars mission data.[9,29,30]

Extending the POST2 capabilities to include trajectory reconstruction as an integral part of the software is a natural continuation of POST2 support for NASA missions. Additionally, further validation of POST2 and mission specific models can be facilitated by an integrated reconstruction capability. An element of this research is to rectify this deficiency and enhance POST2 by developing this integrated reconstruction capability.

2.2 TRAJECTORY RECONSTRUCTION

2.2.1 Current EDL Trajectory Reconstruction Methods

For planetary missions, traditional EDL trajectory reconstruction methods have focused on using accelerometer and gyro (if available) data to integrate a best estimate trajectory. These methods numerically integrate the measured data so that detailed modeling of the flight system (i.e., Reaction Control System thrusters, vehicle aerodynamics) is not required for reconstruction. However, errors in the accelerometer and gyro data (such as bias and noise) directly affect the accuracy of the reconstructed state. The flight data is adjusted (e.g., filtered or smoothed) to reduce these effects. If available, additional measurements (such as radar altimetry and Earth-based tracking) are utilized. Some form of filter or batch process is applied to adjust the state based on available measurements.[29,31,32] However, for missions like Mars Pathfinder and Mars Exploration Rovers many of these other data sources are not available until late in the EDL trajectory, usually at subsonic speeds and within a few kilometers of the surface. That is, these measurements generally do not cover hypersonic entry or the parachute phase until subsonic flight.

While this approach provides trajectory state estimates, assessment of the pre-flight simulation models is not adequately addressed by these initial solutions. Additional analysis using the flight data and the reconstructed trajectory is generally used to provide the model evaluation desired. Furthermore, these trajectory reconstructions are completed using different models and simulations than were used for the pre-flight analyses. Additional effort must be expended to verify the models used for reconstruction beyond those already used to verify the pre-flight simulation.

2.2.2 Kalman Filter Method

As indicated above, many of the approaches used for planetary EDL trajectory reconstruction include methods that use measurements to estimate parameters. Predominately, the Kalman filter (or one of the many modified versions) was used. This section briefly summarizes the Kalman filter method for use in reconstruction since this method is used in the POST2 reconstruction module discussed in more detail below (see section 3.1). Further detail on the Kalman filter can be found in refs. [33] and [34].

The Kalman filter is a mathematical technique to statistically estimate the state of a process by using sensor measurements or system observations to correct for modeling errors. This technique is generally applied computationally and was developed in the early 1960's. The steps of the Kalman filter process include modeling the dynamics of a process, taking sensor measurements or direct observations of the process, using mathematical models of these measurements or observations, and correcting the calculated state of the process. These steps continue until the state of the entire process is estimated. An additional result of this procedure is an estimate of the accuracy of the estimated state.

For trajectory reconstruction, the process is a spacecraft trajectory, measurements (from accelerometers, gyros, etc.) are made and compared to calculated values, and the state of the spacecraft is estimated. The state estimated could be the vehicle position and velocity, or it could be certain mission, environment, or spacecraft specific quantities (such as aerodynamic drag or atmospheric density). Additionally, none of the computational models, sensors, or observation methods is perfect; each has some form of modeling error, measurement noise/corruption, and random perturbation. The Kalman filter method includes the effect of the varying degrees of imperfection in the various models, sensors, and observations into the estimated state and accuracy. Several key

assumptions are made when using the Kalman filter, namely that the process to be estimated can be linearized, the measurement/observation and system errors are evenly distributed about the actual value (Gaussian) and have noise completely uncorrelated with time (also termed white noise). Techniques exist to allow nonlinear problems to be estimated (such as the Extended Kalman filter) by using a partial-derivative matrix (or Jacobian) to effectively linearize the system dynamics and observations about the estimated state.

2.2.3 Trajectory Simulation and Reconstruction Connection

As indicated above, the process from pre-flight simulation to post-flight reconstruction is currently disjoint. A more efficient approach would be to combine the two efforts such that testing and validation of the pre-flight simulation are applicable to the reconstruction. This approach would most benefit missions like MER that had two probes enter Mars within weeks of each other and needed a reconstruction of the first probe before the second one arrived. By following this approach, more time and resources can be focused on preparing for the post-flight analysis as opposed to the pre-flight development of software specific to the reconstruction problem.

In response to this desired capability, a main focus of this research is to connect the pre-flight simulation with the post-flight reconstruction. Many reconstruction applications involve not only a determination of the traditional vehicle state (position, velocity, attitude) but also an estimate of environment, vehicle characteristics, and system responses. For example, MER needed to assess the models of the environment (e.g., dynamic pressure, etc.) and vehicle characteristics (such as aerodynamics of the parachute) as well as the flight software parameter settings chosen for several critical events during EDL. Using the same simulation for pre- and post- flight analyses would

have made that process easier and faster. One product of this research is a general reconstruction module added to the existing POST2 software to provide such a capability for future missions. Another product of this research is the application of such a POST2 module to reconstruct environment, vehicle and trajectory information during EDL for a mission which used a POST2-based, mission specific trajectory simulation: the Huygens probe at Titan.

2.3 HUYGENS TITAN PROBE

2.3.1 Brief Huygens Mission Overview

The Cassini/Huygens mission to Saturn and Titan is a joint NASA/ European Space Agency (ESA) program that is managed by NASA JPL.[35] The Huygens probe portion of the mission is ESA's responsibility. The Cassini/Huygens spacecraft achieved orbit around Saturn following the successful Saturn Orbital Insertion (SOI) burn on July 1, 2004. As scheduled, the Huygens probe separated from NASA's Cassini spacecraft on December 25, 2004. On January 14, 2005, the Huygens probe entered the Titan atmosphere and landed on its surface. This probe used a multiple parachute system to enable atmospheric measurements to be recorded during the probe's more than two-hour descent to the surface. Digital images, radar altimetry, accelerometer data, and Earth-based radio telescope observations were also gathered during the entry, descent, and landing (EDL).[36-38]

Figure 2-1 illustrates the Huygens probe's EDL profile. After atmospheric interface, defined to be 1270 km above the surface, the probe decelerates to around Mach 1.5 at Pilot parachute deploy. This deploy event (designated T0) is triggered by a sequence of time and acceleration conditions and is the epoch time for all subsequent

events and most data sets generated during the parachute descent phase. Three parachutes were used in the Huygens probe system: (1) a 2.5-sec Pilot parachute; (2) a 15-minute Main parachute; and (3) a 2.5-hour Drogue parachute. Data taken during the descent was relayed through the Cassini spacecraft as it flew by Titan.

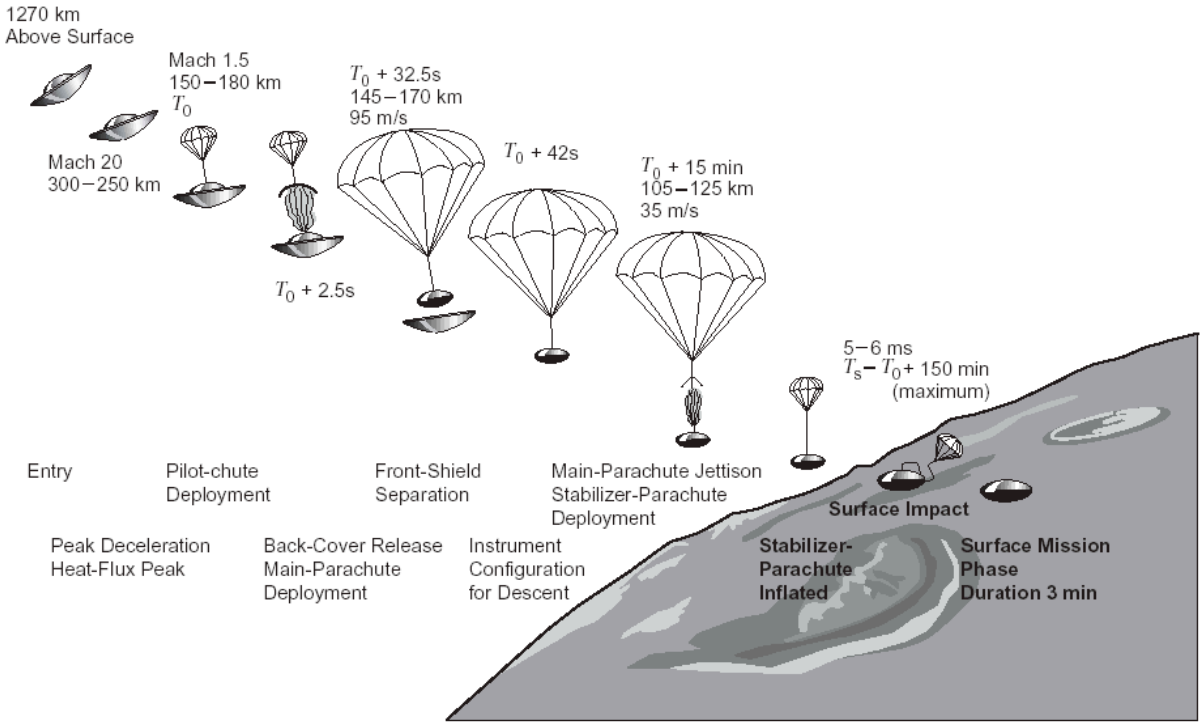

Figure 2-1. Huygens Titan probe Entry, Descent, and Landing (EDL) sequence [37]

NASA Langley was involved in the pre-entry EDL analyses of the Huygens probe. Analyses were conducted under the auspices of the NASA Engineering Safety Center's (NESC) Independent Technical Assessment (ITA) of the Cassini/Huygens probe EDL at Titan.[16] A POST2-based trajectory simulation was developed that included models of the probe aerodynamics, parachute trigger logic and drag models for the Pilot, Main, and Drogue parachutes. As part of the agreement with ESA, NASA provided

results of all analyses and presented findings to both the Cassini and Huygens project teams. In return, NASA was provided the flight data from the probe so that trajectory reconstruction could be done and simulation models assessed. NASA has completed similar assessments using flight data to improve simulation models such as capsule aerodynamics, parachute aerodynamics, and atmospheric density and winds. ESA had a team that provided the official project reconstruction of the Huygens EDL trajectory (the Huygens Descent Trajectory Working Group, or DTWG).[38] The main objective of the NESC sponsored activity was to reconstruct the Huygens Probe data to improve NASA's aerodynamics, atmospheric density and winds, and parachute performance models as well as to provide an independent trajectory reconstruction. The results of these analyses were provided to the DTWG and the Huygens Data Analysis Working Group (DAWG), with interaction between NASA, DTWG, and DAWG to discuss any differences in the reconstructed trajectory.

Chapter 3: Reconstruction Capability for POST2

3.1 General Reconstruction POST2 Module

As indicated above, an extended Kalman filter (EKF) module has been developed for and included into POST2. The motivation for integrating this EKF function into POST2 was to allow more rapid setup and execution of trajectory reconstruction runs using the same POST2-based mission specific simulation that was tested and validated during the design of a particular mission. A key element of this implementation is that any POST2 inputs can be the states to be estimated and any POST2 outputs can be the observations. While the general POST2 software architecture was retained, separate files of observations and their associated weightings versus simulation time must be provided for use with this EKF module.

3.1.1 Extended Kalman Filter Logic

The theory and equations defining this module are well described in the literature.[33,34] A summary of the EKF implementation for the POST2 module is as follows:

1) Define initial covariance matrix and estimated state (P_0 and X_0)

2) Read observations (O) and their weights (W) from files

3) Integrate state and covariance to the next observation time:

$$\dot{\overline{X}} = F(\overline{X}, t)$$

$$\dot{\overline{P}} = A * \overline{P} + \overline{P} * A^T + Q \qquad (3.1)$$

where $\overline{X}$ is the propagated state vector; $\overline{P}$ is the propagated state covariance matrix; A is the matrix of state derivative with respect to time ($\dot{\overline{X}}$) sensitivity to the state ($\frac{\partial \dot{\overline{X}}}{\partial \overline{X}}$); Q is the system noise covariance matrix.

4) At the observation time, calculate:

$$Y = O - G$$

$$H = \frac{\partial G}{\partial X}$$

$$K = \overline{P} H^T * (H * \overline{P} * H^T + R)^{-1}$$

where O is the observation vector (from file), G is the vector of calculated observation values from the simulation, Y is the observation residual, K is the Kalman gain matrix, and R (the measurement noise covariance) is set to the inverse of the observation weightings matrix ($R = W^{-1}$).

5) Next estimate the state:

$$\hat{X} = \overline{X} + K * Y$$

6) And estimate the covariance:

$$\hat{P} = (I - K * H) * \overline{P} * (I - KH)^T + K * R * K^T$$

where I is the identity matrix, $\hat{X}$ is the estimated state, and $\hat{P}$ is the estimated covariance.

Note that the Joseph form of the covariance update is used. As Gelb indicated[33], this form reduces the impact of numerical round off error at the expense of computational speed. However, with current computer speeds, this cost is acceptable for

implementation into POST2. This process is continued from step 3 above with POST2 integrating the state and covariance between observation updates.

3.1.2 Implementation into POST2

As indicated above, the Extended Kalman Filter module for trajectory reconstruction was integrated into POST2. Any POST2 input parameter that has an associated derivative calculated in the software can be an estimated state, and any POST2 output parameter can be an observation. Note that derivative calculations can be added to POST2 for use with the reconstruction module. Additionally, software modifications followed the POST2 optimization module program conventions whenever possible to ensure that reconstruction functions were called in the correct sequence.

The reconstruction process in POST2 follows the basic logic shown in section 3.1.1 and can be expressed as three major procedures. First, all of the reconstruction variables (e.g., states, derivatives) are initialized and POST2 processes (integration list, module activation) are setup. Next, POST2 integrates states and covariance until the next measurement time is reached. Finally, the reconstruction module estimates the states and covariance that are then inserted into the appropriate POST2 variables (based on user input). The process continues with the integration and estimation steps unless a POST2 event occurs. If an event occurs, the setup step is also redone to include any simulation changes.

The POST2 reconstruction module inputs and outputs are shown in Appendix A. The reconstruction inputs specific to each problem are entered in the estimated state, estimated state derivative, and observed parameters using the POST2 input/output variable names RECON_STATE, RECON_STATE_DERIV, and RECON_OBSERV, respectively. Several other parameters are available as well (e.g., system noise, state

variable perturbation size for sensitivity matrix generation). A file of the measurements as a function of time and another file containing measurement weightings must also be provided.

Nearly 30 routines were modified or supplemented to provide the reconstruction capability within POST2. For example, changes were made to allow the simulation state to be updated internally more than once during the trajectory; this operation mode is unlike the POST2 optimization process where a given independent parameter is adjusted only once in a trajectory. Other additions to POST2 for reconstruction included the EKF and its other supporting routines (such as measurement data acquisition, residual calculations, etc.), more variable structures as well as POST2 integration list modifications.

When code modifications were made during the process of developing the reconstruction capability, all POST2 quality assurance tests were conducted. Also, all NASA Langley procedures for quality assurance testing were followed during this development process. Following these procedures means that the modified software had to pass a comparison with the production (certified) POST2 for a suite of over 160 test cases.

3.2 VALIDATION TEST CASES

Several validation test cases were performed using the POST2 reconstruction module. These cases ranged from a single, constant parameter estimate to a case similar to an actual mission. These cases were run in the order of increasing complexity to not only validate the changes to POST2, but also determine issues that had to be resolved before moving to the next case. The cases used to validate and verify the approach and

implementation were: (1) Large J2; (2) 6-DOF entry; and (3) MER Mission specific 6-DOF entry.

The more complex cases were run from multiple starting conditions to measure how well the method produced the "truth" trajectory used to generate the test data. The results of these validation cases were used as a basis for asserting the capability of the method using POST2 to reconstruct the entry trajectory for an actual mission. The following sections detail the results of these validation case runs.

3.2.1 Large J2 Case

As an initial test case, a trajectory with a large J2 component of the gravity harmonic on an orbit around Mars was simulated using POST2. The magnitude of the gravity vector was recorded at 100 sec intervals. This observation set was then used with POST2 in reconstruction mode to estimate the value of J2. Table 3-1 gives the pertinent parameters used in the simulation and reconstruction. A large value of J2 was used to quickly have an impact on the trajectory. This trajectory was terminated after 10000 sec.

As indicated above, this test case estimates a constant J2 zonal harmonic of the gravity field for observed gravity magnitudes over several orbits. To facilitate code error identification, the large J2 value of 1.9595 was used in generating the test case observation values. The inputs used in this case are summarized in Table 3-2. Also, the

Table 3-1 Large J2 Test Parameters and Values

Parameter	Simulation Run	Reconstruction Run
Initial Conditions		
Periapse Altitude	50000 m	50000 m
Apoapse Altitude	600000 m	600000 m
J2 used/initial estimate	1.9595	0
Gravitational Parameter	4.2828287 E13 m^2/s^3	4.2828287 E13 m^2/s^3
Mars Equatorial Radius	3393940 m	3393940 m
Mars Equatorial Radius	3376780 m	3376780 m

associated POST2 variables are shown in the table. Note that the POST2 variable GENV1 is set to zero providing the appropriate derivative value for the constant J2. Also, the gravity vector magnitude (the observation in this test) was calculated in the POST2 variable SPCV1.

Table 3-2. J2 Estimation Test Case Reconstruction Variable Inputs

POST2 Input	Initial Value	POST2 Variable Name
RECON_STATE	0.0	J2
RECON_STATE_DERIVS	-	GENV1
RECON_OBSERV	-	SPCV1
COVARIANCE	4	-

Figures 3-1 to 3-3 show the results of using the EKF reconstruction module in POST2 for estimating the J2. Figure 3-1 shows the error in the estimated J2 as a function of time. The initial error of just over 1.9 is also indicated on this plot. As seen in the figure, after one observation the error overshoots to almost an equal amount as the initial error. However, after four observations, the error is near zero. Figures 3-2 and 3-3 show the difference in the observed and actual gravity values. Again, after four observations are included, the gravity of the reconstructed trajectory is aligned with the observed values from the “truth” trajectory. The circles in the last two plots show the time (and value) of the observations for this test case. These results provided initial confidence that the reconstruction module was functioning as an integrated part of POST2.

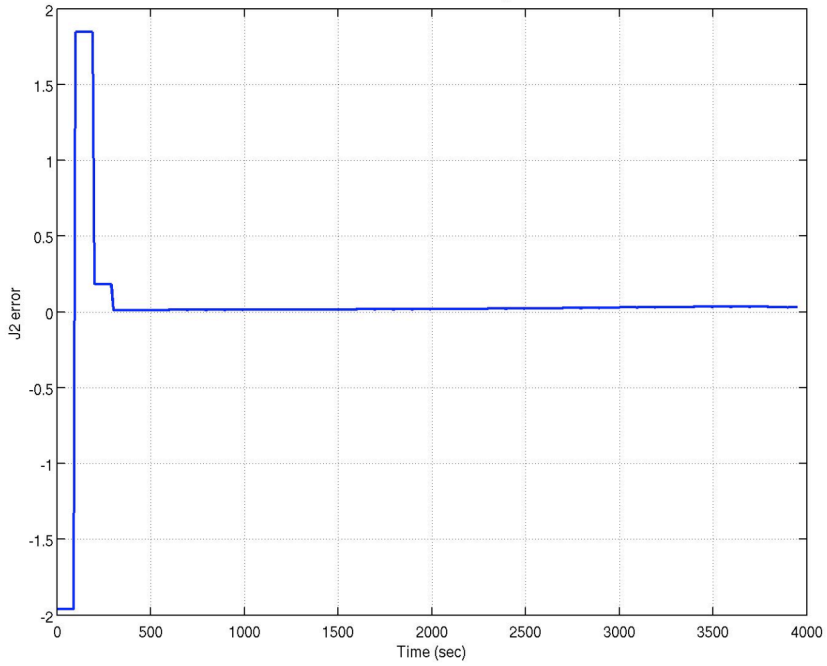

Figure 3-1. Error in Actual versus Estimated J2

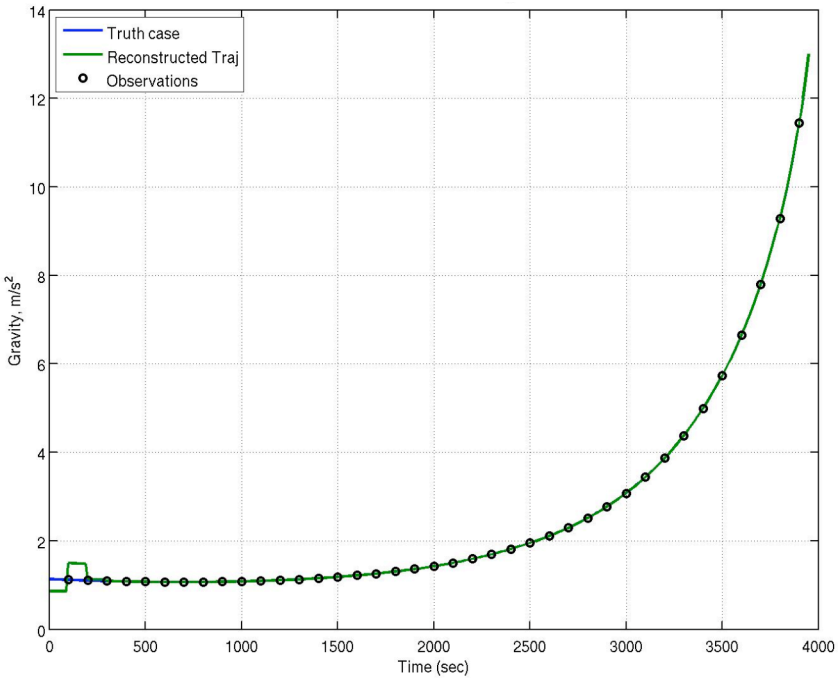

Figure 3-2. Comparison of Observed versus Actual Gravity

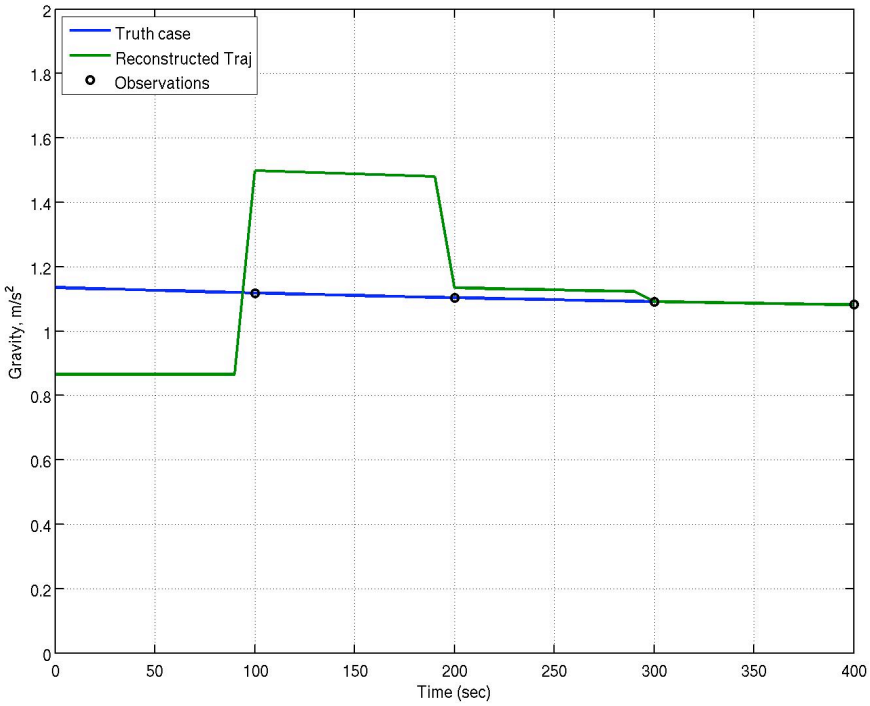

Figure 3-3. Magnification of Initial Four Observations

3.2.2 6DOF Entry Trajectory

The next test case uses a POST2 simulated six degree-of-freedom ballistic entry trajectory at Mars. This ballistic trajectory is similar to the hypersonic entry portion of the Huygens EDL trajectory to be reconstructed. POST2 variables are used for the states and calculated observations so that additional coding and checkout of those quantities is not needed. This entry trajectory at Mars was simulated using a nominal initial state (position, velocity, attitude and attitude rate). The observed quantities (acceleration vector and attitude rates) were sampled from the nominal trajectory run every 0.1 sec, or every ten integration steps. Additionally, 3-σ noise values of 10 μ-g's (or 9.81e-5 m/s^2) and 0.01 deg/root-hr (or 1.667e-4 deg/sec) were sampled and added to the observations.

Using these values and a random number generator, noisy measurements were created from perfect measurement values captured from the nominal trajectory.

For the reconstruction run in POST2, the inertial position and velocity were estimated. Also, the aerodynamic angles (for vehicle attitude) and body angular velocity vector were estimated. A MER covariance was used to generate an off-nominal initial position and velocity. The attitude error was assumed no larger than 0.5 deg 3-σ per angle and attitude rate error of less than 0.01 deg/sec per axis. Using these values and a random number generator, three separate sets of initial conditions for the state to be estimated (inertial position, velocity, attitude and attitude rates) were generated. The values above were used to initialize the vehicle state and covariance in the reconstruction run. The reconstruction run did not start from the same initial state as the nominal case used to generate the observed quantities.

The vehicle parameters (e.g., mass properties, dimensions, aerodynamics) for these test cases were based on the MER entry vehicle. Table 3-3 gives the reconstruction inputs using POST2 variables. Table 3-4 shows the reconstruction states and their initial value uncertainties, whereas Table 3-5 indicates the initial conditions for the three entry

Table 3-3. 6-DOF Entry Trajectory Test Case Reconstruction Inputs

POST2 Input	POST2 Variable Name
RECON_STATE	XI, YI, ZI, VXI, VYI, VZI, ALPHA, BETA, BNKANG, ROLBD, PITBD, YAWBD
RECON_STATE_DERIVS	VXI, VYI, VZI, AXI, AYI, AZI, ALPDOT, BETDOT, BNKDOT, ROLBDD, PITBDD, YAWBDD
RECON_OBSERV	AXI, AYI, AZI, ROLBD, PITBD, YAWBD

trajectory test cases used. Note that the observation values from the same "truth" trajectory were used in each case and that total accelerations were measurements for this test.

Table 3-4. Entry Test Case Reconstruction States and Initial Value Uncertainties

State	POST2 Variable Name	1-σ Uncertainty	3-σ
Inertial Position X Coordinate, m	XI	5887	17661
Inertial Position Y Coordinate, m	YI	2100	6300
Inertial Position Z Coordinate, m	ZI	2145	6435
Inertial Velocity X Coordinate, m/s	VXI	1.46	4.38
Inertial Velocity Y Coordinate, m/s	VYI	1.14	3.42
Inertial Velocity Z Coordinate, m/s	VZI	1.02	3.06
Angle of Attack, deg	ALPHA	0.1667	0.5
Sideslip Angle, deg	BETA	0.1667	0.5
Bank Angle, deg	BNKANG	0.1667	0.5
Angular Velocity Body X, deg/s	ROLBD	0.0033	0.01
Angular Velocity Body Y, deg/s	PITBD	0.0033	0.01
Angular Velocity Body Z, deg/s	YAWBD	0.0033	0.01

Table 3-5. Three Entry Test Case Initial Values

POST2 Variable Name	Truth Case	Test Case 1	Test Case 2	Test Case 3
XI	-2833460.1	-2840685.2	-2833267.4	-2824923.5
YI	-1796348.4	-1799150.9	-1796194.1	-1793427.2
ZI	-1072627.1	-1070834.3	-1071217.6	-1072989.5
VXI	3532.51	3530.88	3532.75	3534.57
VYI	-4171.4	-4172.58	-4171.23	-4169.80
VZI	1338.9	1337.35	1338.67	1340.29
ALPHA	0.0	-0.4	-0.45	0.45
BETA	0.0	0.4	0.35	-0.35
BNKANG	0.0	-0.35	0.2	-0.25
ROLBD	12.0	12.010	11.991	12.005
PITBD	0.0	0.008	-0.008	-0.009
YAWBD	0.0	-0.0065	-0.0045	0.008

Figures 3-4 through 3-15 show the results of using the EKF reconstruction module in POST2 for estimating the position, velocity, attitude and angular velocity for three separate cases. These cases compare the error between the test case estimated state and the "truth" state generated from nominal inputs using POST2. These figures show the state estimate errors in groups of three: position components, velocity components, aerodynamic angles, and angular velocity components.

Each one of these test cases indicates improvement in the state estimate error (relative to the "truth" state) as more observations are included. Test case 1 results for position error (Fig. 3-4), velocity error (Fig. 3-5), aerodynamic angle errors (Fig. 3-6), and angular velocity errors (Fig. 3-7) illustrate this assessment. As seen in Fig. 3-4, the total position error vector magnitude that begins around 7900 m is reduced to less than 200 m after 15 sec of observations. Note that once the appreciable atmosphere is reached (increased dynamic pressure) at around 130 sec and aerodynamic forces begin to affect the vehicle motion, the errors still remain much lower than their initial values. The final position error is on the order of 20 m. The velocity errors and attitude rate errors (Figs. 3-5 and 3-7) show a very similar trend as the position error (significant reduction in initial error after 15 s). While the angle of attack and sideslip angle also show the same trend in Fig. 3-6, the bank angle does not reduce as rapidly. Since the attitude errors in the angles that align the vehicle body X-axis with the velocity vector are quickly reduced, the bank angle is effectively the vehicle roll angle after about 15s. Since this vehicle has no lift once the X-axis aligns with the velocity vector, the observed accelerations have little contribution to determining the orientation of the other two axes, and hence the roll (or bank) angle.

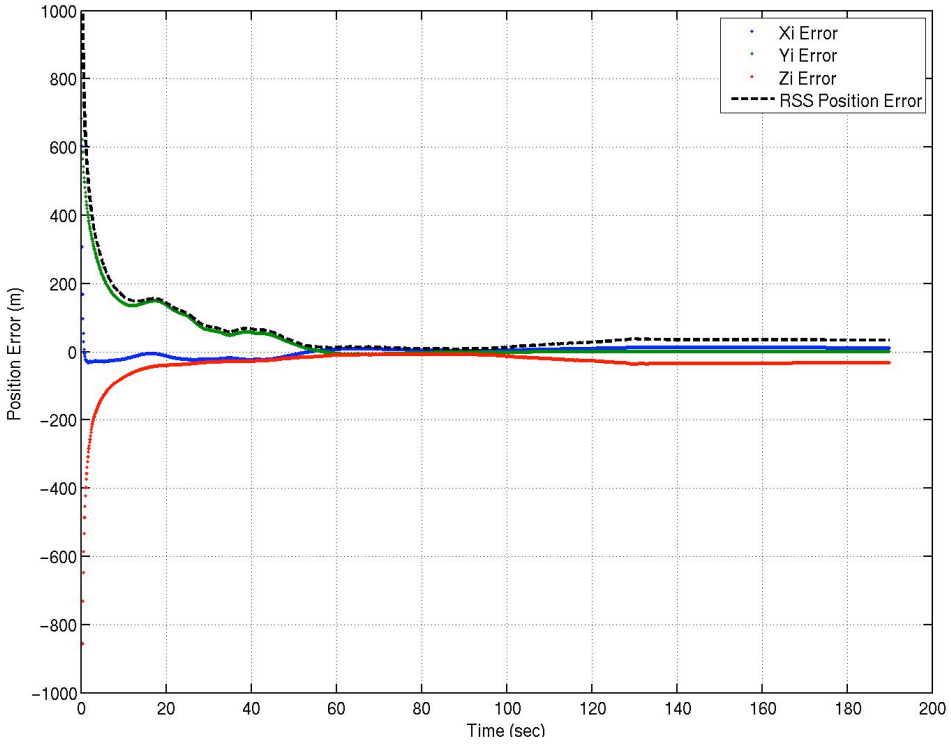

Figure 3-4. Entry Test Case 1 Position Component Error

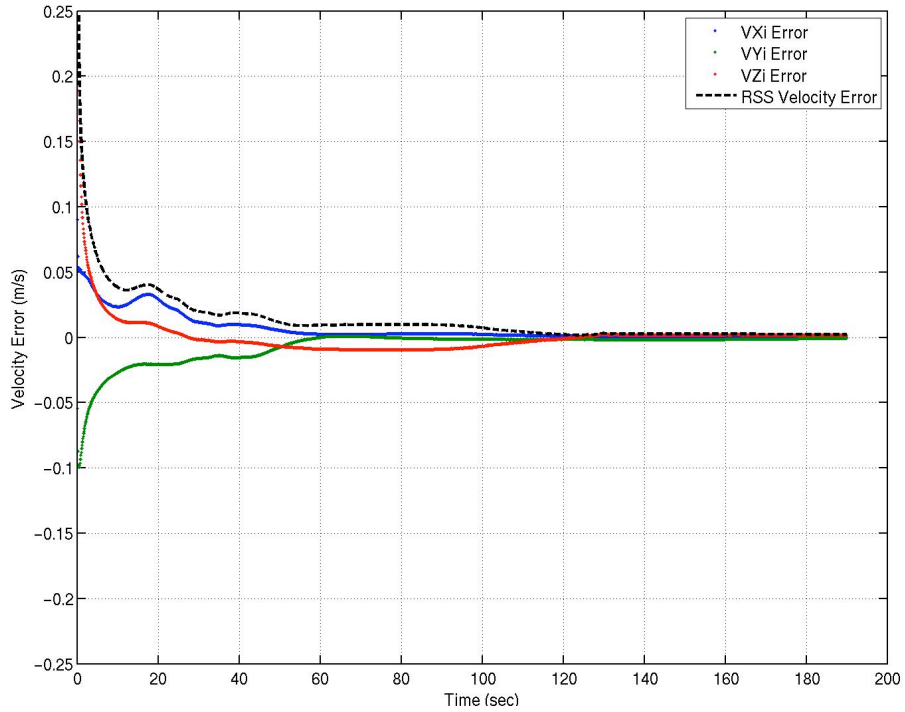

Figure 3-5. Entry Test Case 1 Velocity Component Error

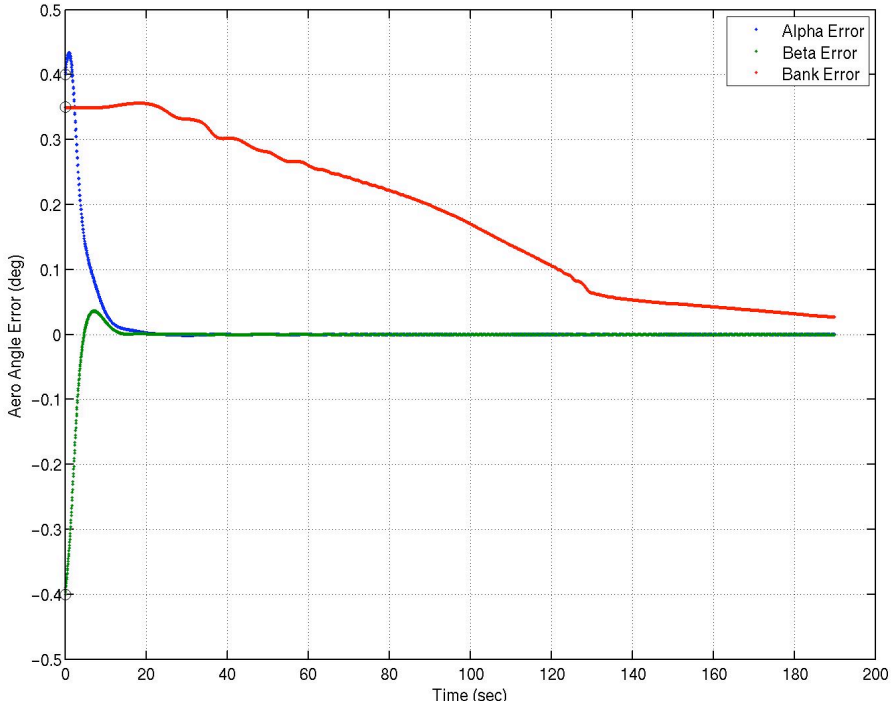

Figure 3-6. Entry Test Case 1 Aerodynamic Angle Error

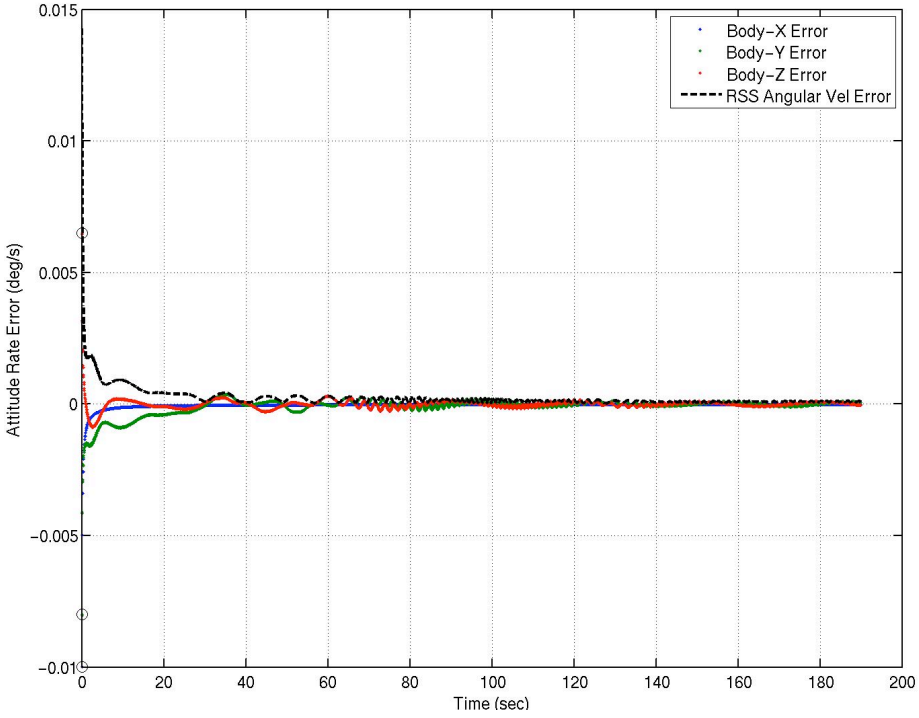

Figure 3-7. Entry Test Case 1 Angular Velocity Component Error

The remaining two test cases show trends similar to those indicated above. Test Case 2 results are given in the same order as Test Case 1 in Figs. 3-8 to 3-11, and Test Case 3 results are shown in Figs. 3-12 to 3-15. All the cases result in reduced errors between the estimated and "truth" states. This analysis did not include either observation weights or system noise covariance matrices. These options will be investigated further in the next series of test cases.

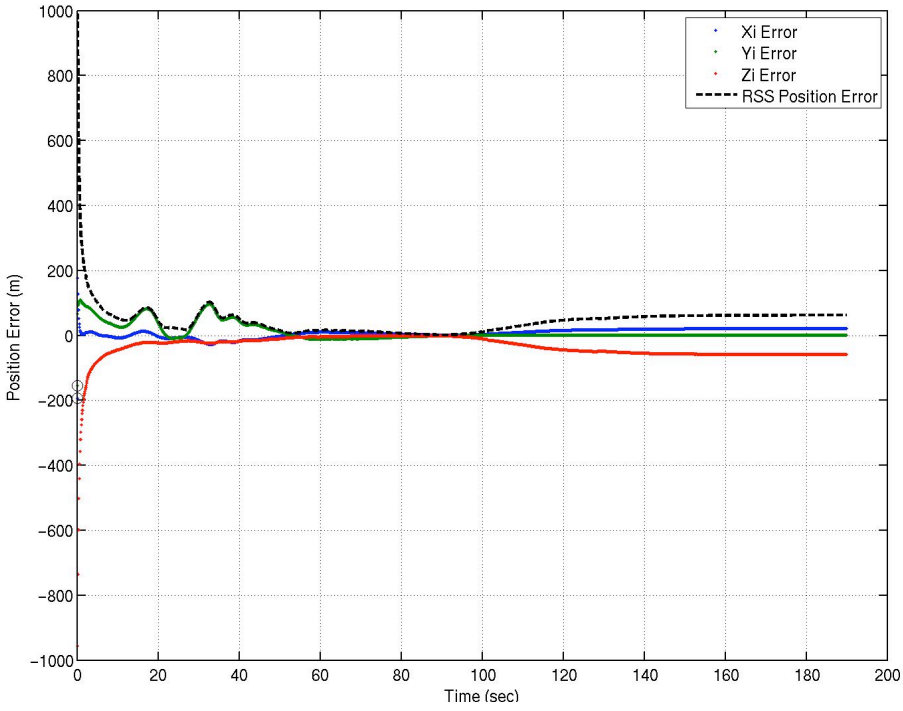

Figure 3-8. Entry Test Case 2 Position Component Error

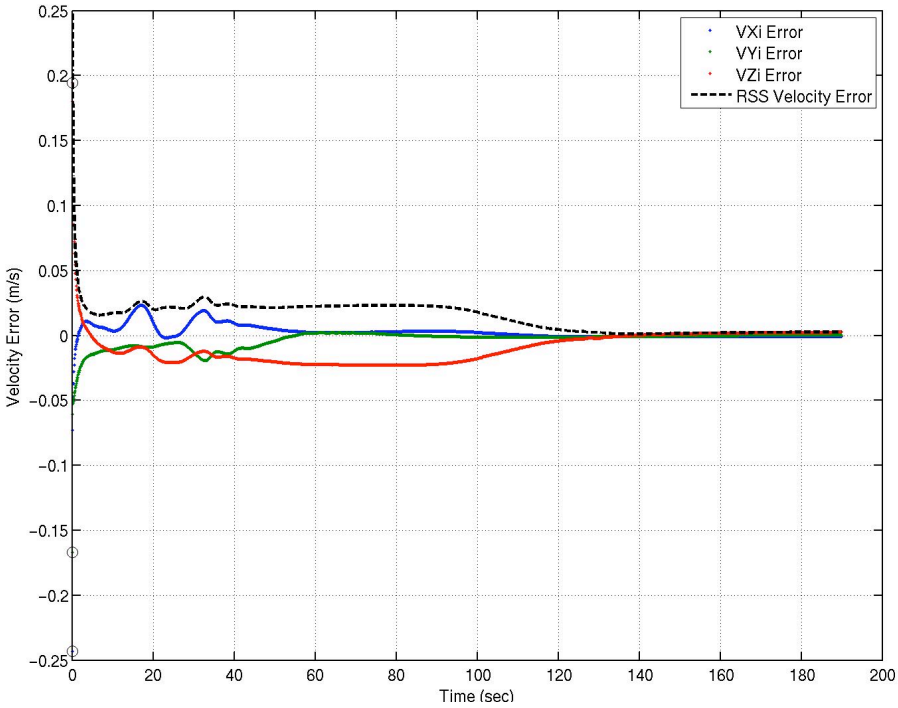

Figure 3-9. Entry Test Case 2 Velocity Component Error

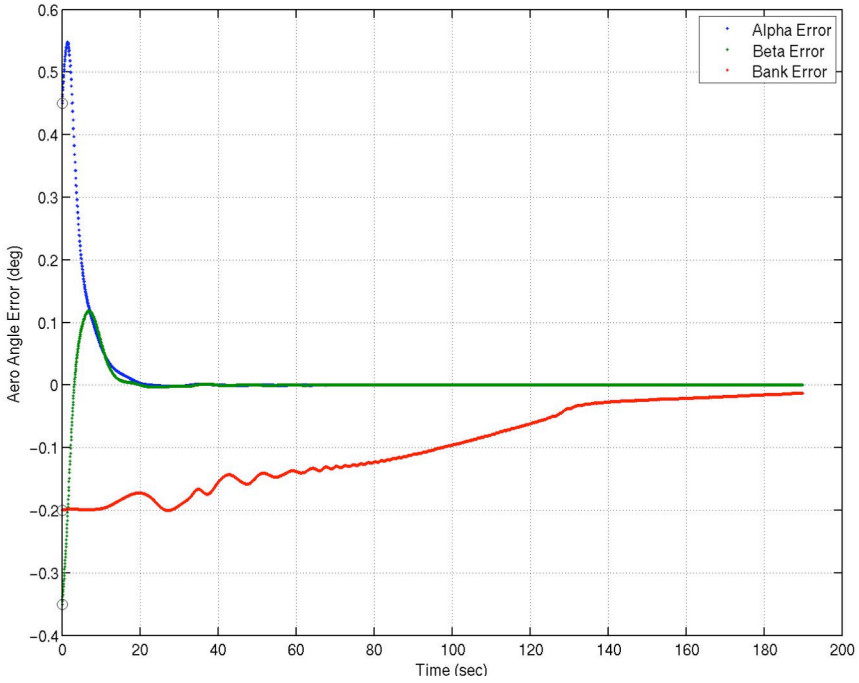

Figure 3-10. Entry Test Case 2 Aerodynamic Angle Component Error

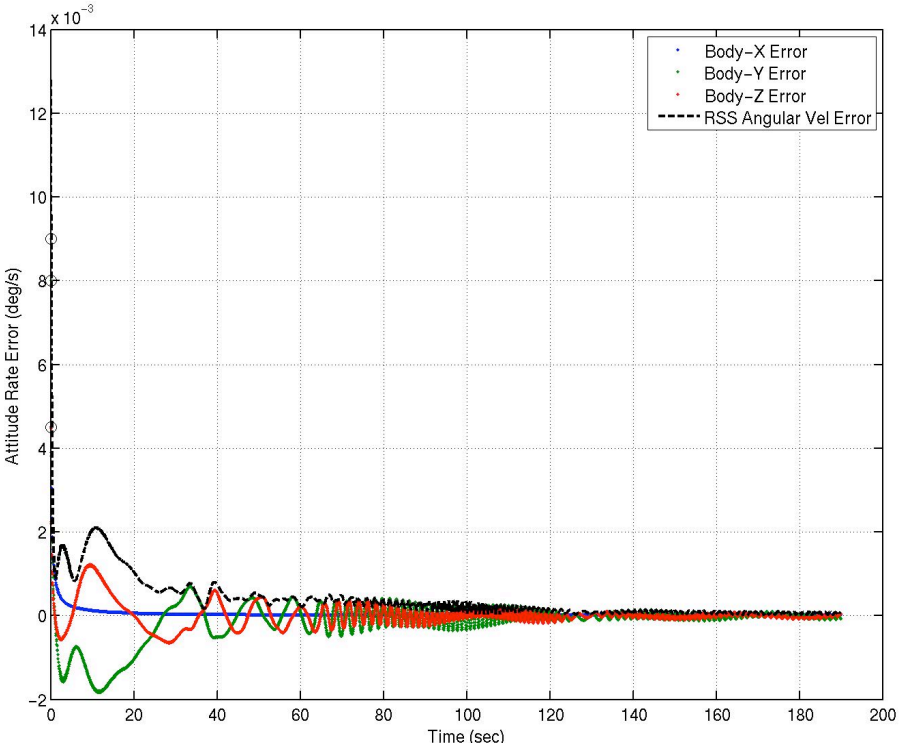

Figure 3-11. Entry Test Case 2 Angular Velocity Component Error

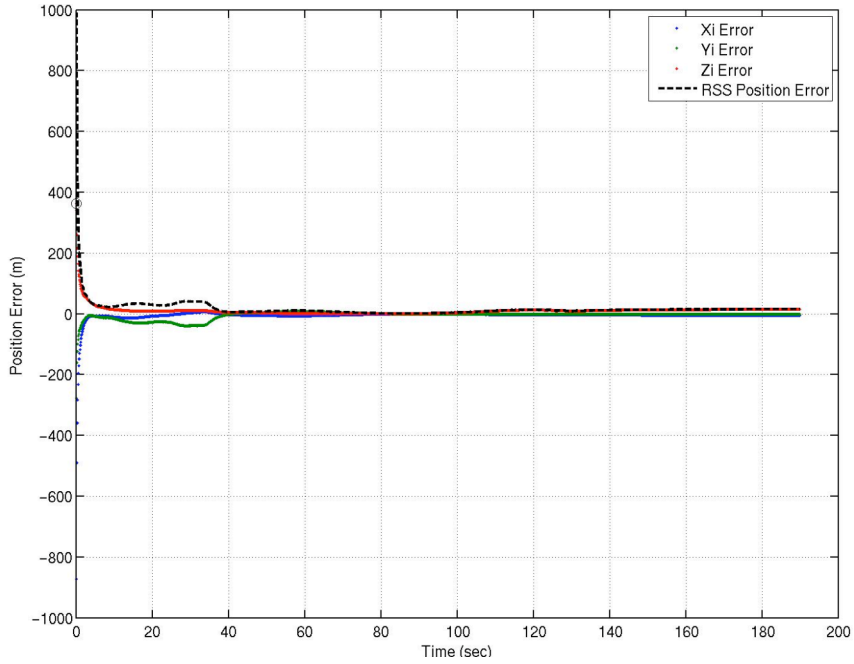

Figure 3-12. Entry Test Case 3 Position Component Error

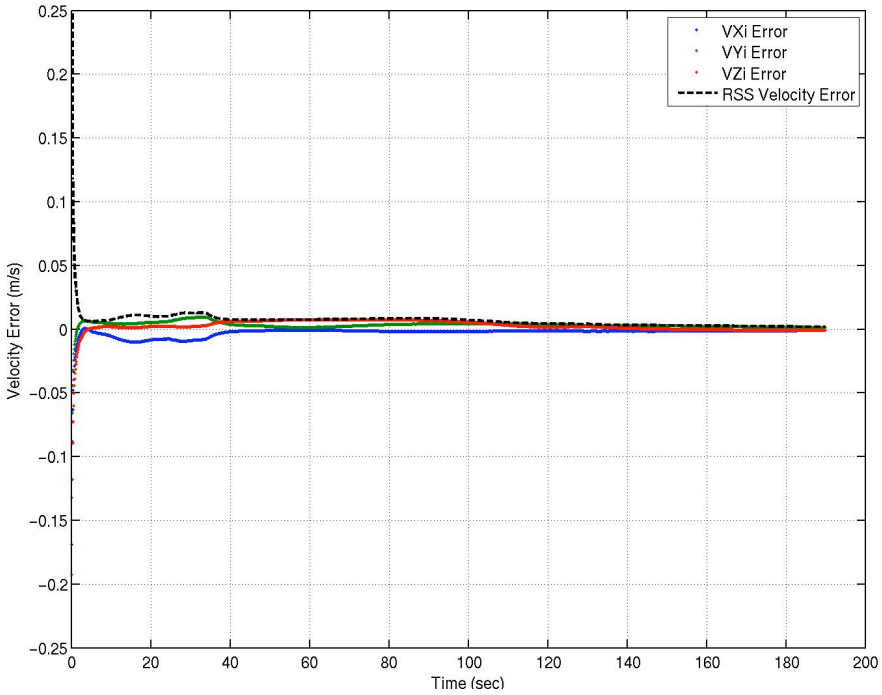

Figure 3-13. Entry Test Case 3 Velocity Component Error

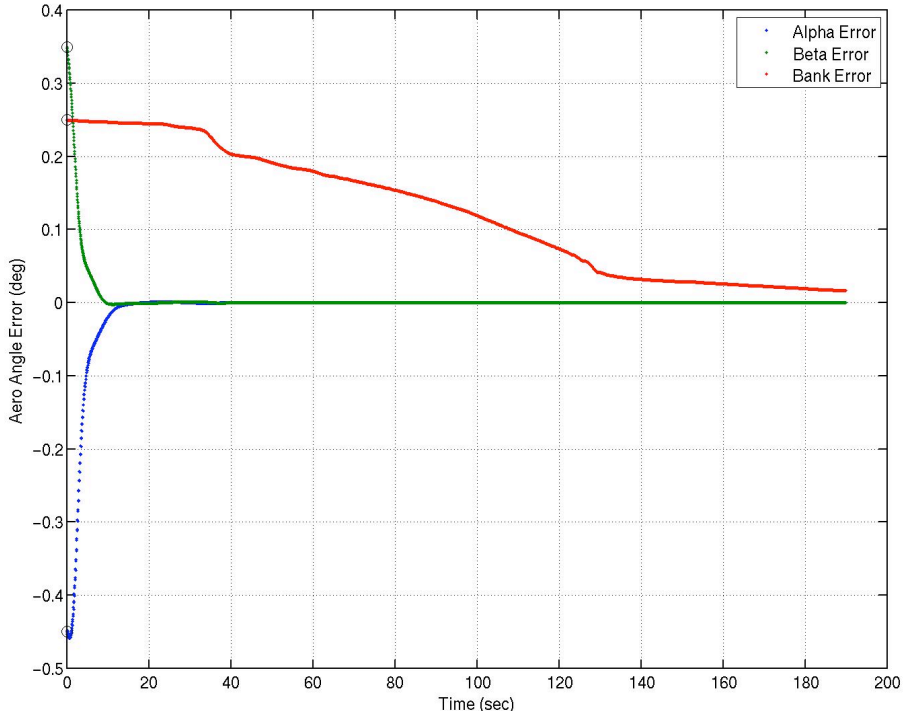

Figure 3-14. Entry Test Case 3 Aerodynamic Angle Component Error

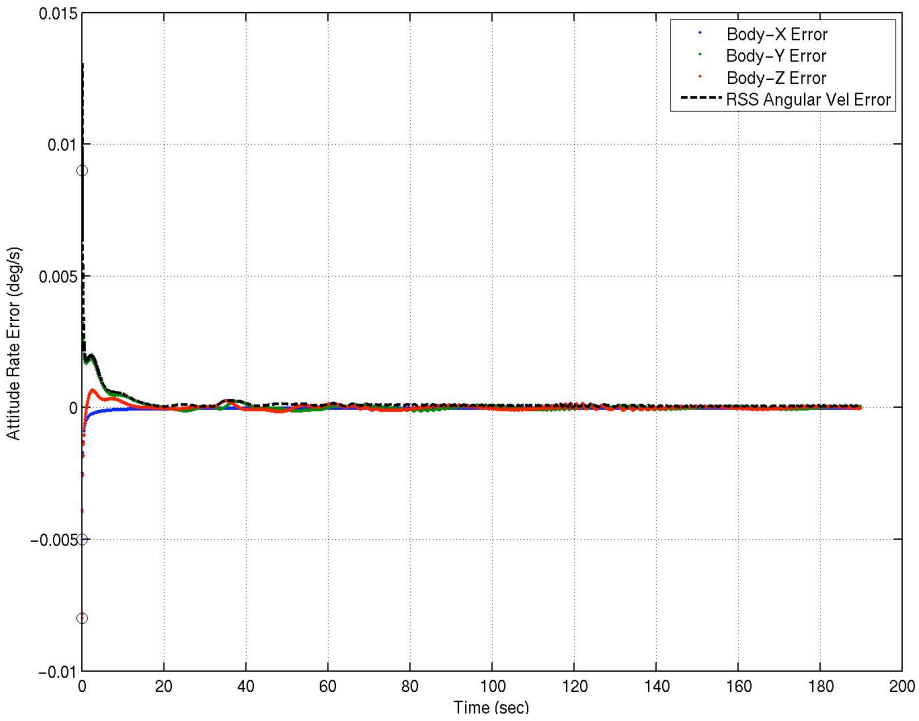

Figure 3-15. Entry Test Case 3 Angular Velocity Component Error

When no "truth" case is available, as for a flight reconstruction, the observation residuals will be examined to determine how closely the filtered trajectory matches the observations. Figures 3-16 to 3-19 show the residuals for Test Case 1. The residuals quickly diminish, which is consistent with the state error plots above. The added observation noise is evident on the acceleration residual plots (Figs. 3-16, 3-17). From Figs. 3-16 and 3-17 it can be seen that the acceleration residuals drop from about 0.002 m/s^2 to a final value on the order of 0.0001 m/s^2. Figures 3-18 and 3-19 show the attitude rate observation residuals. These figures also illustrate the observation noise and the rapid decrease in the residuals. Test Cases 2 and 3 exhibit similar behavior, but are not shown here. These results indicate that the Kalman filter components tested thus far are correctly implemented in POST2.

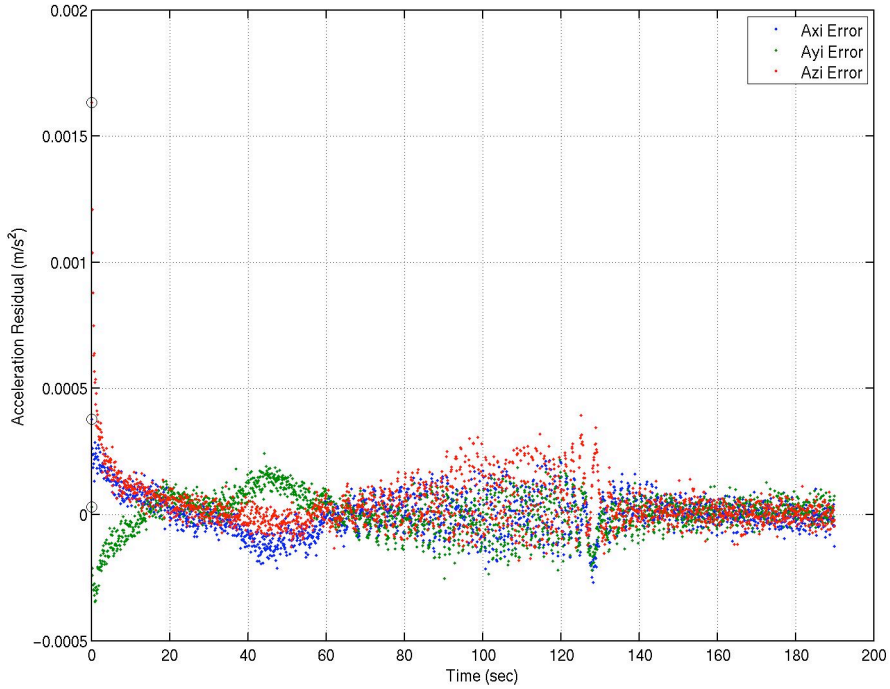

Figure 3-16. Entry Test Case 1 Observed Acceleration Residuals

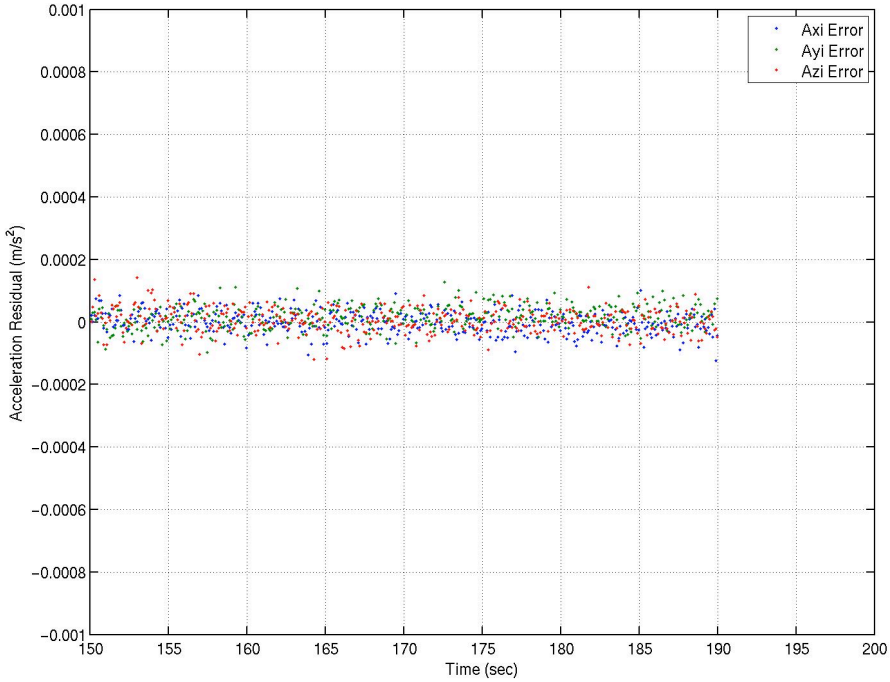

Figure 3-17. Entry Test Case 1 Observed Acceleration Residuals (End of Trajectory)

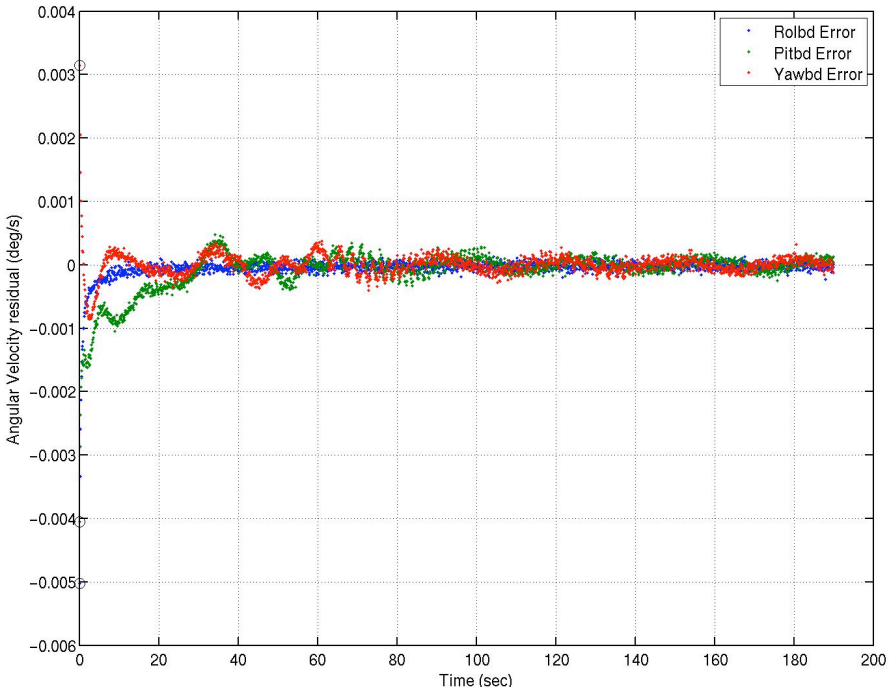

Figure 3-18. Entry Test Case 1 Observed Angular Velocity Residuals

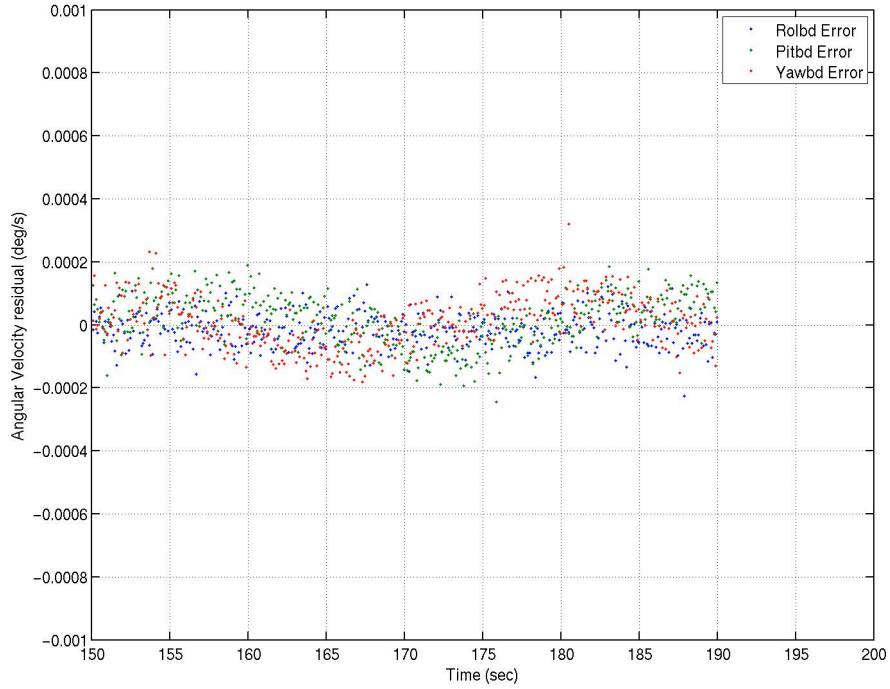

Figure 3-19. Entry Case 1 Observed Angular Velocity Residuals (End of Trajectory)

A comparison between a simulation-only run (without reconstruction) and a reconstructed trajectory was made using the same initial state errors for both. This test evaluated the tendency of similar entry trajectories to naturally approach a common flight path; that is, could the propagated trajectory reduce the residual error as well as the reconstructed case if the same system models were used that generated the "truth" trajectory? Figures 3-20 through 3-23 clearly show that the answer to this question is no. These figures indicate a significant impact on the trajectory estimate when using the reconstruction module in POST2: tens of kilometers for the position X-component (Fig. 3-20); hundreds of m/s for the velocity X-component (Fig. 3-21); as large as half a degree for Angle of Attack (Fig. 3-22); and angular velocity body X-component (Fig. 3-23) never really improves the initial error. That is, just propagating the initially provided states with very good models of the system used to generate the observations produces unacceptably large errors in the propagated trajectory when compared with the "truth". These results confirm that the Kalman filter module implemented into POST2 definitely impacts the trajectory produced by simulation and in a positive manner relative to a "truth" trajectory.

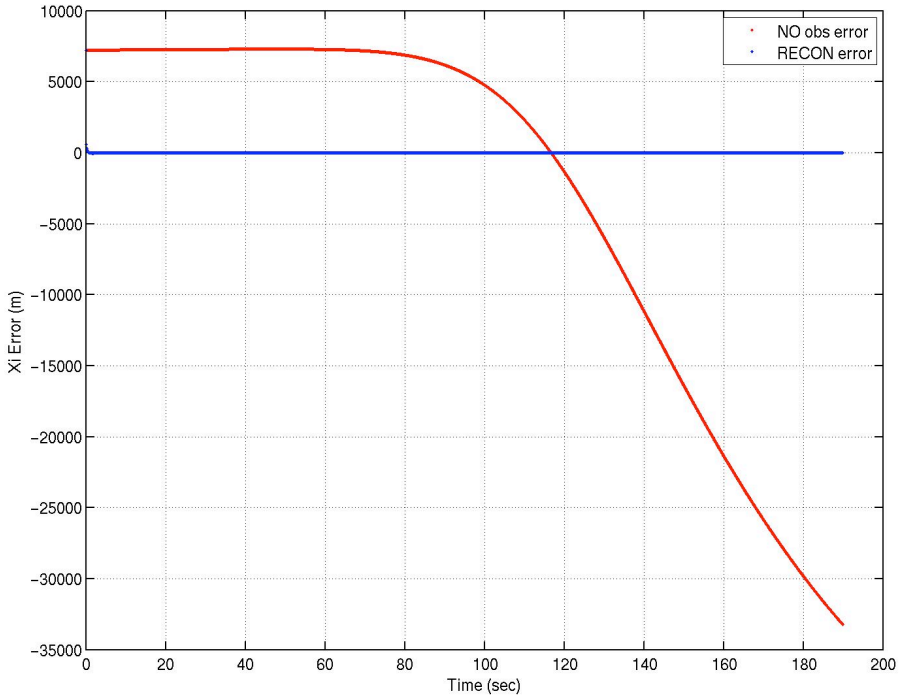

Figure 3-20. Entry Case 1 Estimated versus Propagated Position X-Component

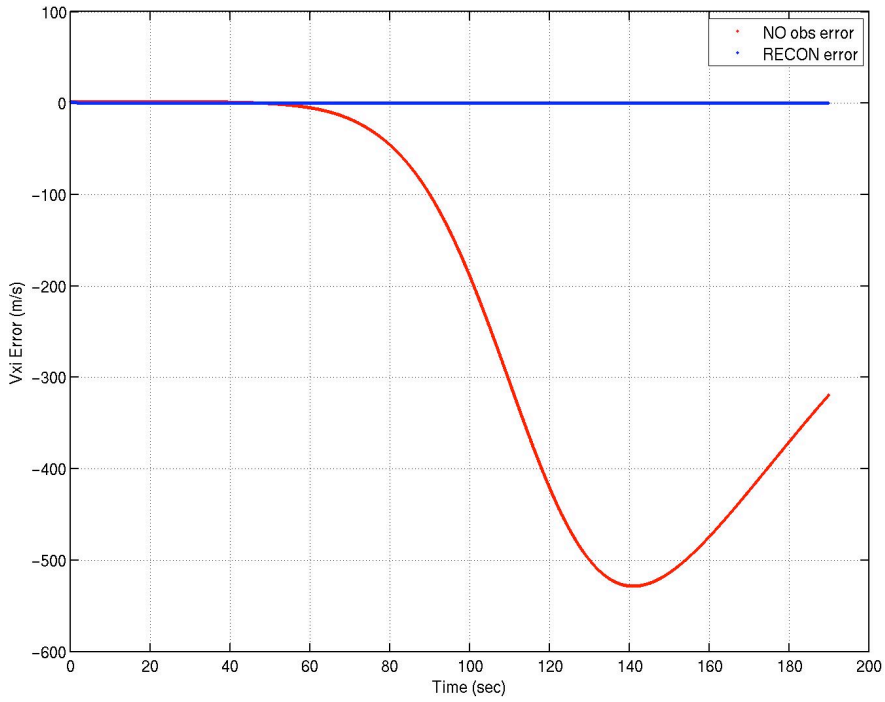

Figure 3-21. Entry Case 1 Estimated versus Propagated Velocity X-Component

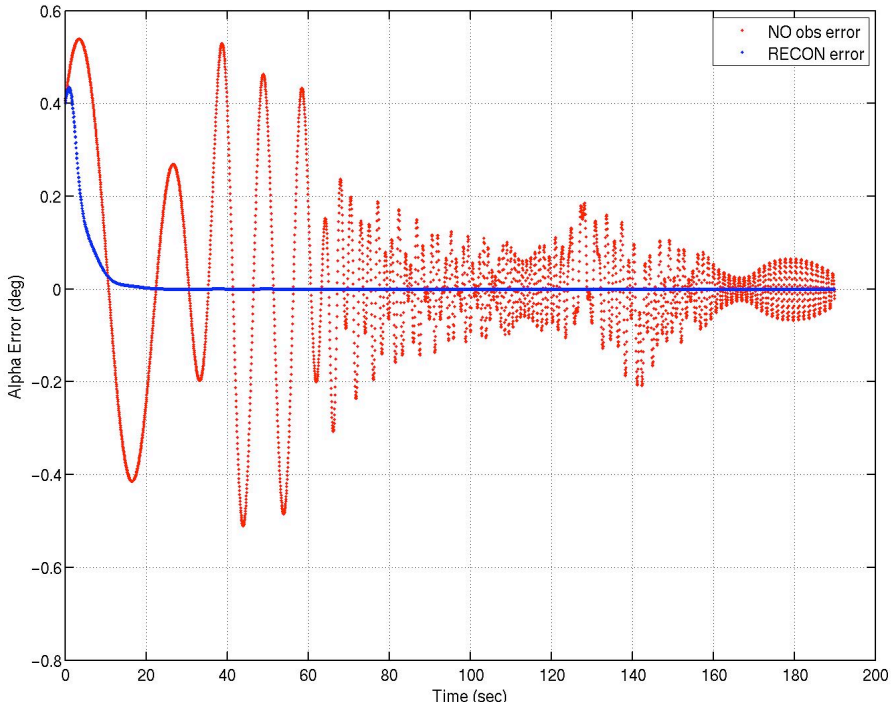

Figure 3-22. Entry Case 1 Estimated versus Propagated Angle of Attack

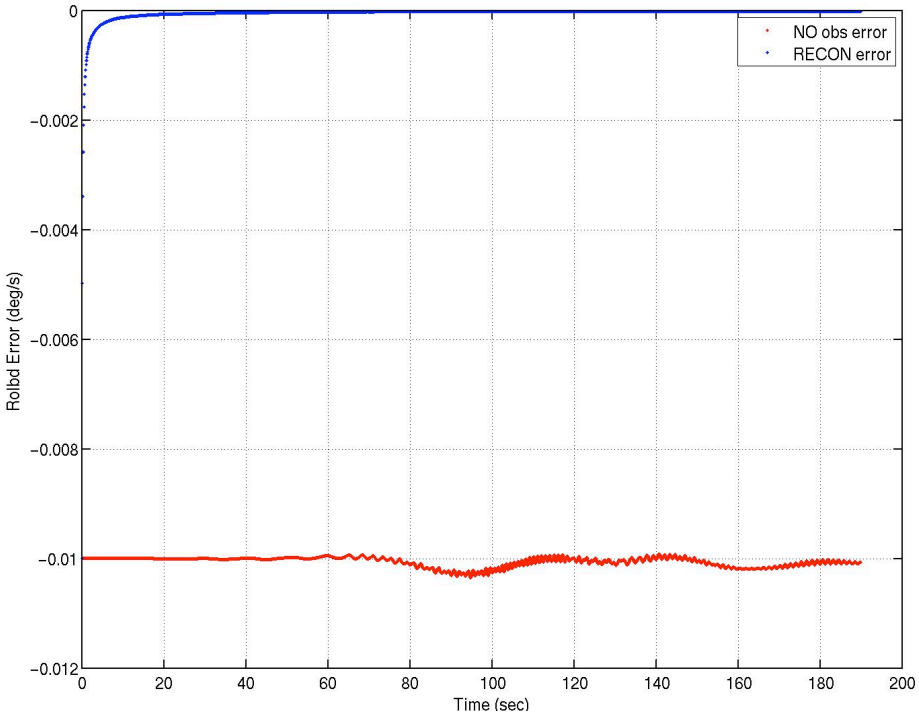

Figure 3-23. Entry Case 1 Estimated versus Propagated Angular Velocity X-component

A useful metric generated by the Kalman filter process is the expected variation in the state estimates. The standard deviation generated from the covariance matrix for Entry Test Case 3 is shown in Figs. 3-24 through 3-35. In each of these plots the state error with respect to the "truth" trajectory (as was also presented above) as well as the standard deviation (σ) determined from the covariance matrix and three times the standard deviation ($3\text{-}\sigma$) are shown. Figures 3-24 to 3-26 indicate the standard deviation of the position components, while Figs. 3-27 to 3-29 show velocity. Figures 3-30 to 3-32 indicate aerodynamic angles, and Figs. 3-33 to 3-35 show angular velocity. Generally, the standard deviation decreases with time for each of the states estimated, even the bank angle. The limited acceleration information for other than the axis aligned with the velocity vector (since angle of attack and sideslip are small) impacts the observability of the bank angle; however, the standard deviation for bank angle does definitely decrease with time. Several of the estimated states start around the $3\text{-}\sigma$ values (consistent with the inputs noted above), but all finish well within the $1\text{-}\sigma$ bound. This result provides confidence that the covariance is being propagated and updated in the reconstruction capability added to POST2.

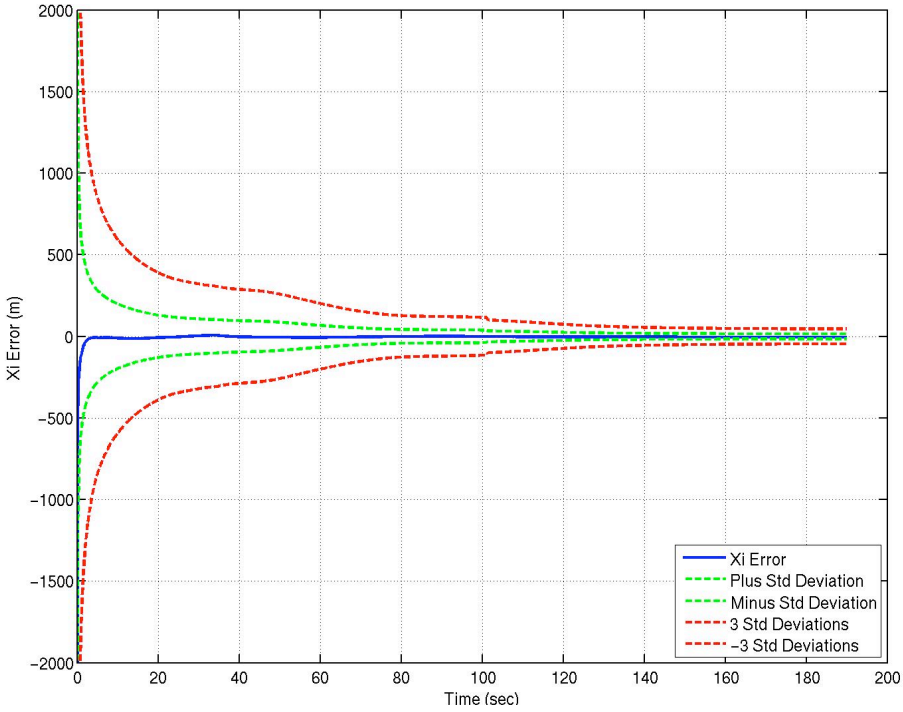

Figure 3-24. Entry Case 3 Position X-component Standard Deviation from Covariance

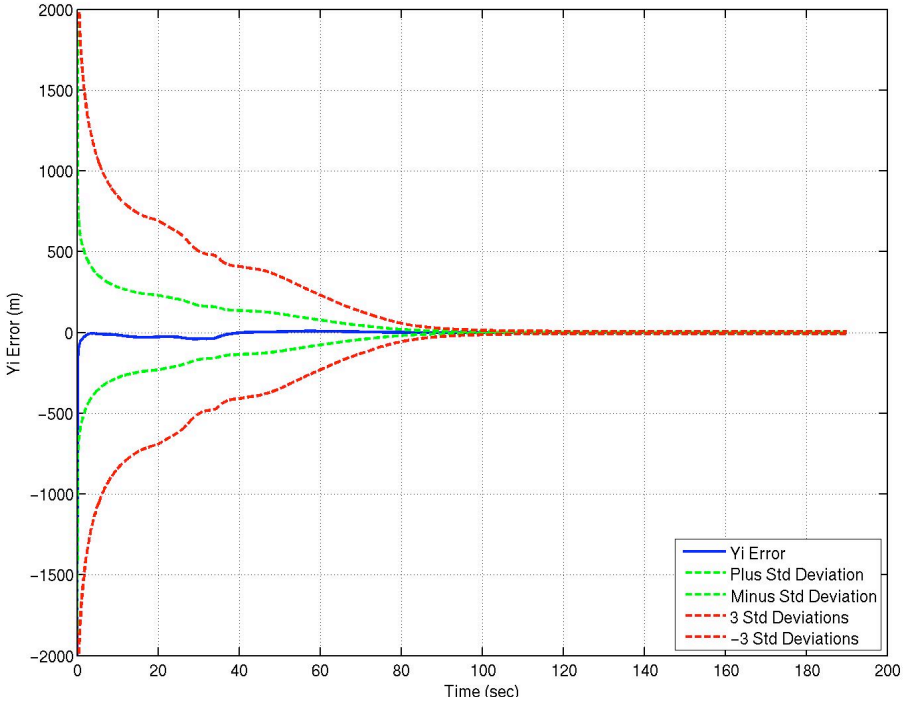

Figure 3-25. Entry Case 3 Position Y-component Standard Deviation from Covariance

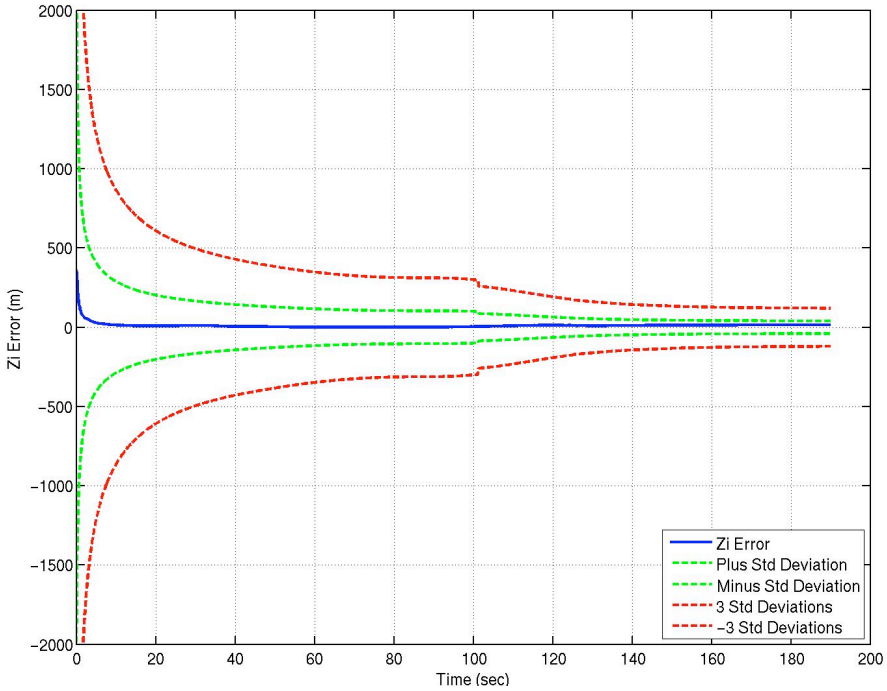

Figure 3-26. Entry Case 3 Position Z-component Standard Deviation from Covariance

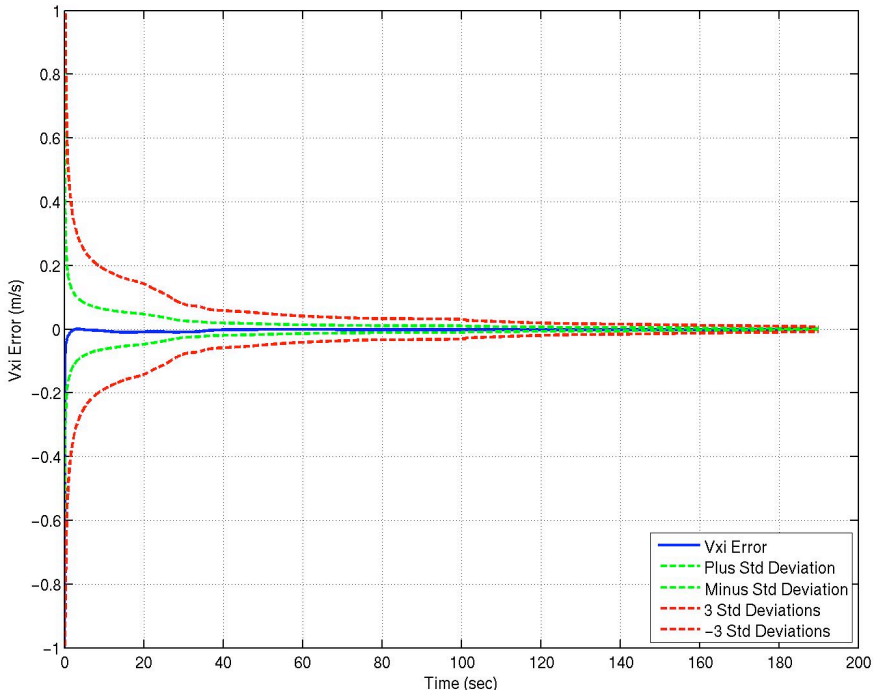

Figure 3-27. Entry Case 3 Velocity X-component Standard Deviation from Covariance

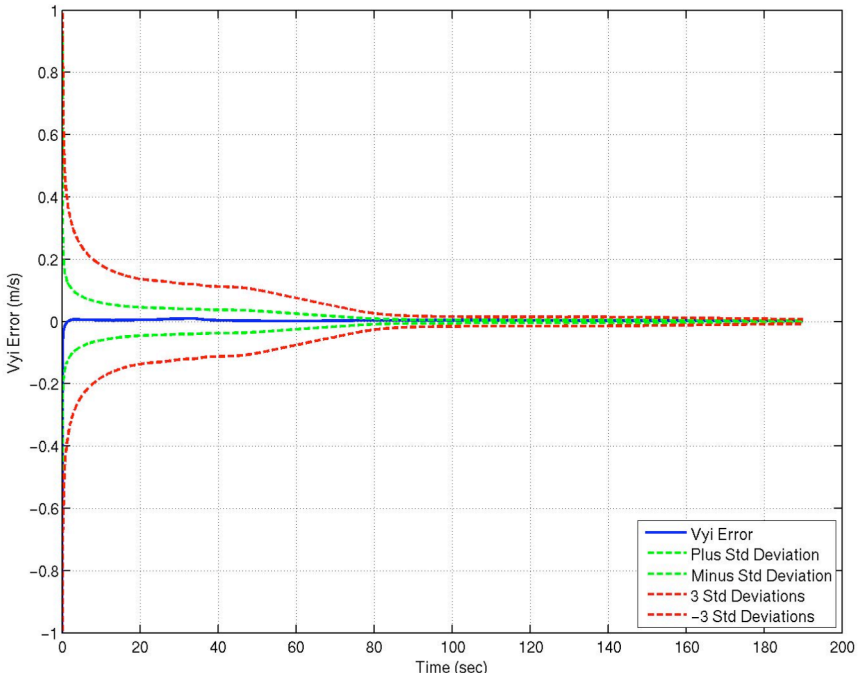

Figure 3-28. Entry Case 3 Velocity Y-component Standard Deviation from Covariance

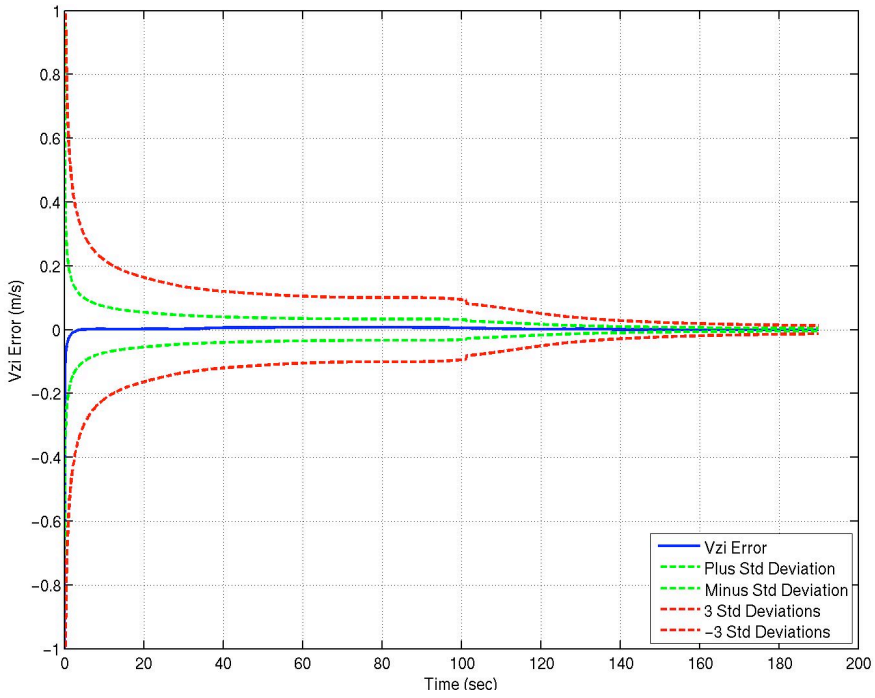

Figure 3-29. Entry Case 3 Velocity Z-component Standard Deviation from Covariance

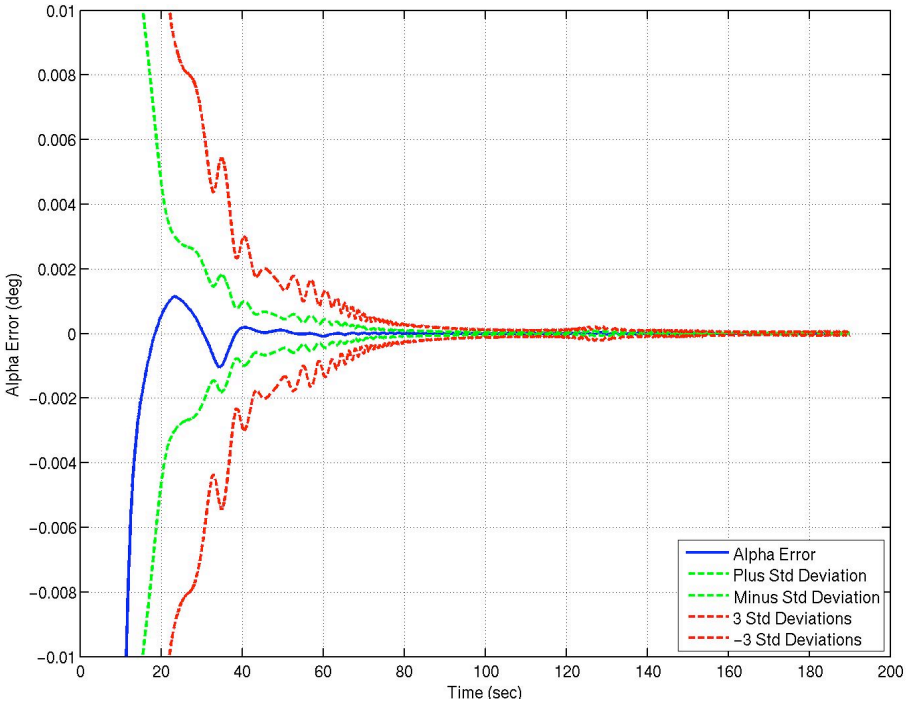

Figure 3-30. Entry Case 3 Angle of Attack Standard Deviation from Covariance

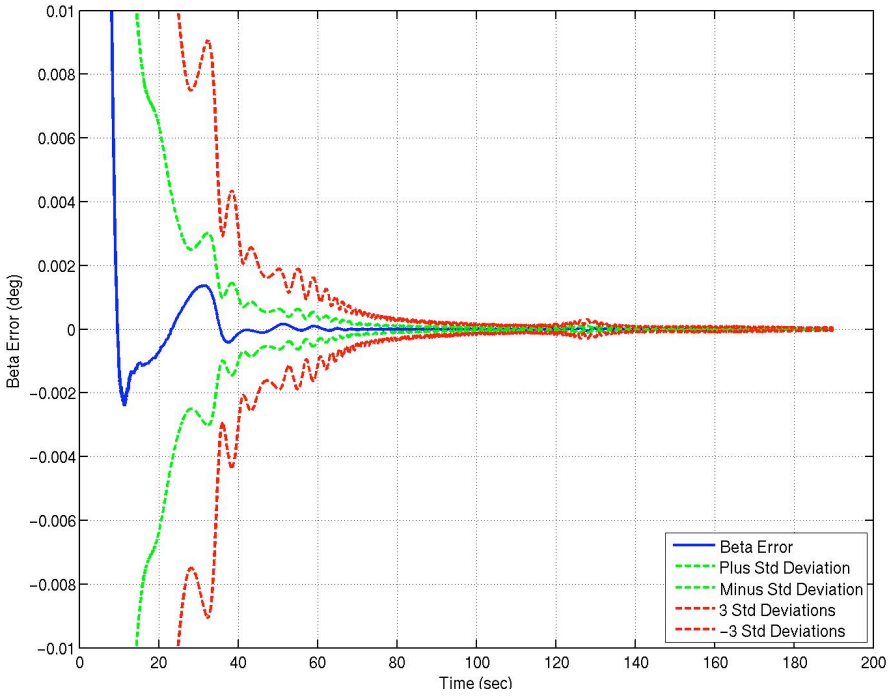

Figure 3-31. Entry Case 3 Sideslip Angle Standard Deviation from Covariance

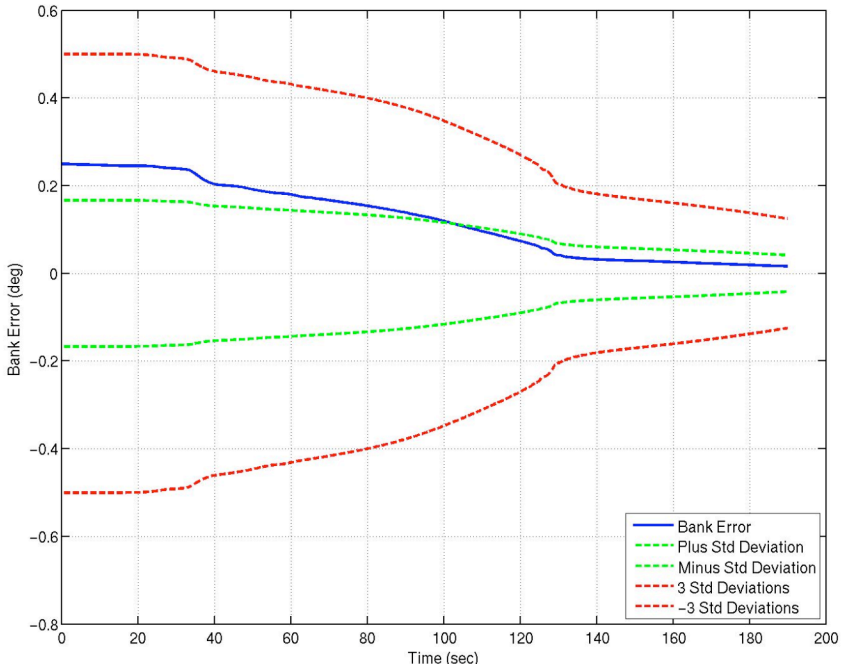

Figure 3-32. Entry Case 3 Bank Angle Standard Deviation from Covariance

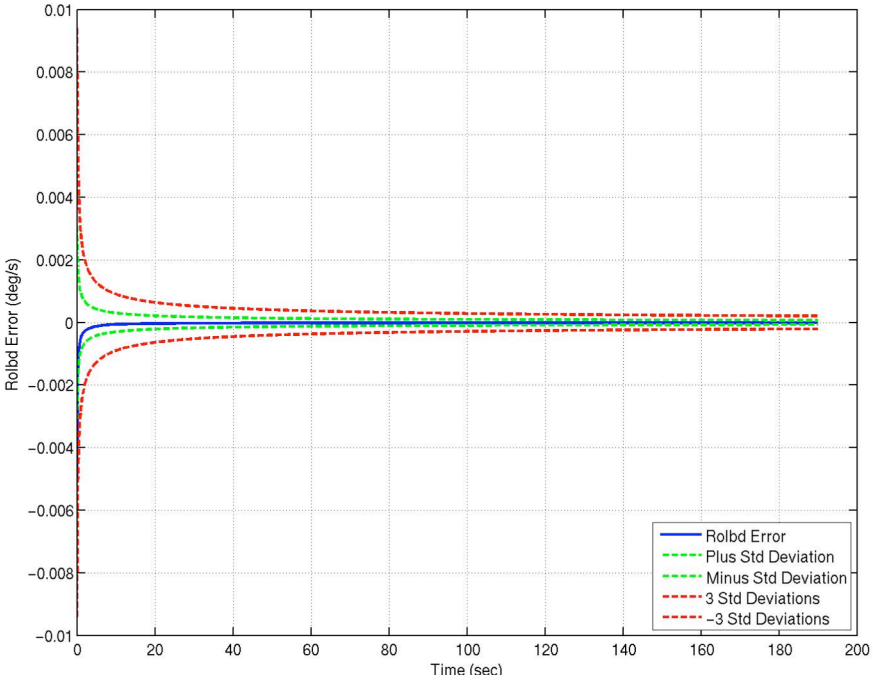

Figure 3-33. Entry Case 3 Angular Velocity X-component Standard Deviation from Covariance

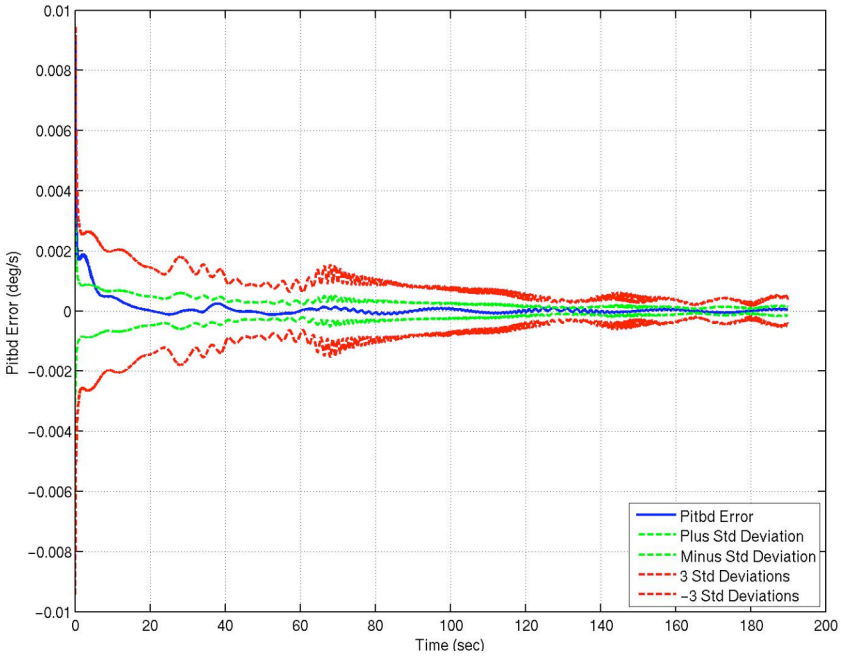

Figure 3-34. Entry Case 3 Angular Velocity Y-component Standard Deviation from Covariance

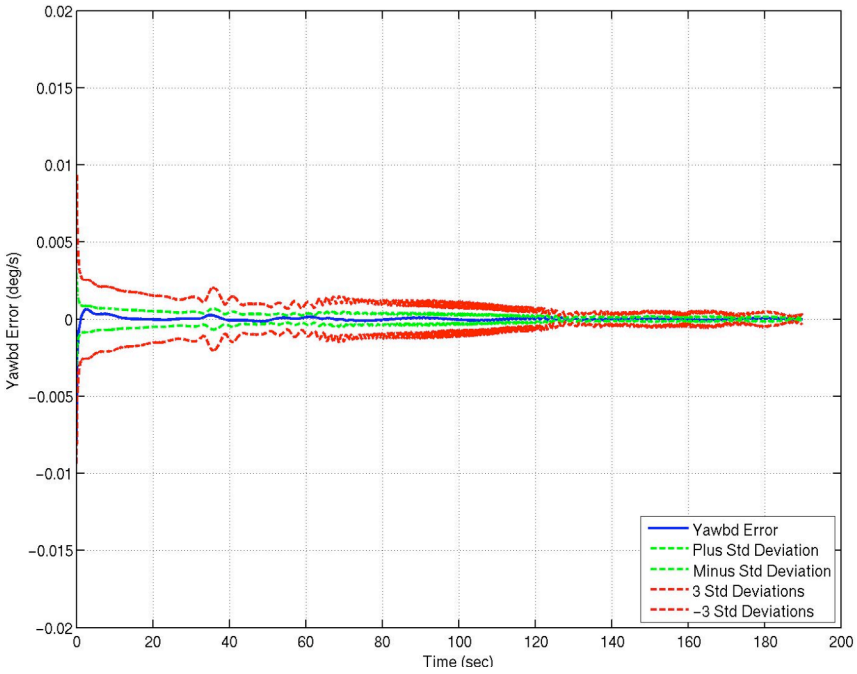

Figure 3-35. Entry Case 3 Angular Velocity Z-component Standard Deviation from Covariance

3.2.3 MER 6-DOF Entry Trajectory

This test case is similar to the previous one, but includes flight software generated quantities. While this test also uses the MER entry parameters and a simulation of a ballistic entry using POST2, the observations for this case were generated using the software included in the mission specific version of POST2 that supported the MER entry, descent, and landing. [13] Calculations of onboard quantities to be used for trajectory reconstruction were included in the POST2 version used to generate the test case.

A nominal entry trajectory was simulated using a POST2 executable with MER specific modules included. The observation set included the sensed acceleration in three body axes and the quaternion calculated using the accelerometer and gyroscope package included on the back shell. The observations were taken at a frequency of 8 Hz, or 0.125 sec intervals, which is the frequency that the actual mission data was generated. The parameters to be estimated were the same as those in the ballistic entry test case above: inertial position vector, inertial velocity vector, attitude using aerodynamic angles, and body angular velocity vector.

The position and velocity at simulation start were generated from an actual MER initial state covariance. Three-sigma error values of 0.5 deg and 0.01 deg/s per axis were assumed for the initial attitude and attitude rate, respectively. These initial state uncertainty values are compiled in Table 3-6. The initial values selected for the three test cases are shown in Table 3-7.

Table 3-6. MER-type Entry Test Case Reconstruction States and Initial Value Uncertainties

State	POST2 Variable Name	1-σ Uncertainty	3-σ
Inertial Position X Coordinate, m	XI	174.5	524
Inertial Position Y Coordinate, m	YI	39.6	119
Inertial Position Z Coordinate, m	ZI	210.9	633
Inertial Velocity X Coordinate, m/s	VXI	0.10	0.30
Inertial Velocity Y Coordinate, m/s	VYI	0.025	0.075
Inertial Velocity Z Coordinate, m/s	VZI	0.18	0.54
Angle of Attack, deg	ALPHA	0.1667	0.5
Sideslip Angle, deg	BETA	0.1667	0.5
Bank Angle, deg	BNKANG	0.1667	0.5
Angular Velocity Body X, deg/s	ROLBD	0.0033	0.01
Angular Velocity Body Y, deg/s	PITBD	0.0033	0.01
Angular Velocity Body Z, deg/s	YAWBD	0.0033	0.01

Table 3-7. MER-type Entry Test Case Initial Values

POST2 Variable Name	Truth Case	Test Case 1	Test Case 2	Test Case 3
XI (m)	-3333417.7	-3333672.1	-3333431.0	-3333479.0
YI (m)	-1343510.2	-1343492.7	-1343517.1	-1343489.4
ZI (m)	-202236.8	-201973.4	-202231.5	-202238.4
VXI (m/s)	3361.65	3361.50	3361.64	3361.60
VYI (m/s)	-4527.64	-4527.61	-4527.64	-4527.64
VZI (m/s)	386.75	386.52	386.74	386.74
ALPHA (deg)	-0.12	-0.25	-0.33	-0.33
BETA (deg)	-1.80	-1.45	-2.00	-1.29
BNKANG (deg)	89.8	89.4	90.1	90.3
ROLBD (deg/s)	12.0	11.99	12.005	12.0085
PITBD (deg/s)	0.0	0.012	0.0075	-0.0075
YAWBD (deg/s)	0.0	0.008	0.0038	-0.0058

For the actual reconstruction, an evaluation of the observation residual was used to determine if the POST2 module was generating an acceptable reconstruction of the trajectory. In order to determine how well the reconstruction was working, comparison was made with the case of no reconstruction. Figures 3-36 and 3-37 show the acceleration and quaternion observation residuals, respectively, for Test Case 1 without activating the reconstruction mode of POST2. The initial reconstruction run used the same weight for each observation just as was done in the previous test (see Section 3.2.2). Recall that the flight code generated quaternion measurements were used to generate the residual, whereas aerodynamic angles are used for the attitude estimate. The Kalman gain as defined above will not be optimal when using quaternion measurements, however reasonable estimates can still be obtained in this problem. Since the quaternion is a four number representation of the attitude (three independent quantities plus a constraint), caution must be taken if the quaternion is part of the estimated state (which is not the case in this test).

The residuals for this run are shown in Figs. 3-38 and 3-39 (note that the scale changed for these plots). First analysis does indeed indicate a reduction in acceleration residual, but the quaternion residual at the start of reconstruction (around 60 sec) appears about the same as the no reconstruction case. Also note from Fig. 3-39, the quaternion residuals are smaller than the no reconstruction case once the vehicle begins to appreciably decelerate. This result indicates that the acceleration observation affects the attitude estimate, thus the quaternion observation weighting was set equal to the acceleration weight when vehicle deceleration begins (around 130 sec). The weight on the attitude rate measurements in the observation weighting file was set for higher importance early in the trajectory and reduced to equal the acceleration weighting when the deceleration becomes appreciable. The impact on residuals for this observation

weight approach is shown in Figs. 3-40 and 3-41. Both observation residuals are reduced significantly at the start of reconstruction and remain small throughout. Thus, increasing the weight on the initial quaternion observations rectified the situation noted above.

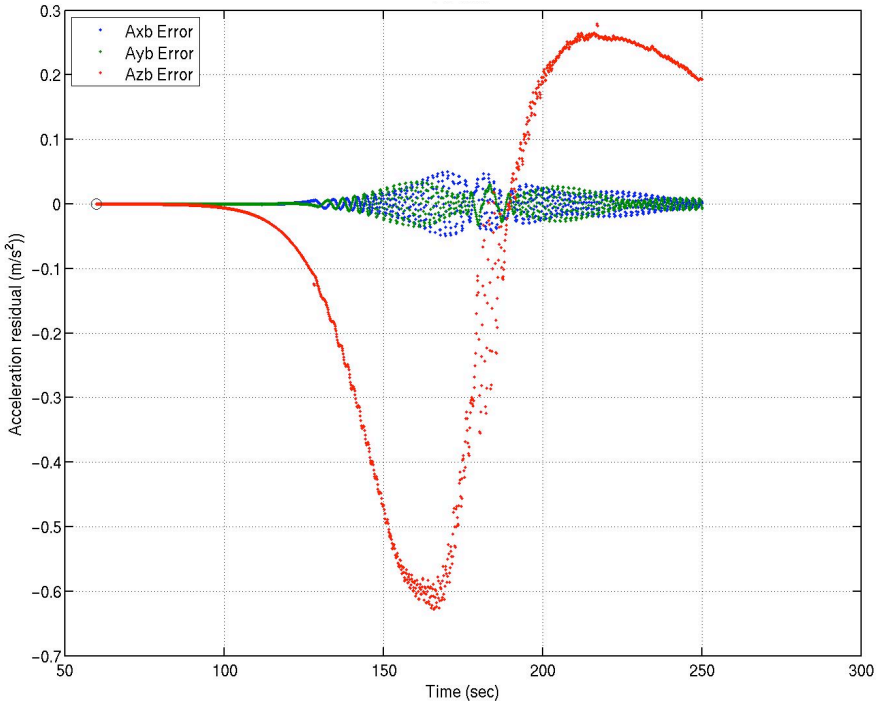

Figure 3-36. MER Case 1 Acceleration Residual – No Observations

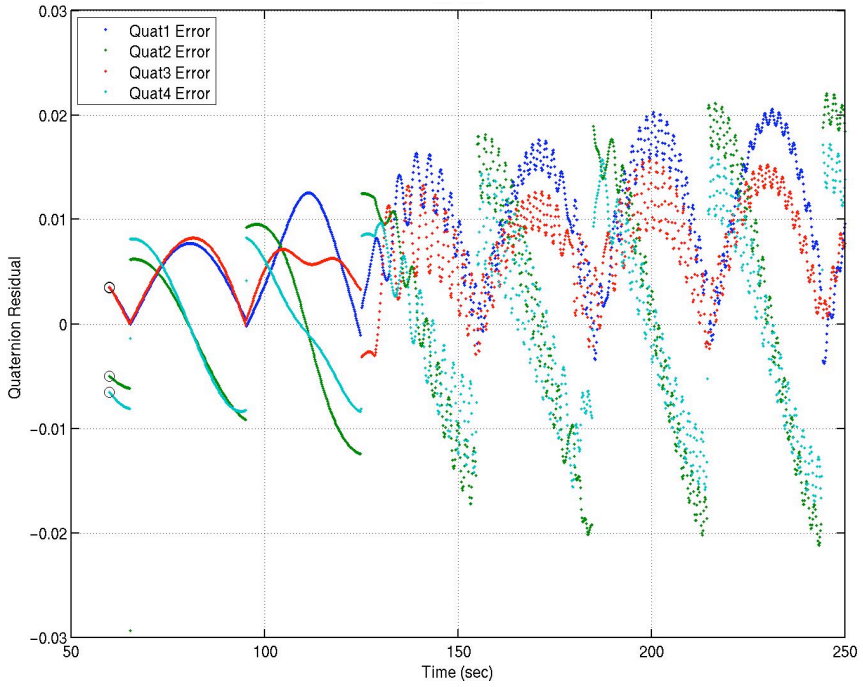

Figure 3-37. MER Case 1 Quaternion Residual – No Observations

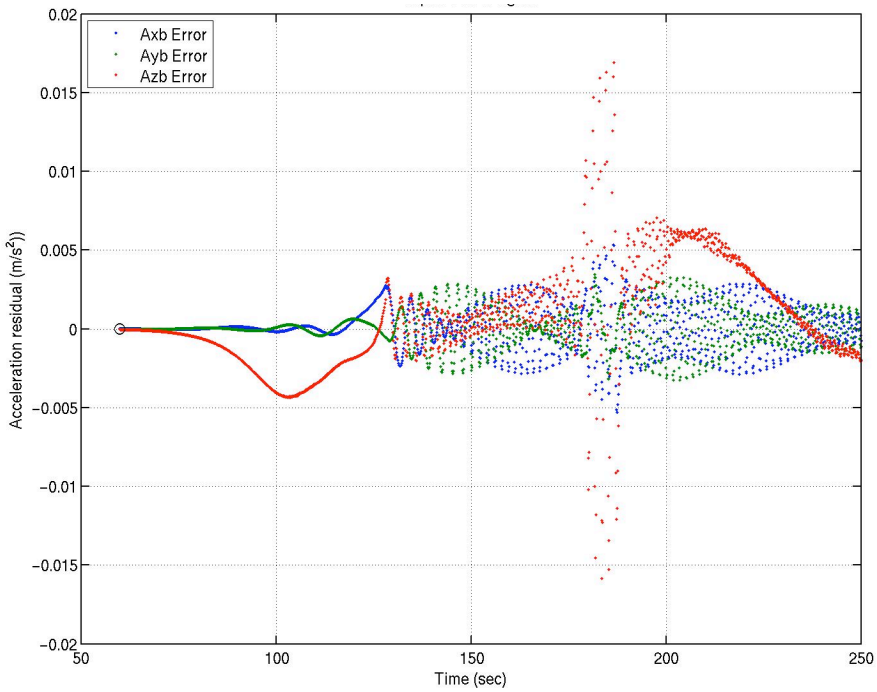

Figure 3-38. MER Case 1 Acceleration Residual – Equal Obs Weights

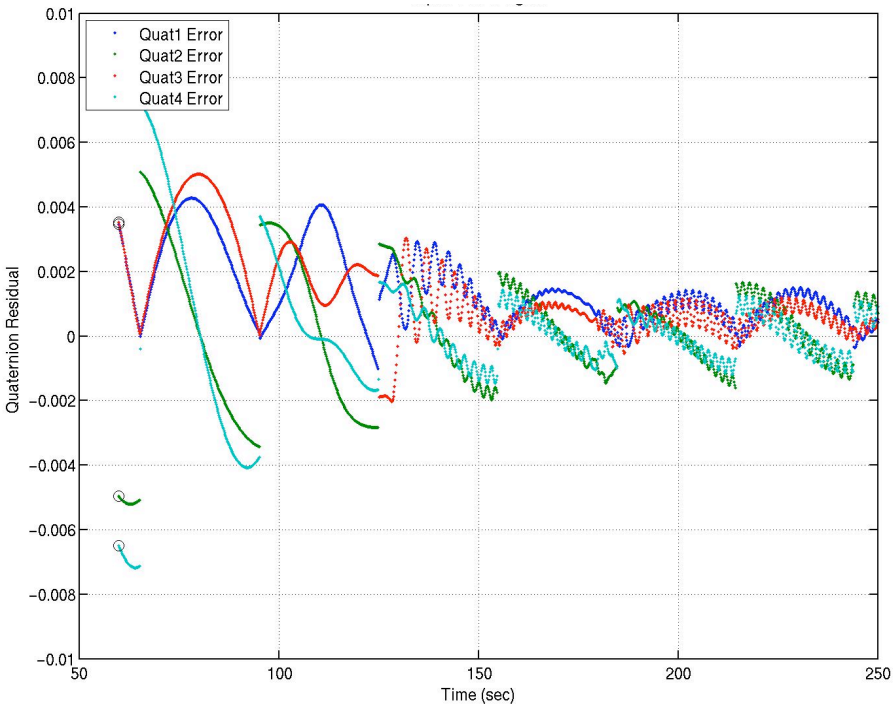

Figure 3-39. MER Case 1 Quaternion Residual – Equal Obs Weights

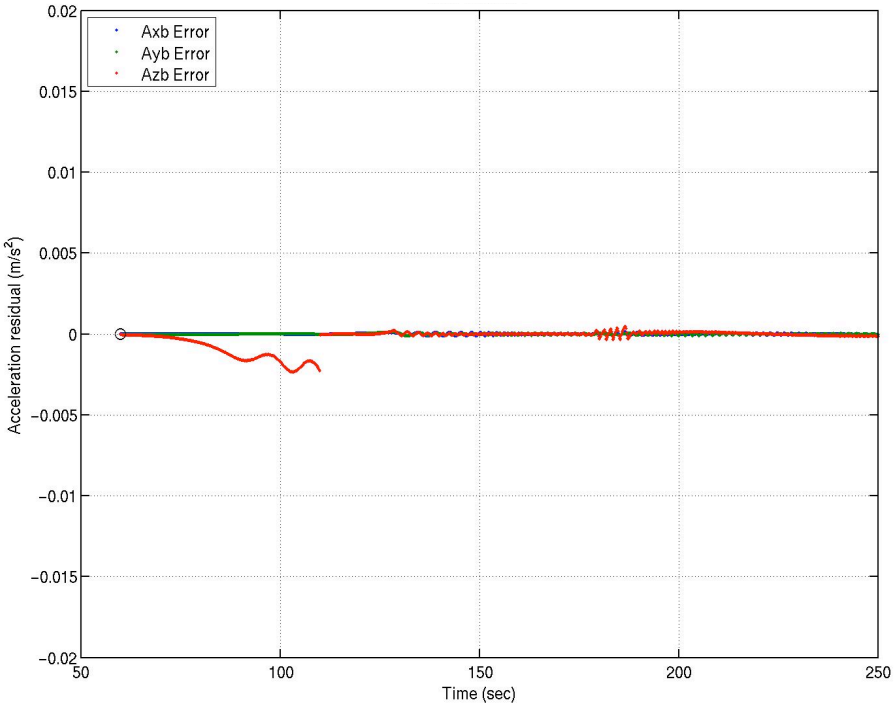

Figure 3-40. MER Case 1 Acceleration Residual – Higher Quaternion Weights Early

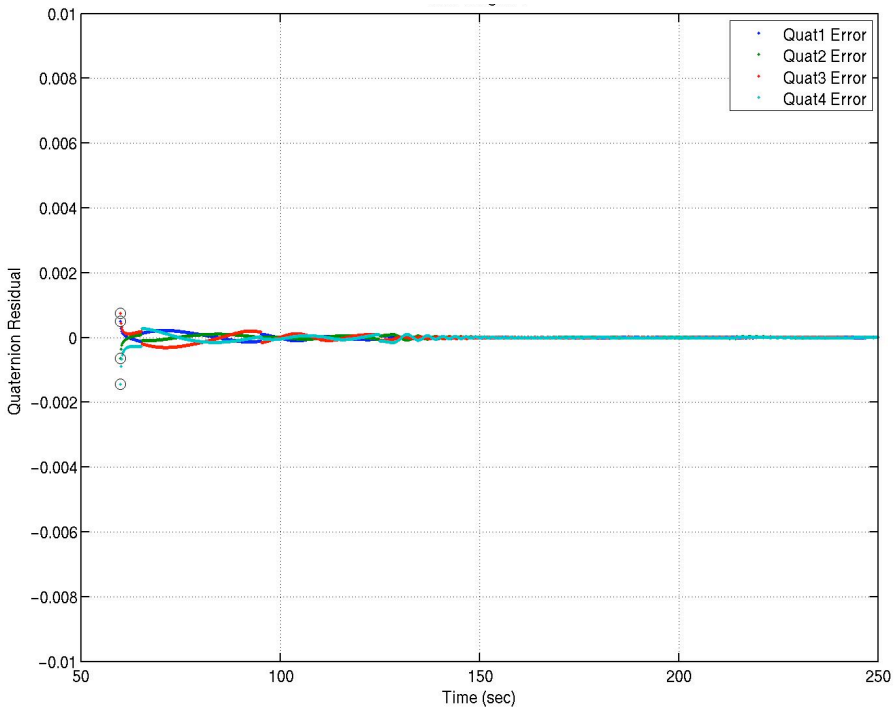

Figure 3-41. MER Case 1 Quaternion Residual – Higher Quaternion Weights Early

The situation where the quaternion observation was not being used is more clearly shown in Figs. 3-42 and 3-43. The initial angle of attack error (difference between the "truth" and the reconstructed trajectories) plotted in Fig. 3-42 is nearly the same for the equal observation weight and no reconstruction cases indicating that the EKF had little effect on vehicle attitude before the deceleration starts. Figure 3-43 indicates the same conclusion for the sideslip angle error. However, these figures show a definite impact when the weight on the quaternion observation is increased in the initial reconstruction, between 60 and 110 sec (note that the dark blue and green dots lie on top of each other during this early phase). However, there is an issue with this case.

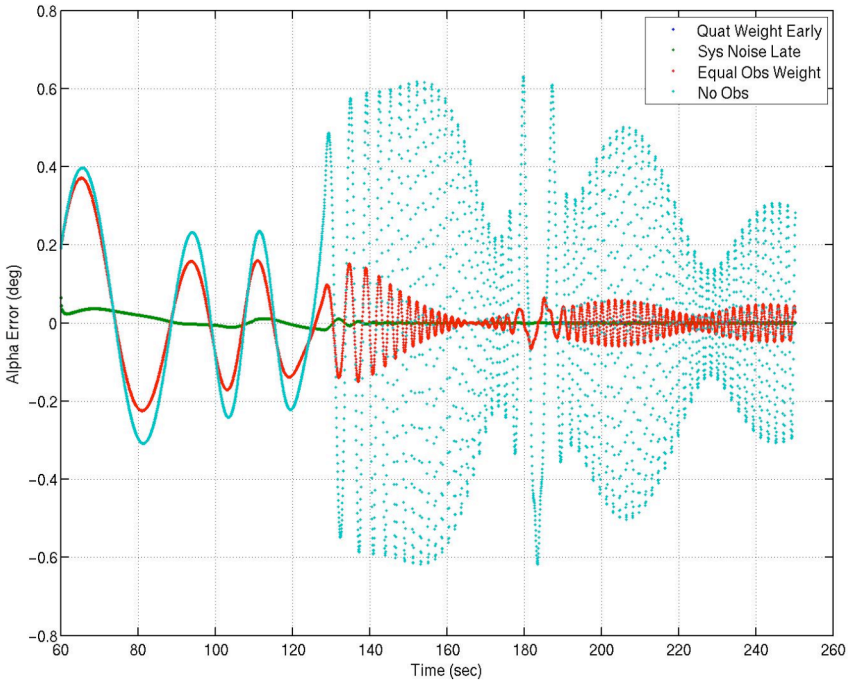

Figure 3-42. MER Case 1 Angle of Attack Error Comparison

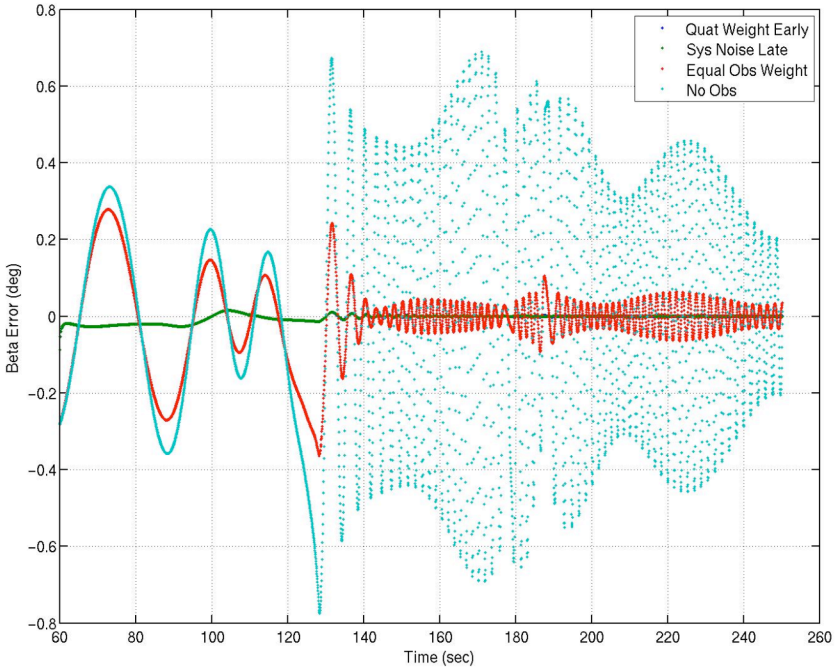

Figure 3-43. MER Case 1 Sideslip Angle Error Comparison

Comparisons for the test cases with increased quaternion observation weights against the "truth" trajectory are shown in Figs. 3-44 to 3-47. The results shown for position errors (Fig. 3-44), velocity errors (Fig. 3-45), and aerodynamic angle errors (Fig. 3-46) look acceptable for this case. However, the angular velocity errors (Fig. 3-47) while initially damped, return to about the same order as the starting error. The effect starts after the observation weights are equated again (when the vehicle starts to decelerate). Since this MER simulation includes more complex models, the reconstruction simulation does not exactly model the system, especially when the aerodynamics begins to affect the vehicle motion. Thus, adding system noise to the EKF can help alleviate this issue. System noise input values tend to slow the estimation process thus preventing the filter from achieving smugness in the trajectory reconstruction run; filter smugness causes the estimator to ignore additional observations since the covariance elements become small. Since this issue does not arise until around 130 sec, the system noise inputs were added at that point (if system noise was included earlier, the rapid error reduction seen before 130 sec would not be as fast). The impact of including the system noise inputs is shown in the angular velocity error plot (Fig. 3-48). This error is reduced to near zero by around 160 sec.

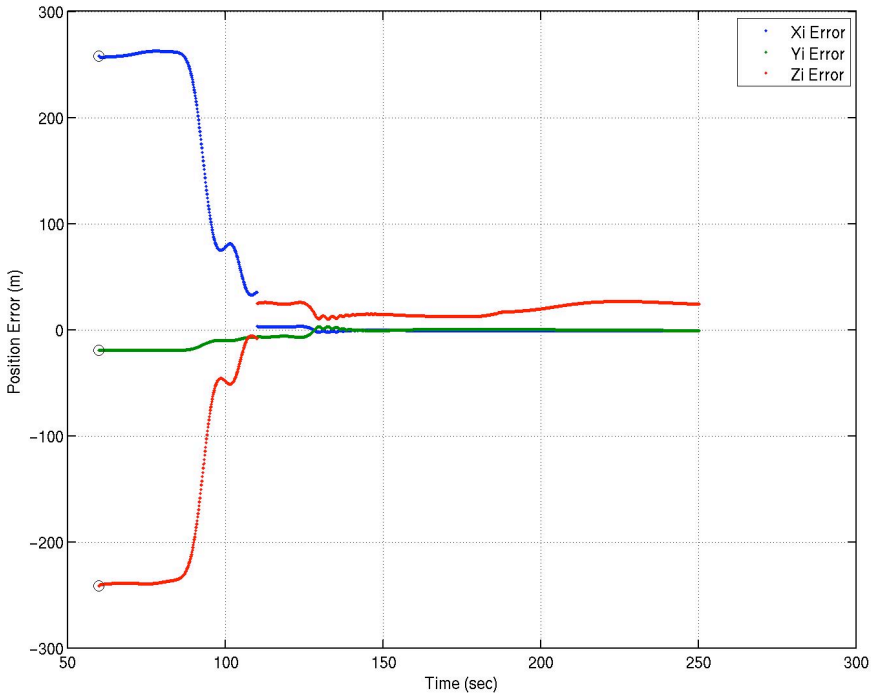

Figure 3-44. MER Case 1 Position Component Error – Higher Quaternion Weights

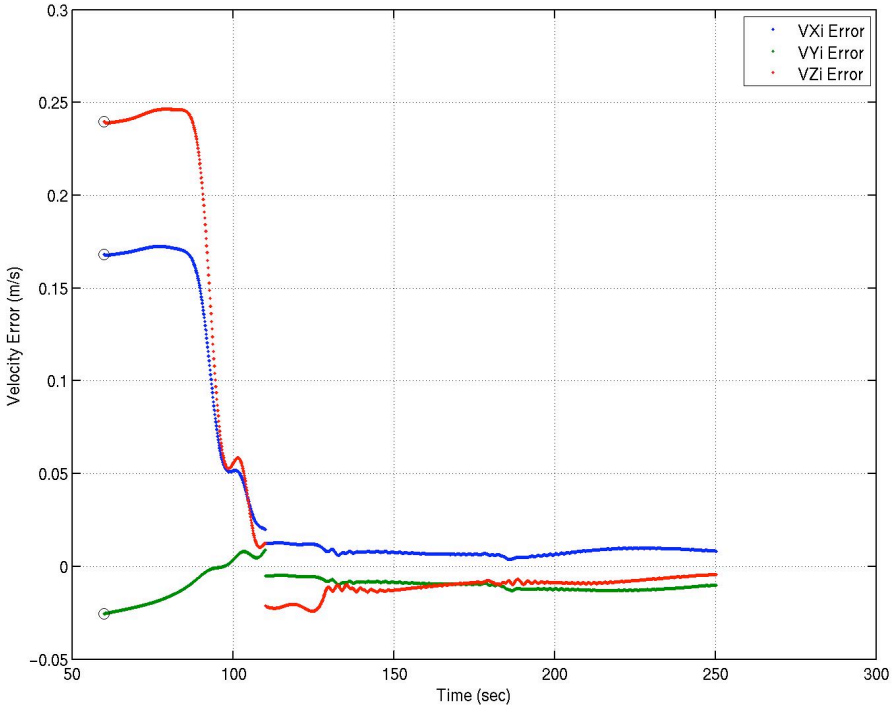

Figure 3-45. MER Case 1 Velocity Component Error– Higher Quaternion Weights

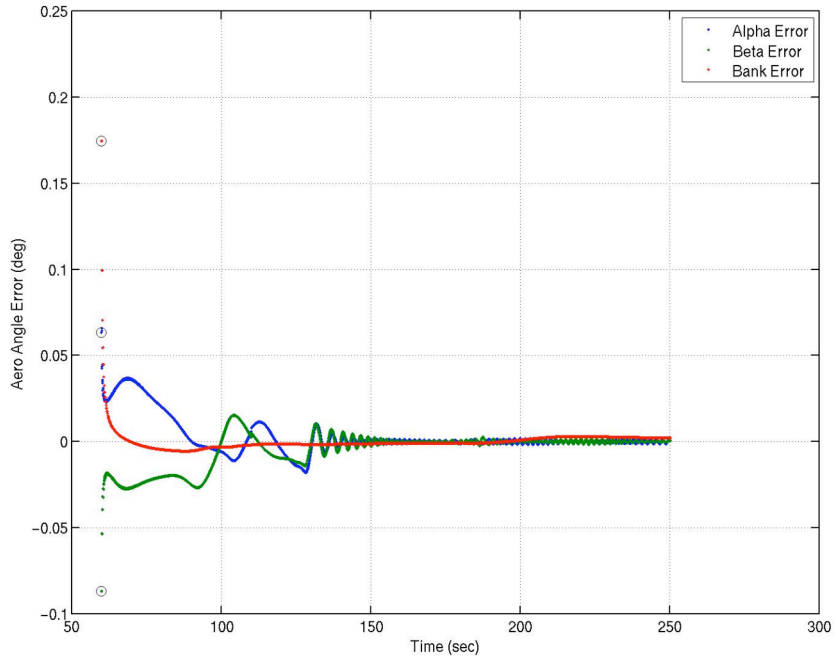

Figure 3-46. MER Case 1 Aerodynamic Angle Error– Higher Quaternion Weights

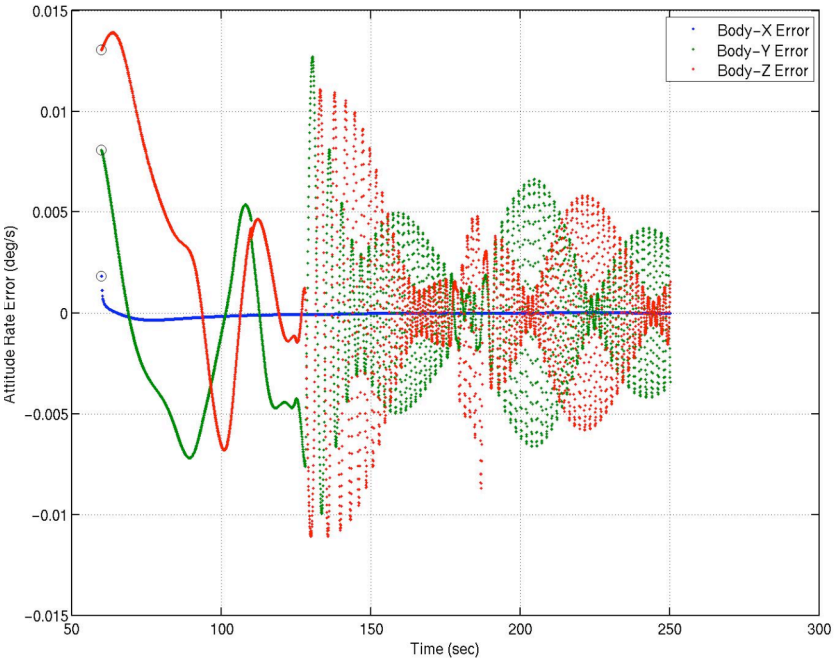

Figure 3-47. MER Case 1 Angular Velocity Component Error– Higher Quaternion Weights

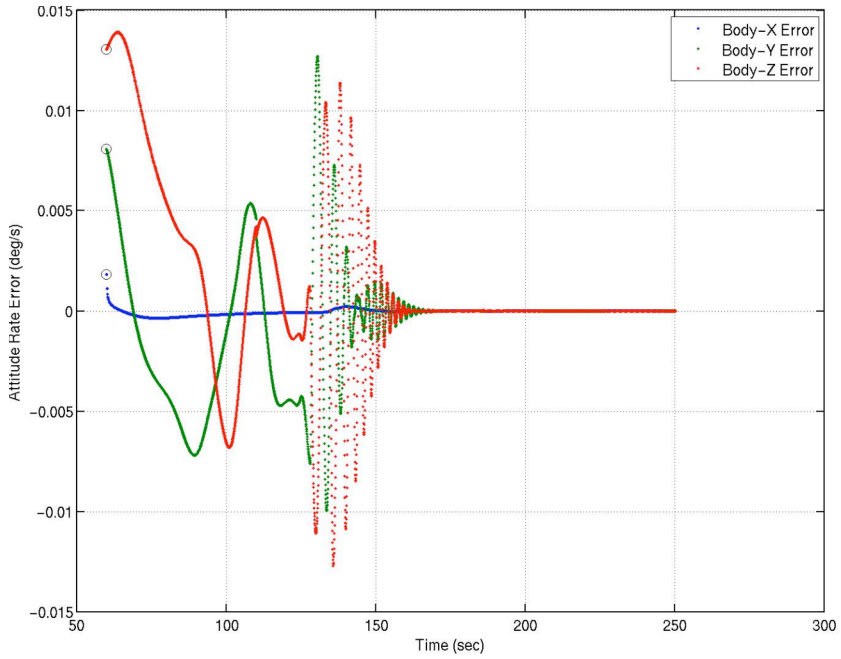

Figure 3-48. MER Case 1 Angular Velocity Component Error –System Noise Late

Figures 3-49 and 3-50 show that the acceleration and quaternion observation residuals are not changed noticeably compared with the case without system noise. However, the velocity error (Fig. 3-51) indicates one impact of using the system noise. That is, some errors will initially increase due to increased covariance values when system noise inputs are made to the filter.

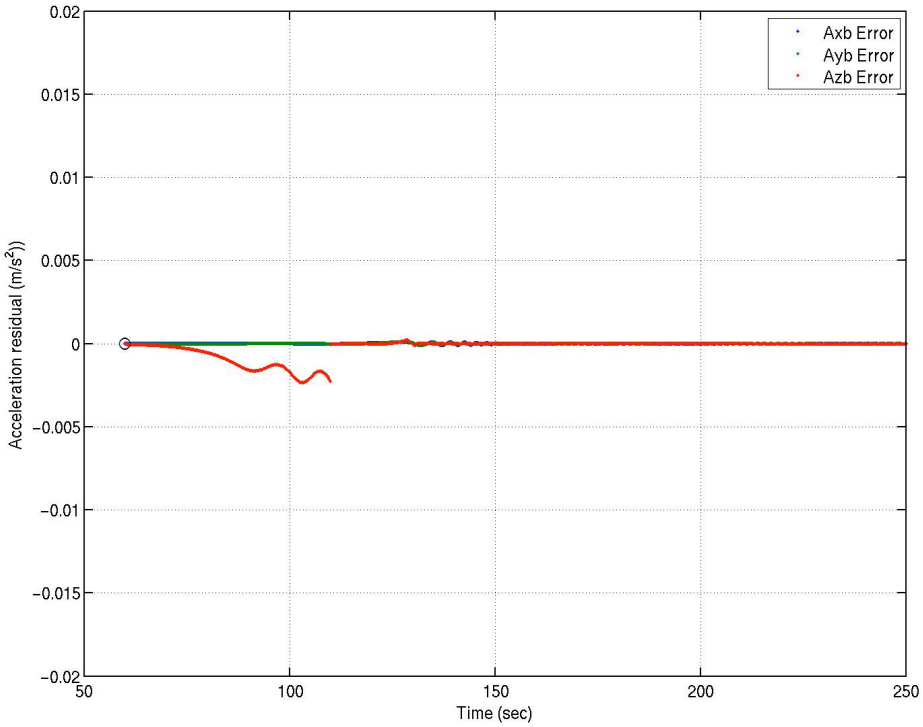

Figure 3-49. MER Case 1 Acceleration Residual – With System Noise

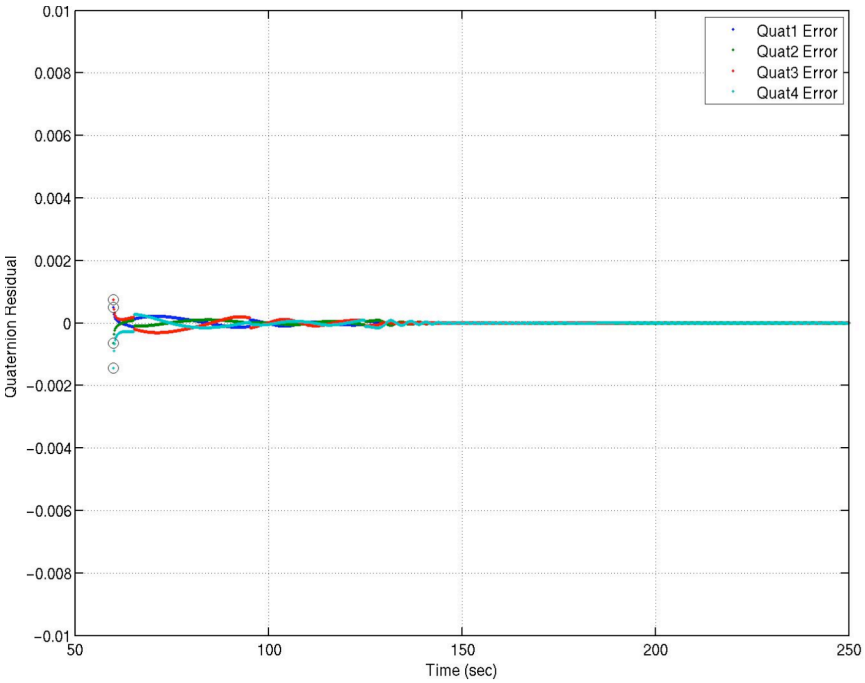

Figure 3-50. MER Case 1 Quaternion Residual – With System Noise

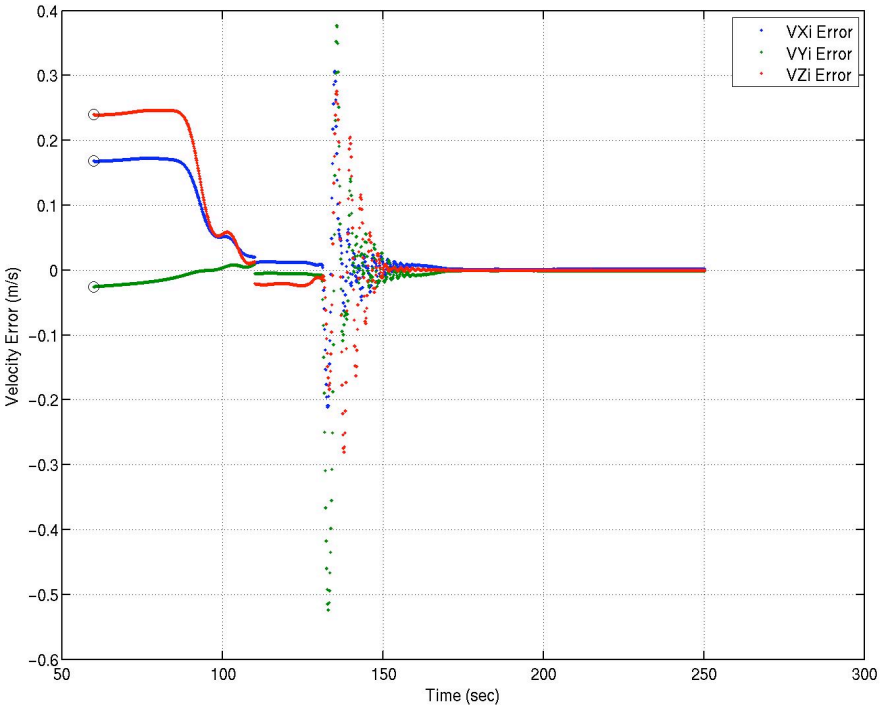

Figure 3-51. MER Case 1 Velocity Component Error –With System Noise

The effect of adding system noise at 130 sec on the covariance can be seen in Figs. 3-52 through 3-55. Each of these plots show the state error (when compared to the "truth" trajectory) and standard deviation determined from the covariance. Either the standard deviation is increased or it does not decrease at the same rate as was previously noted after 130 sec. Even though the covariance values increased, the state errors stay small or decrease.

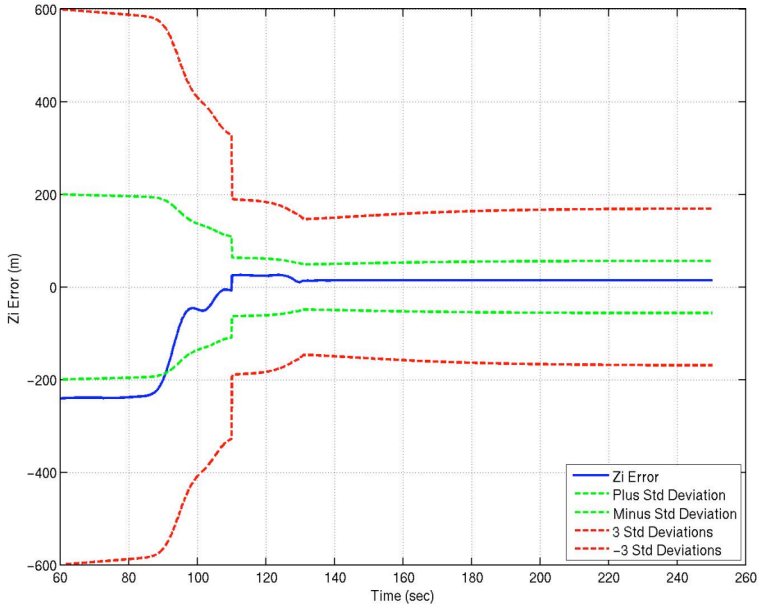

Figure 3-52. MER Case 1 Position Z-component Standard Deviation from Covariance-With System Noise

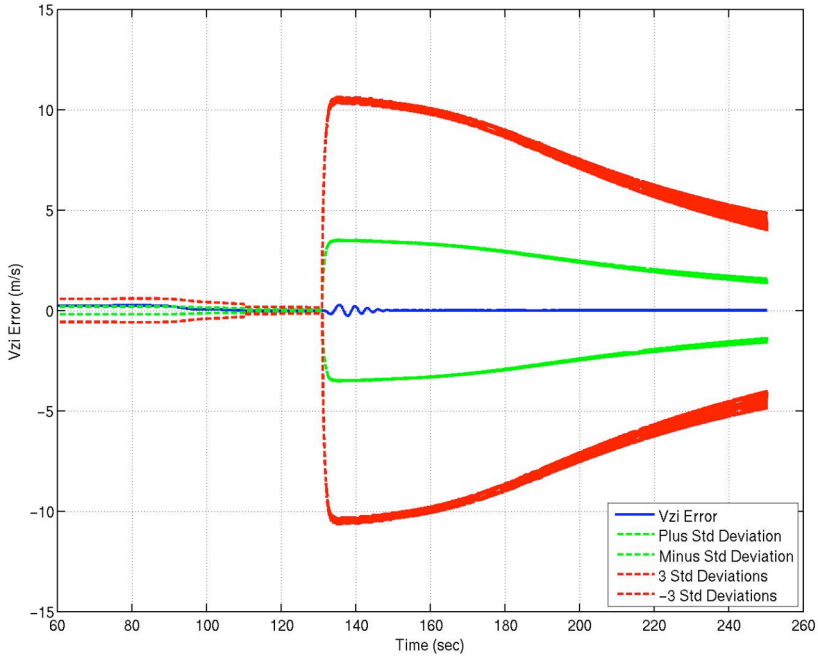

Figure 3-53. MER Case 1 Velocity Z-component Standard Deviation from Covariance – With System Noise

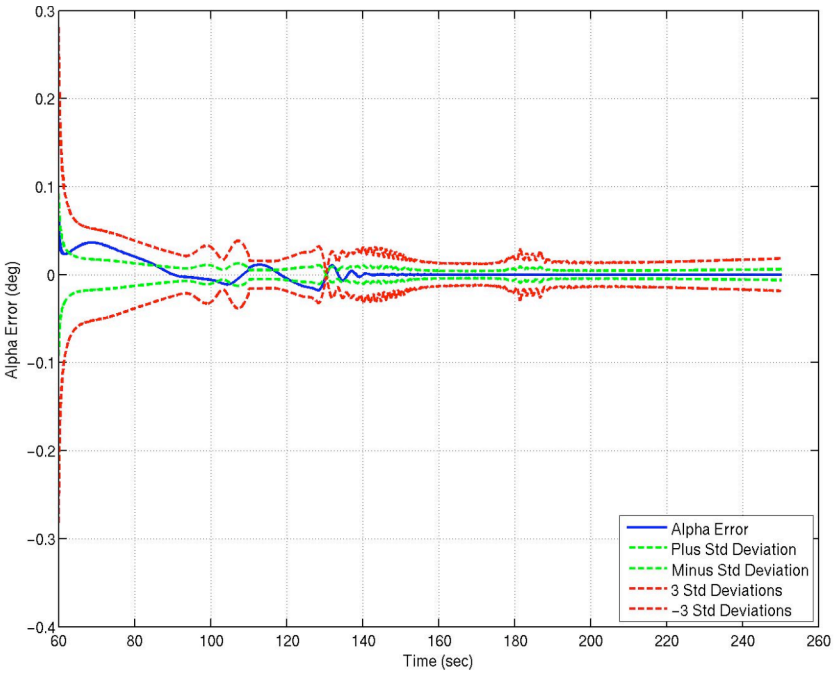

Figure 3-54. MER Case 1 Angle of Attack Standard Deviation from Covariance–With System Noise

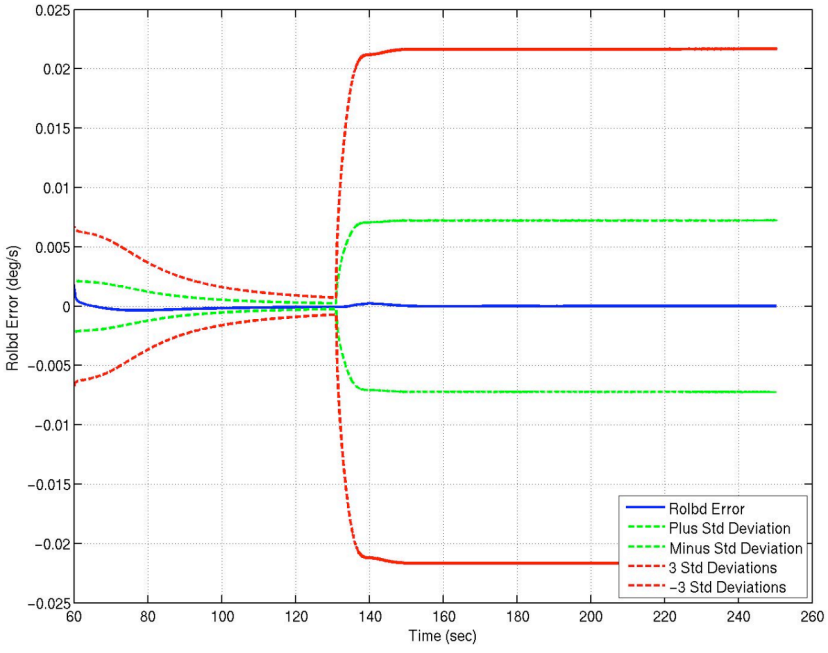

Figure 3-55. MER Case 1 Angular Velocity X-component Standard Deviation from Covariance – With System Noise

These test cases provide confidence that several key features of the EKF reconstruction module in POST2 are functioning well. The observation weight inputs are read in correctly and are applied appropriately. The system noise inputs are also working as expected. Also, this test case shows that the POST2 simulation using MER specific models appears able to handle the MER specific reconstruction.

Chapter 4: Huygens Trajectory Reconstruction Approach and Data

4.1 Huygens Trajectory Reconstruction Background

NASA's trajectory reconstruction of the Huygens entry probe at Titan was accomplished using two independent approaches.[39] One was a traditional approach to trajectory reconstruction that integrates the accelerometer measurements directly during the entry phase (forward) and integrates the hydrostatic equation using the temperature and pressure measurements to determine altitude and velocity (backwards). The other approach used a Kalman filter module developed for reconstruction in conjunction with the POST2-based simulation. The POST2-based reconstruction uses accelerometer measurements to adjust an estimated state using a POST2-based simulation developed prior to entry to support EDL analyses and design. The latter approach is the focus of the current research, and thus the results from the POST2-based reconstruction are discussed in this report.

In the current research, the main emphasis of the Huygens probe reconstruction was to evaluate the simulation models used prior to entry at Titan with actual flight data. Another objective of the Huygens reconstruction was to compare the NASA derived trajectory and the Huygens DTWG solution to the trajectory profile. This second objective became more important as several datasets appeared not to be in agreement with other direct measurements taken during the probe's descent. Several issues were raised with the ESA science teams and DTWG resulting from this analysis; the findings of this assessment were provided to these two teams as well as the NASA NESC.

4.1.1 POST2 Use Supporting Huygens Probe EDL

POST2 [22] was used to simulate the Huygens entry, descent, and landing trajectory into Titan to support analyses as part of a NESC ITA.[16] A six degree-of-freedom atmospheric entry and three degree-of-freedom parachute descent trajectory of the Huygens probe was simulated. The POST2-based flight simulation incorporated several models specific to the Huygens probe entry: a 6-DOF aerodynamics model; Titan's gravity and Titan-GRAM atmosphere (including wind) models; attitude inputs and initial states; trigger criteria, inflation, and drag models for the pilot, main, and drogue parachutes; as well as vehicle geometric parameters. This simulation was used to produce trajectory data and was an integral element of the Monte Carlo analyses discussed below.

Version 1.0 of the Titan-GRAM atmospheric model[40] was implemented into POST2. This model was updated from Cassini measurements of Titan. In POST2, the Titan-GRAM atmosphere model was initialized at the atmospheric interface event (altitude of 1270 km above the reference surface of 2575 km radius).

The primary and backup trigger for the pilot parachute deployment was based on acceleration logic provided by ESA and was incorporated into the POST2 simulation. Parachute inflation models developed by NASA were introduced into the simulation. The sequence for the pilot parachute modeled in POST2 started with acceleration logic for deployment initiation, mortar fire, inflation model, and fully inflated flight. The main and stabilizer drogue parachutes had similar sequences; the primary difference being that the main and drogue parachutes were triggered on time, while the pilot parachute trigger was based on acceleration.

NASA developed the Huygens probe 6-DOF aerodynamic database based on Genesis data and Huygens probe-shape ballistic range data. [16] The database was then

incorporated into an aerodynamics subroutine and used in the 6DOF-3DOF trajectory simulation. ESA-generated aerodynamics data was also introduced as a separate subroutine used in the pre-entry simulation, but was not evaluated in this reconstruction analysis.

This POST2-based simulation was used in a Monte Carlo analysis of the Huygens probe entry, descent, and landing on Titan.[16] The Monte Carlo technique involves the variation of key input parameters to encompass the level of uncertainty in these inputs. That is, once the range of uncertainty in the inputs was established, random numbers were used to determine the specific input value selected for a given simulation run. Several thousand runs (normally around 10000 for each analysis run) were made in this fashion and statistics of the resulting outputs were analyzed. The Monte Carlo dispersed inputs are assumed to have a certain distribution (e.g., Gaussian, Uniform, etc.) with a given mean and extreme values. Discipline experts were consulted to define ranges for the various input variables. Other inputs were taken from previously defined ranges. For example, the dispersions of the mass properties were developed from previous NASA missions, such as Genesis and MER. Table 4-1 shows the inputs and dispersion ranges for the entry phase used in the Monte Carlo assessments.

Table 4-1. Huygens Titan Probe 6DOF Entry Dispersions

Quantity	Nominal Value	Distribution Type	3-σ or min/max
Mission Uncertainty			
Initial Roll Angle, deg	80.36	Gaussian	2.7
Initial Pitch Angle, deg	18.42	Gaussian	2.7
Initial Yaw Angle, deg	7.46	Gaussian	2.7
Initial Roll Rate, deg/sec	43.725	Gaussian	10%
Initial Pitch Rate, deg/sec	0.0	Gaussian	0.4
Initial Yaw Rate, deg/sec	0.0	Gaussian	0.4
Aerodynamic Uncertainty			
Probe Axial Force Coeff Mult. ($K_n \geq 0.1$)	1.0	Gaussian	5 %
Probe Normal Force Coeff Incr ($K_n \geq 0.1$)	0	Gaussian	0.01
Probe Axial Force Coeff Mult. (Mach > 10)	1.0	Gaussian	3 %
Probe Normal Force Coeff Incr (Mach > 10)	0	Gaussian	0.01
Probe Axial Force Coeff Mult. (Mach < 5)	1.0	Gaussian	10 %
Probe Normal Force Coeff Incr (Mach < 5)	0	Gaussian	0.01
Probe Pitch Moment Coeff Incr. ($K_n \geq 0.1$)	0	Gaussian	0.005
Probe Pitch Moment Coeff Incr. (Mach > 10)	0	Gaussian	0.003
Probe Pitch Moment Coeff Incr. (Mach < 5)	0	Gaussian	0.005
Probe Pitch Damping Coeff Incr. (Mach > 6)	0	Gaussian	0.15
Probe Pitch Damping Coeff Incr. (Mach < 3)	0	Gaussian	0.15
Mass Property Uncertainty			
Mass, kg	320.0	Gaussian	1.0
Axial CG position, m	0.47176	Uniform	0.03175
Lateral CG position (Y), m	0.00154	Uniform	0.0069
Lateral CG position (Z), m	0.00491	Uniform	0.0069
Ixx, kg-m^2	127.97	Gaussian	10 %
Iyy, kg-m^2	75.85	Gaussian	10 %
Izz, kg-m^2	71.9	Gaussian	10 %
Ixy, kg-m^2	0.45	Gaussian	2.0
Ixz, kg-m^2	0.096	Gaussian	2.0
Iyz, kg-m^2	-0.338	Gaussian	2.0
Atmospheric Uncertainty			
Initial Seed Value	1	Uniform	1/29999
Fminmax input	0	Uniform	+/- 1.0

The nominal states and the corresponding covariance for the entry vehicle were provided by NASA's Jet Propulsion Laboratory based on their last best estimate of the probe location and orbit. The position and velocity coordinates were provided in the Titan Equatorial, Prime Meridian of the Epoch frame. The coordinate frame epoch was

established at 9 hours, 6 minutes, and 56.707 seconds on 14 January 2005. Table 4-2 shows the final best-estimated entry state and covariance provided on 16 January 2005.

Table 4-2. Huygens Titan Probe Final Entry State and Covariance

Parameter Name	Nominal Value
Probe Initial State (PME)	
XI, km	-3.785052917E+03
YI, km	3.666228396E+02
ZI, km	-5.684286346E+02
VXI, km/s	5.704491572E+00
VYI, km/s	1.918924348E+00
VZI, km/s	3.903063895E-01
Covariance	
(XI,XI)	9.968263850758179E+02
(XI,YI)	-2.409369480191529E+02
(XI,ZI)	3.257636252284417E+01
(XI,VXI)	1.030485908591312E-01
(XI,VYI)	1.910293598571988E-02
(XI,VZI)	1.726213988938161E-02
(YI,YI)	6.673675637097152E+01
(YI,ZI)	-6.236480565254642E+00
(YI,VXI)	-2.482536389707811E-02
(YI,VYI)	-5.080711008612633E-03
(YI,VZI)	-4.256843534812582E-03
(ZI,ZI)	1.159175790596700E+01
(ZI,VXI)	3.580276609460046E-03
(ZI,VYI)	5.415253848133445E-04
(ZI,VZI)	-1.920652296503984E-05
(VXI,VXI)	1.065741245612198E-05
(VXI,VYI)	1.970458965786453E-06
(VXI,VZI)	1.772749694250542E-06
(VYI,VYI)	3.913553702168093E-07
(VYI,VZI)	3.350492678937892E-07
(VZI,VZI)	3.313941373440683E-07

4.1.2 Huygens Trajectory Reconstruction Plan

The Huygens trajectory reconstruction process started with an analysis to determine the initial state (inertial position and velocity vectors) within the delivered final covariance that best fits the flight data through the entry phase (where the main deceleration pulse occurs); this initial state was used for all of the subsequent reconstruction runs. Next, the POST2 reconstruction was set up to focus on the three specific phases in EDL: entry, main parachute and drogue parachute phases. Finally, an end-to-end state (position and velocity) estimate was determined.

The entry phase starts at entry interface (1270 km altitude) and ends at pilot parachute deploy. Aerodynamic uncertainties in the Free Molecular, Hypersonic, and Supersonic flight regimes are included in the capsule aerodynamics model used with the pre-flight simulation. In the pre-flight analyses, an uncertainty for each regime was randomly selected and used throughout that regime. The reconstruction run estimated the uncertainty values at each acceleration measurement point. That is, the constant uncertainty value normally used in the Monte Carlo runs was estimated at each observation for the reconstruction run. Note that the aerodynamics model provides a smooth transition between flight regimes, so there are certain times during the trajectory that uncertainties from two flight regimes will be active. During this reconstruction of the capsule aerodynamics, all of the observation error is assumed to be from aerodynamics only; that is, the nominal atmospheric density and wind model used prior to entry is assumed to be correct.

For the parachute phases, the pre-flight model of the parachute inflation is assumed correct since the frequency of the acceleration measurements is not high enough to capture these very dynamic events. Thus, the measurements during the inflation

periods are weighted such that the measurements are not a large factor in the reconstruction run.

Let us now summarize the Huygens reconstruction analysis plan. After determining an initial state, the reconstruction effort will focus on the entry, main parachute and drogue parachute phases. Finally, an end-to-end position and velocity estimate will be generated.

4.2 HUYGENS FLIGHT DATA FOR RECONSTRUCTION

The ESA Huygens probe science teams provided several sets of data to NASA as part of an agreement with ESA for analyses NASA performed prior to entry. These data included acceleration measurements throughout EDL, atmospheric pressure and temperature after heat shield jettison, and radar altimetry for the last 40 kilometers. Additionally, radio telescopes at Earth received the Huygens signal throughout the descent and provided an estimate of wind velocity. The Descent Imager (DI) team also contributed an estimate of vertical velocity based on sequentially captured images. Various Principal Investigators were responsible for the instruments that provided this data; the various groups responsible for this data are identified, along with details about their instruments, in Refs. [36] and [37]. Additional information on the datasets is given in Ref [39], but datasets used in this analysis are also included here.

4.2.1 Accelerometer Data

Three accelerometers were available on the Huygens probe: the HASI Servo-type Axial Accelerometer (Sandstrund QA2000-030 model)[41], the HASI Piezo three-axis accelerometer (Endveco 7264A-2000T)[41], and the Central Accelerometer Sensor Unit (CASU) axial only accelerometer set. In brief, the Servo-type accelerometer has

resolution on the order of μ-g, Piezo resolution is milli-g, and the CASU system is an order of magnitude larger (approximately tens of milli-g).[42] The three datasets are shown with the POST2 pre-flight simulation (using the JPL post-flight estimate of the initial conditions) results in Fig. 4-1. As seen in the figure, two datasets (Servo and CASU) compare well with the POST2 pre-flight simulation and each other. All three have nearly the same slope on both sides of the deceleration pulse and same peak decelerations. The third dataset (Piezo) does not match up well. The Piezo accelerations do show the correct basic profile, but not the slope or peak deceleration. However, as seen in Fig. 4-2, the Piezo is consistent with the other datasets on time of parachute deploy. Based on this comparison, the Piezo data was deemed not acceptable. This decision meant that the only dataset with lateral components could not be used (Fig. 4-3 shows the lateral accelerations from the Piezo dataset). Thus, none of the results in this report use the Piezo acceleration datasets for quantitative analyses; however, qualitative assessment is still possible using the Piezo dataset.

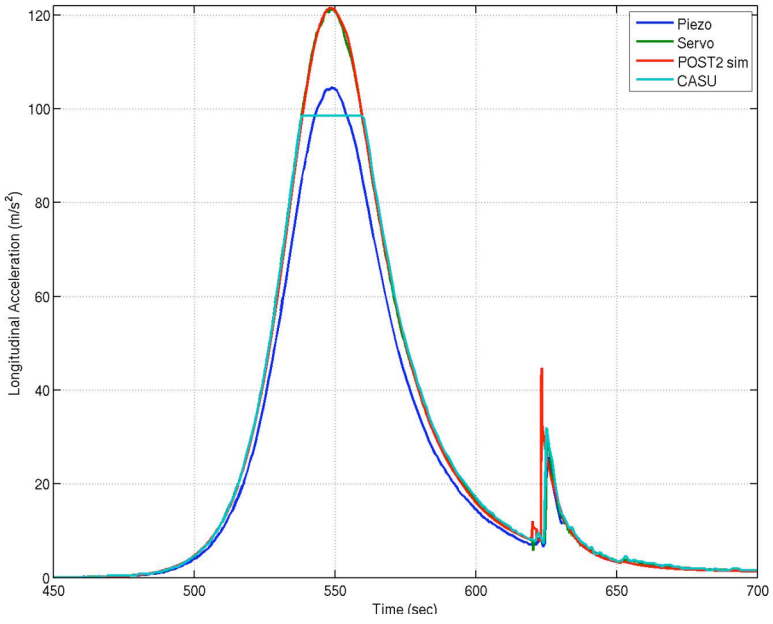

Figure 4-1. Huygens Probe Accelerometer Flight Data Comparison to POST2 Simulation

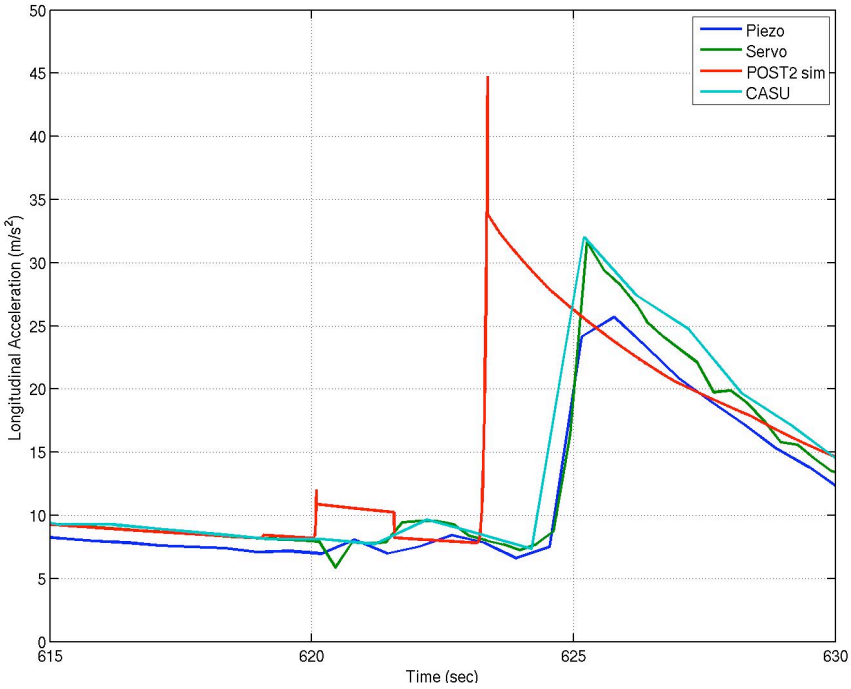

Figure 4-2. Accelerations from Flight Data around Parachute Deployment

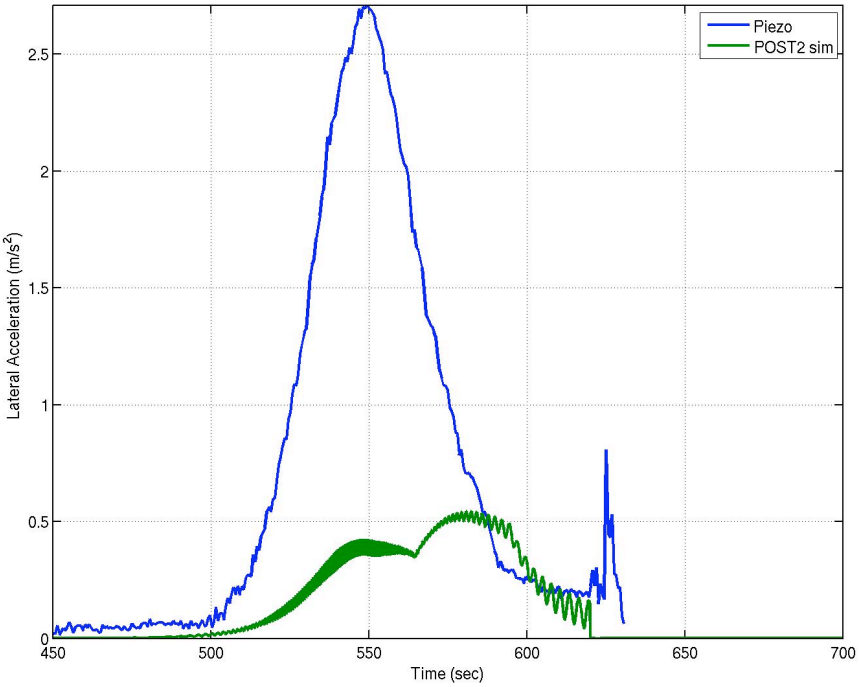

Figure 4-3. Lateral Accelerations from the Piezo Accelerometer and the POST2-based Simulation

The CASU accelerometer data was used as an engineering backup to the other accelerometers to ensure EDL sequence initiation as part of the parachute trigger logic. Also, this dataset is limited to measurements less than ten times Earth's gravity, or 98.1 m/s^2, and the data was taken at a lower frequency (1 Hz) and resolution (by a factor of 10000) than the HASI Servo accelerations. Therefore, the analysis in this report uses the HASI Servo accelerations for quantitative assessments.

Figure 4-4 shows the HASI Servo acceleration dataset after parachute deploy. This data was taken at various frequencies throughout the trajectory: entry, 3.125 Hz; descent, 4.167 Hz; and after radar initiated to touchdown, 1.754 Hz. As can be seen in the figure, significant noise is apparent on this dataset. A simple data smoothing technique (a sliding 200-point median) was applied to this dataset to facilitate reconstruction. The result of this smoothing is the solid green line shown in Fig. 4-4. Note that neither the data prior to Main parachute deployment nor the last 100 data points were smoothed.

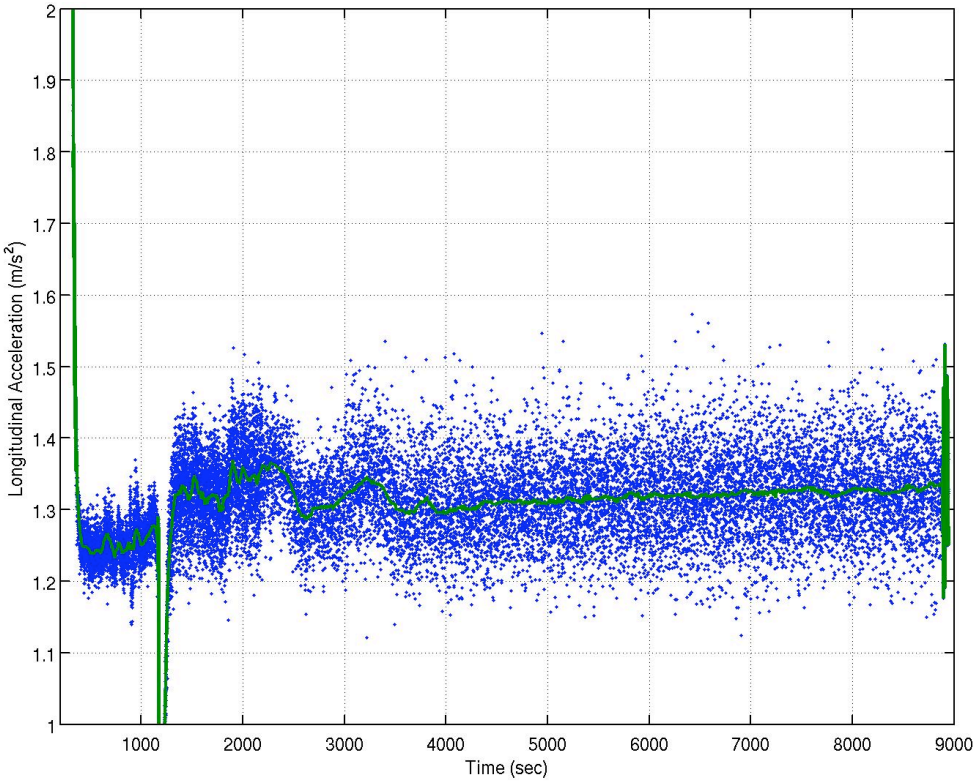

Figure 4-4 Huygens HASI Servo Accelerometer Data – Raw and Smoothed

4.2.2 Altitude Radar Measurements

Another Huygens flight dataset was the altimetry data from two separate Huygens Radar Altimeter (HRA) units, designated A and B, mounted on opposites sides of the probe. Figure 4-5 shows the altitude data generated by these radars after correction by the Principal Investigator for temperature and digital errors. Both A and B units generated very similar data. Thus, the analyses done for this report used the data from unit A.

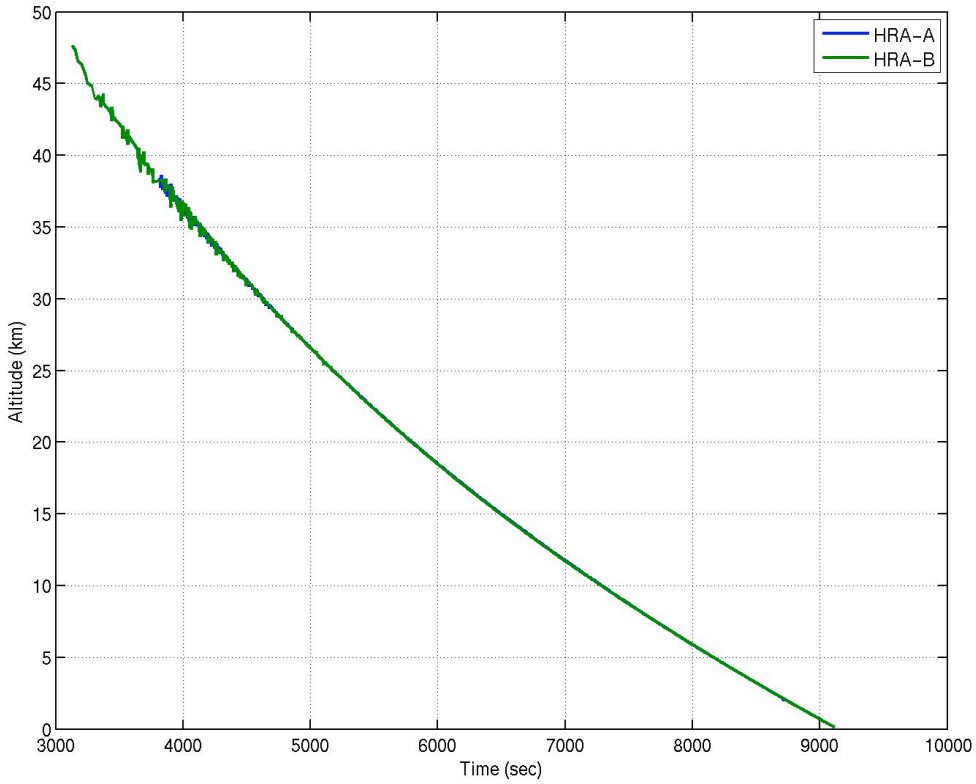

Figure 4-5. Altitude Data from Huygens Altimetry Radar Units A and B

4.2.3 Atmospheric Properties

The time histories of the atmospheric pressure and temperature were obtained from ESA. Figure 4-6 shows the free-stream pressure from the onboard pressure transducer as a function of time from entry interface. Figure 4-7 shows the time history of the free-stream temperature after motion correction and other calibration factors have been applied. Density can be found from the equation of state:

$$\rho = C_f \frac{W_{MM} p}{RT} \tag{4-1}$$

where C_f is compression factor, W_{MM} is mean molecular weight, R is the Universal gas constant (8313.34 N-m/kmole-K), p is atmospheric pressure, and T is temperature.

Reference [39] discusses further the selection of W_{MM} and C_f from the science data. The density resulting from these measurements is shown in Fig. 4-8.

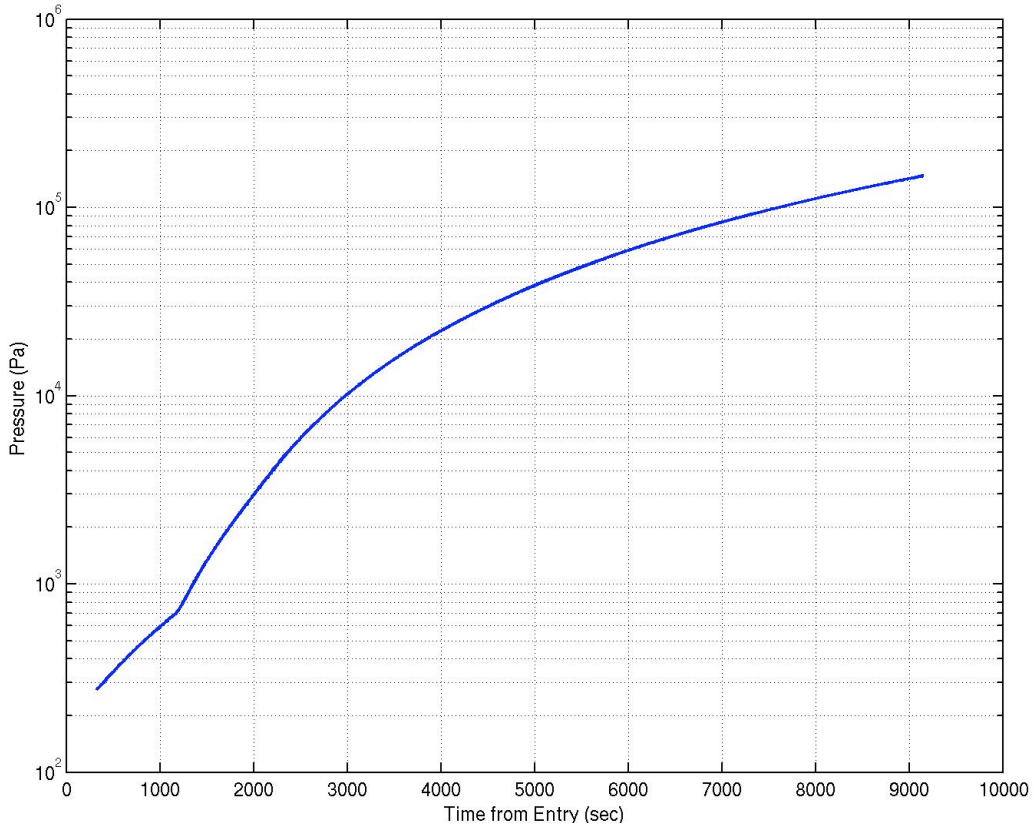

Figure 4-6. Huygens Atmospheric Pressure Measurements

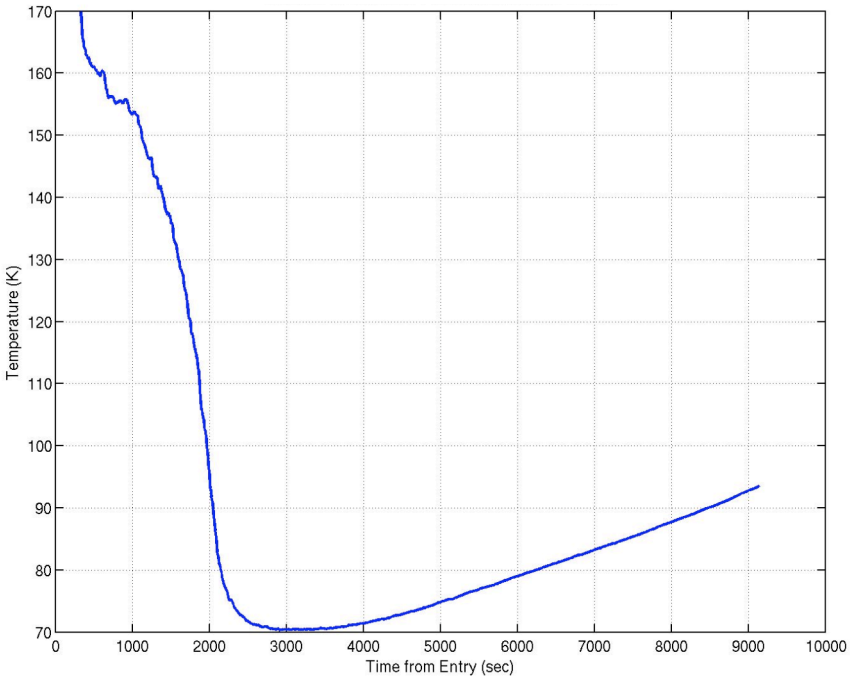

Figure 4-7. Huygens Atmospheric Temperature Measurements

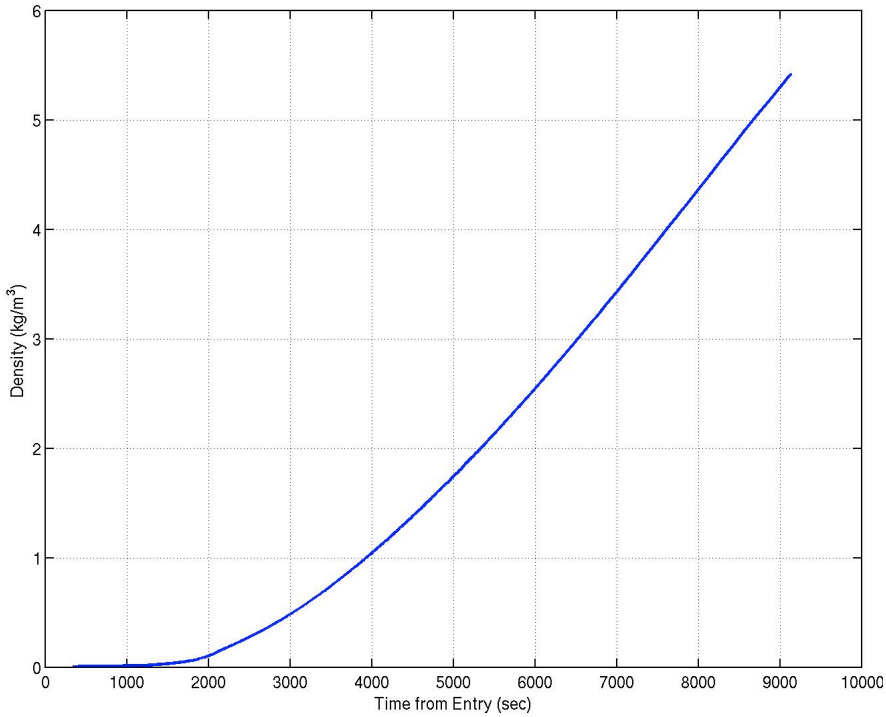

Figure 4-8. Titan Atmospheric Density Derived from Huygens Measurements

4.2.4 Tilt Sensor

Figures 4-9 and 4-10 show the measured probe tilt sensor data from the surface science package (SSP) instrument. These figures also indicate the smoothed dataset that was generated using the median of a 200 point moving window. Lorenz indicated that the probe had a mean tilt of approximately 8 deg based on the TILY sensor.[43] Using the tilt sensor orientation (indicated in Fig. 4-11), the total angle between the local vertical and probe axial axis can be found from acos ($\cos(\theta_X)\ \cos(\theta_Y)$) where θ_X and θ_Y are the angles about the sensor X and Y axes. The resulting total tilt angle is presented in Figure 4-12. Due to the tilt sensor location (see Fig 4-11), Lorenz noted that the X-axis tilt sensor will be impacted by probe spin and an unexpectedly high spin rate peaked at around 1200 sec in the plot shown. However, the time of interest for this analysis is after 3600 sec at which time the probe spin had decreased substantially (from a maximum of 10 rpm at 1200 sec down to 2 and less after 3600 sec). Eliminating the period of high rate, the mean value of tilt over the Drogue parachute phase is around 8.7 deg.

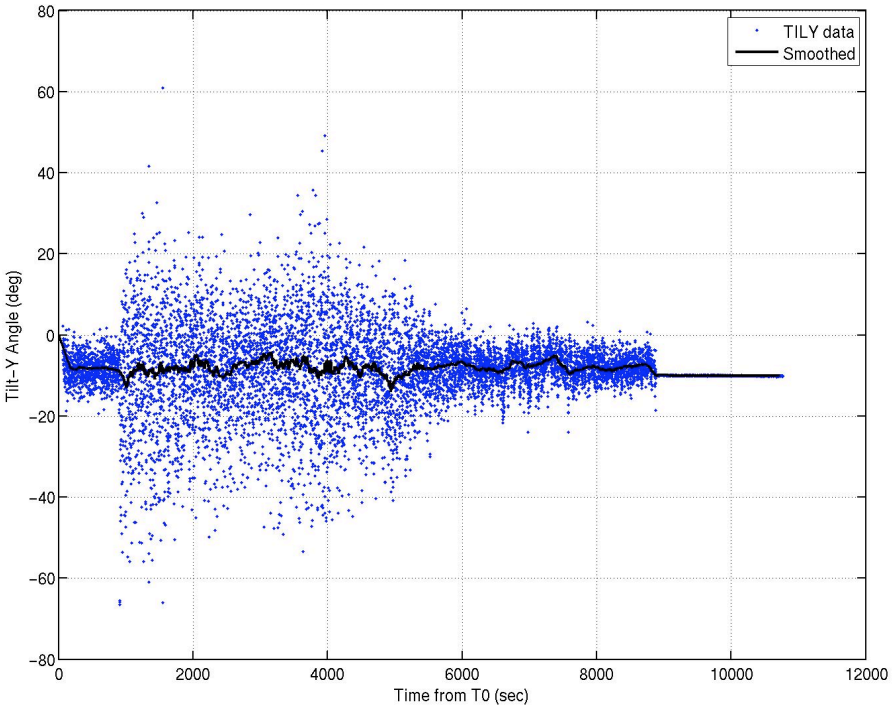

Figure 4-9 Huygens tilt sensor Y-axis angle measurements (TILY)

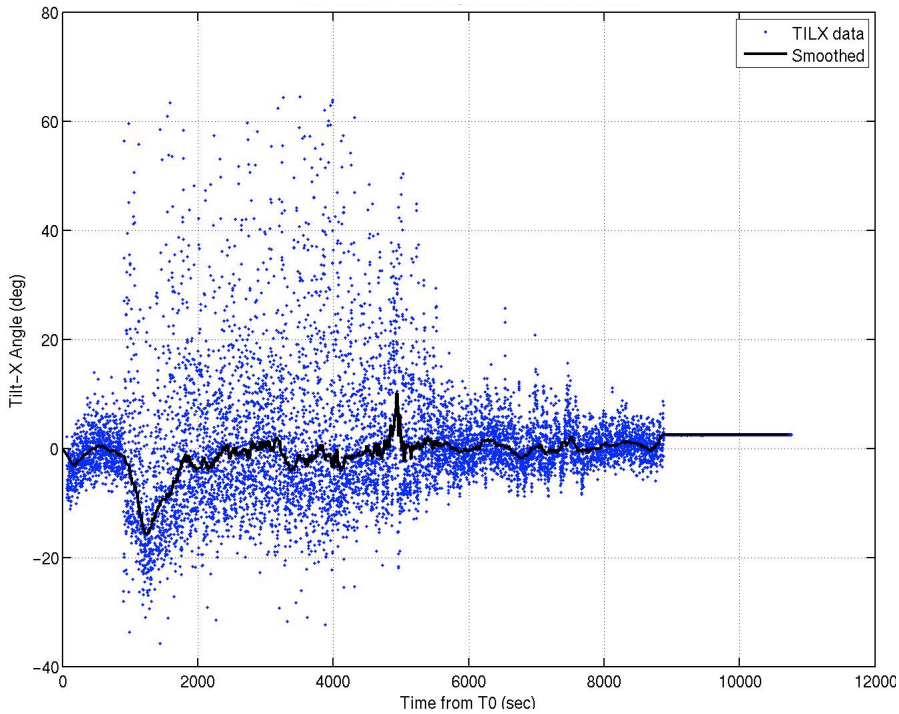

Figure 4-10 Huygens tilt sensor X-axis angle measurement (TILX)

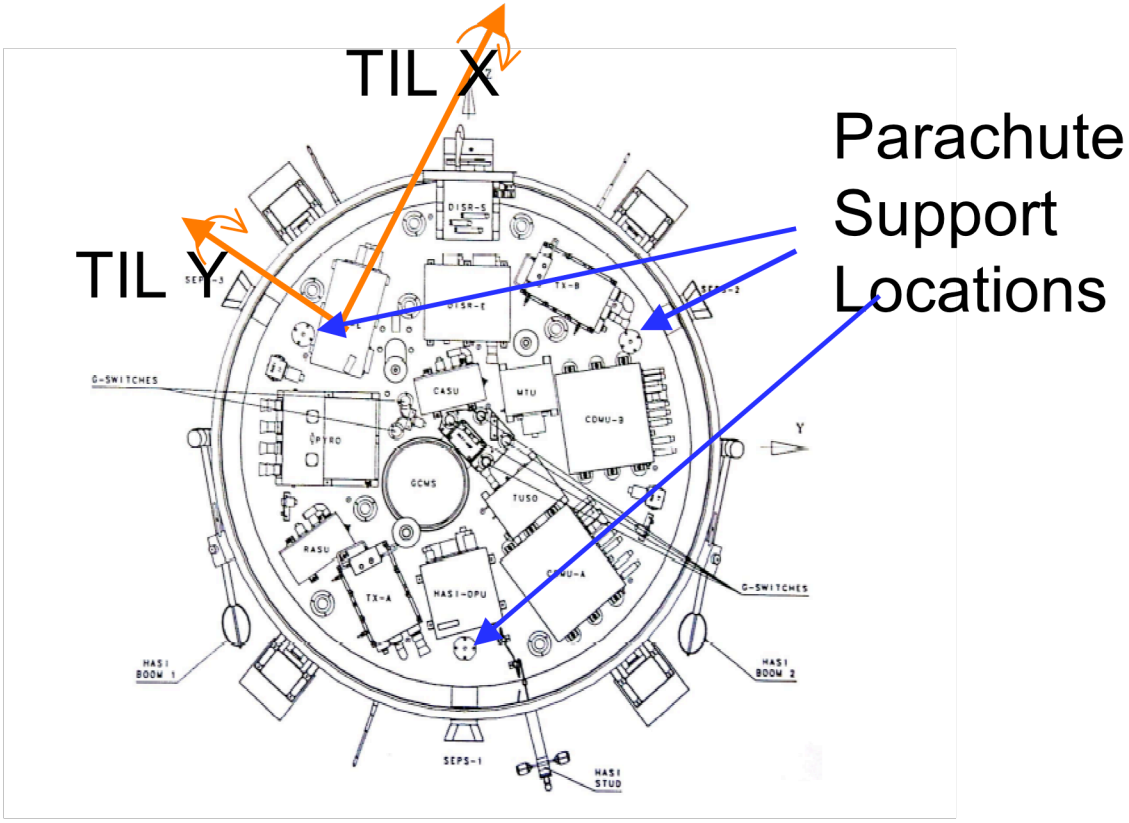

Figure 4-11 Tilt sensor location, axes and positive rotation directions

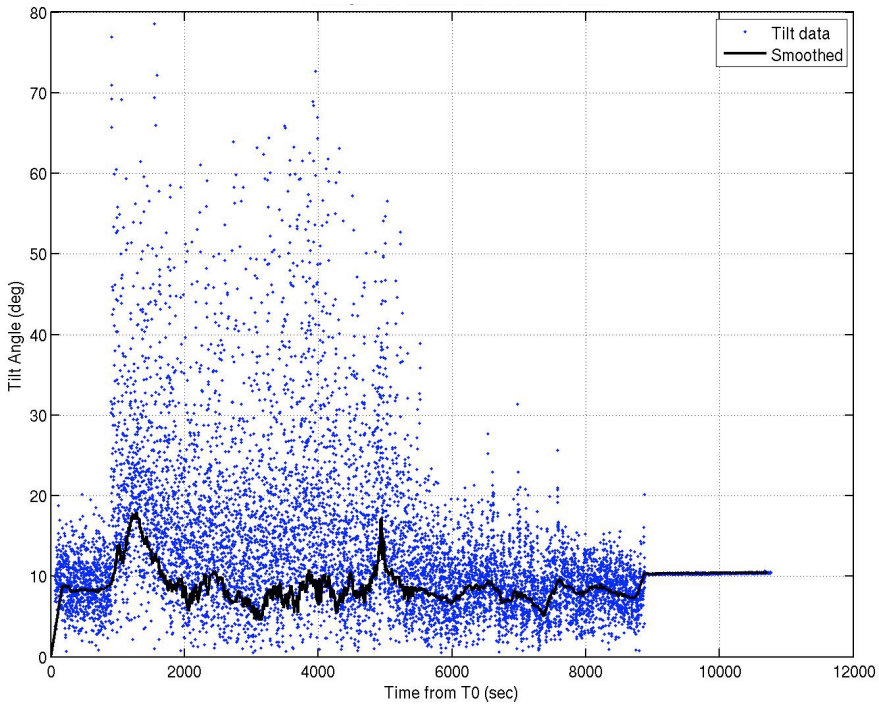

Figure 4-12 Tilt angle from vertical using tilt sensor data

4.2.5 Measured Wind Profile

Figure 4-13 shows the zonal wind velocity provided by ESA.[44] Zonal winds are applied in the East-West direction only. As no North-South winds are assumed, zonal winds provide the total horizontal wind velocity. Note that the winds were not directly measured, but rather were inferred from measured probe motion. That is, this wind estimate assumes that the horizontal component of probe motion while on the parachutes directly represents the movement of the atmosphere.

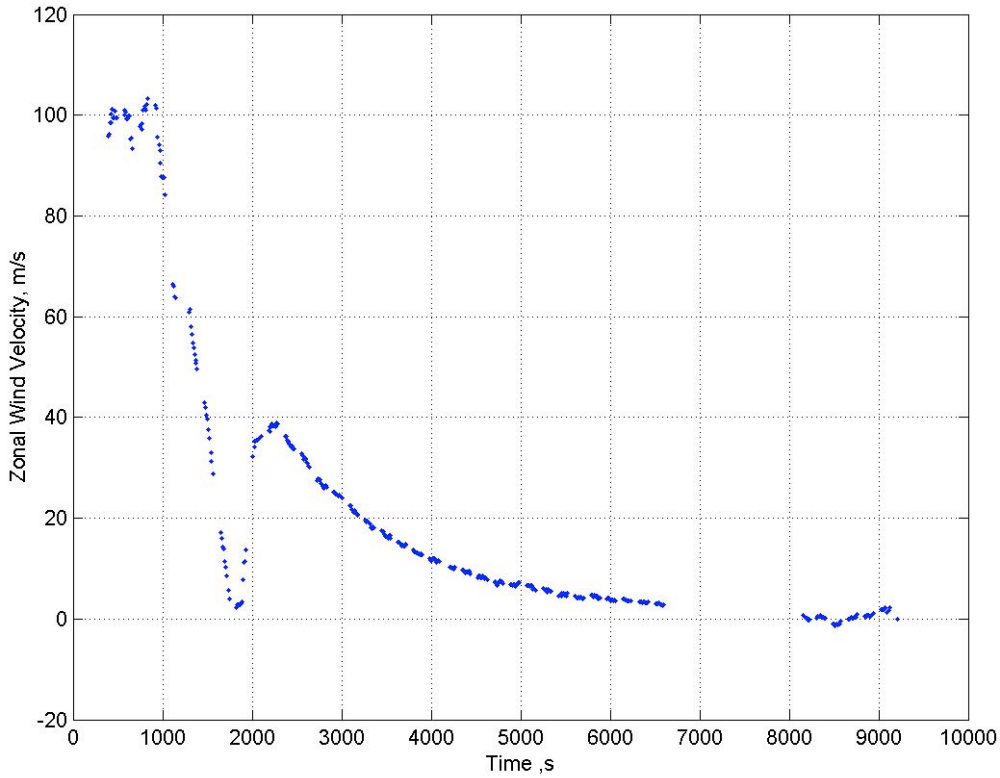

Figure 4-13 Zonal wind velocity provided by ESA

Chapter 5: Huygens Probe EDL Trajectory Reconstruction Results

5.1 Initial State from Monte Carlo Assessment

Although the simulation results using the JPL-determined last estimated nominal entry state generally follows the flight data, a Monte Carlo analysis was used to determine the initial state that best fits the flight data. The last JPL delivered initial state covariance was used to generate 10000 dispersed states. Each of the 10000 cases was simulated and the sum of the acceleration observation residual absolute value was accumulated as the simulation progressed. The final value of this metric (at parachute deploy) was then compared and the smallest value cases were used for subsequent reconstruction efforts. A time adjustment at around 0.5 m/s^2 measured axial acceleration was determined to align each case with the accelerometer. Since the states were generated at a fixed time but position was varied, this time adjustment was necessary to ensure that that once the atmosphere was reached, the times of the acceleration due to aerodynamic drag on the probe and the measured accelerations would align. Table 5-1 compares the nominal best estimated entry state generated by JPL and the initial state determined by

Table 5-1. Comparison of JPL Last Initial State Estimate and Monte Carlo Determined Initial State

	JPL last estimate	3-σ bounds	Monte Carlo determined	Difference
Inertial X Position (km)	-3785.053	94.718	-3810.021	24.968
Inertial Y Position (km)	366.623	24.508	367.226	-0.603
Inertial Z Position (km)	-568.429	10.214	-566.418	-2.011
Inertial X Velocity (km/s)	5.704492	0.009794	5.701933	0.002559
Inertial Y Velocity (km/s)	1.918924	0.001877	1.918745	0.000179
Inertial Z Velocity (km/s)	0.390306	0.001727	0.389695	0.000611

the Monte Carlo process. Case 8724 had the best agreement between the flight data and the simulation for the entry phase. The accumulated measurement error just prior to parachute deploy for the JPL state was 169.8 m/s^2, whereas case 8724 had an error of 159.0 m/s^2. This relative improvement indicates the latter case is closer to the dataset than the former since an error of zero would indicate an exact match between the simulated trajectory and the actual measured accelerations. Results for case 8724 are illustrated in the following plots.

Figure 5-1 shows the entry deceleration pulse for case 8724. The blue curve shows data from the simulation and the green dots indicates the flight data. As noted in the figure, the simulation matches the flight data very well on the up and down slope of this peak. Recall that only the entry phase was used in this Monte Carlo analysis, hence errors after parachute deploy (around 270 sec in the plot) were not included in the calculated metric. Figure 5-2 shows detail near the maximum deceleration pulse region and includes data from the simulation run using the JPL last best estimate of initial entry state (shown in Table 5-1 above). It is clear from this figure that case 8724 is closer to the flight data by a small amount.

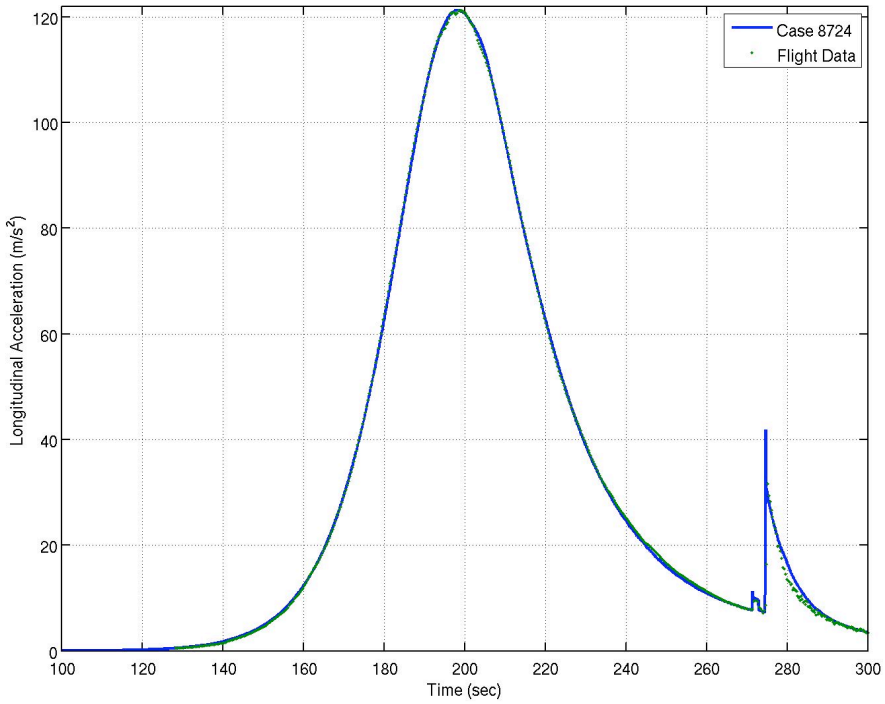

Figure 5-1. Huygens Flight Data Compared to Simulation Run Only – Entry Phase

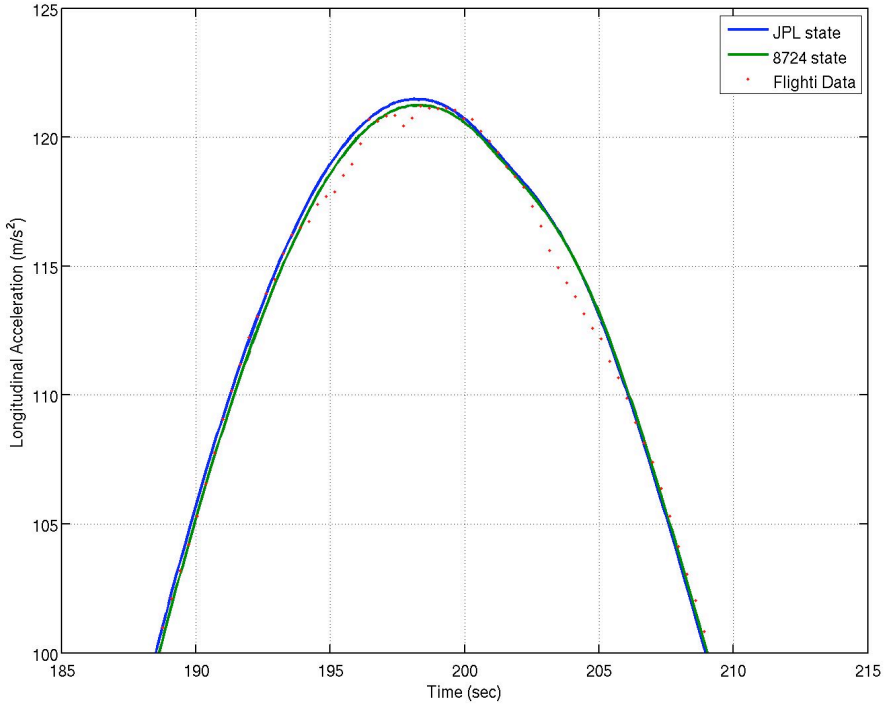

Figure 5-2. Maximum Deceleration Region Comparison - JPL Final State & Case 8724

The altitude-velocity profile for the entire end-to-end trajectory of this case is shown in Figure 5-3. The Pilot parachute deploys at about Mach 1.4 or 350 m/s relative velocity. Figure 5-4 shows the altitude-velocity profile in the parachute descent phase. Note that the heat shield is released at about 157 km and 90 m/s changing probe aerodynamics and mass. Also, the smaller Drogue parachute deploys around 115 km and 75 m/s. Both events are characterized by an increase in velocity due to the changing configuration (aerodynamics, mass, etc.).

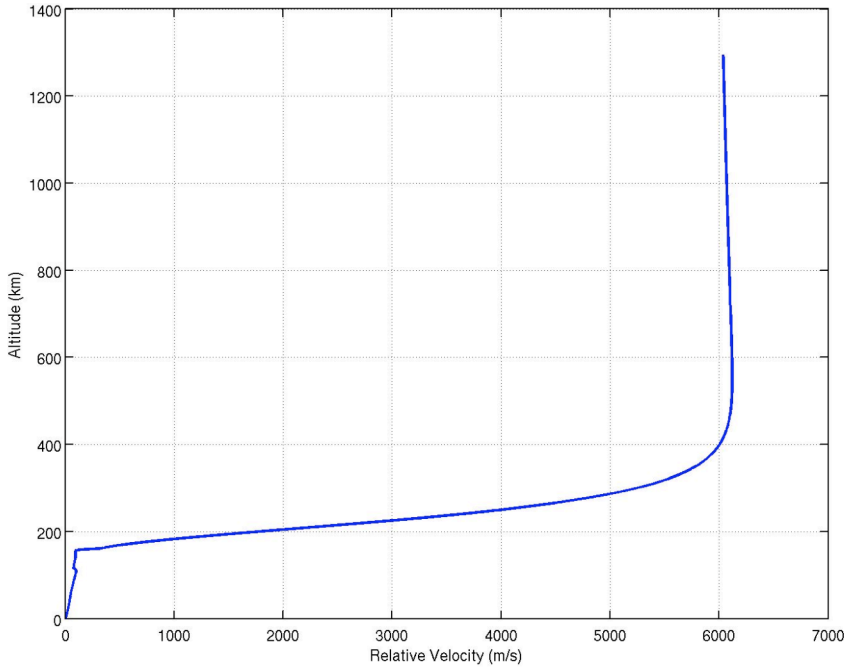

Figure 5-3. Case 8724 Simulation Run Only – Altitude-Velocity Profile

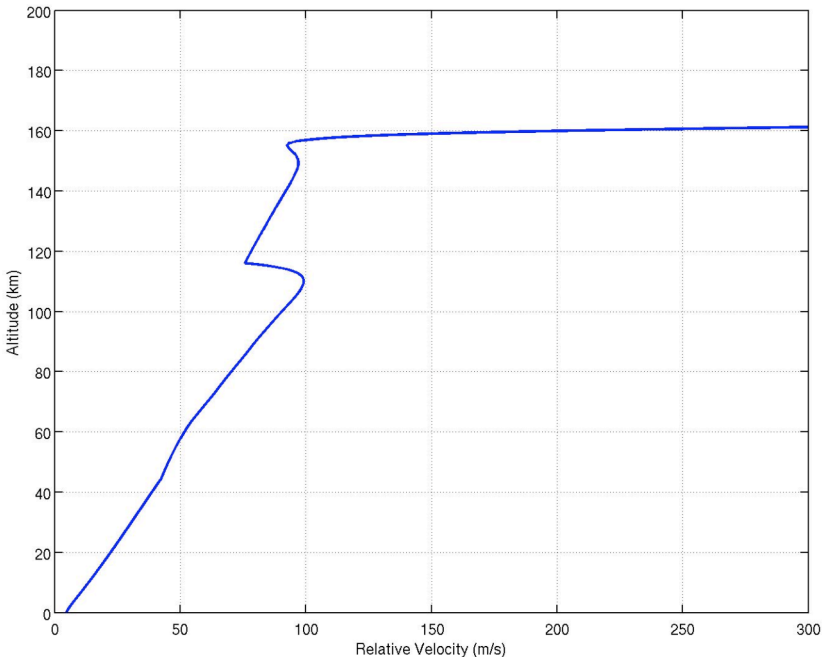

Figure 5-4. Case 8724 Simulation Run Only – Altitude-Velocity Profile – Parachute Phase

The Pilot and Main parachute deployment are shown in Figure 5-5. The simulation matches the flight data well for the few seconds that the Pilot parachute was active (about 271 to 274 sec on the plot). Even the Main parachute deploy is comparable near 275 sec. However, shortly after main parachute deploy the simulation and flight data diverge for about 15 sec from 275 to around 290 sec. This difference could be a temporary bias in the accelerometer after the rapid deceleration parachute deploy event. The difference could also be caused by different parachute aerodynamics or opening profile. The Main parachute and early Drogue parachute phase are shown in Fig. 5-6. As expected, the simulated case does not follow the flight data exactly, but tends to be roughly in the mean of the data, again indicating that the simulated case appears near the flight profile.

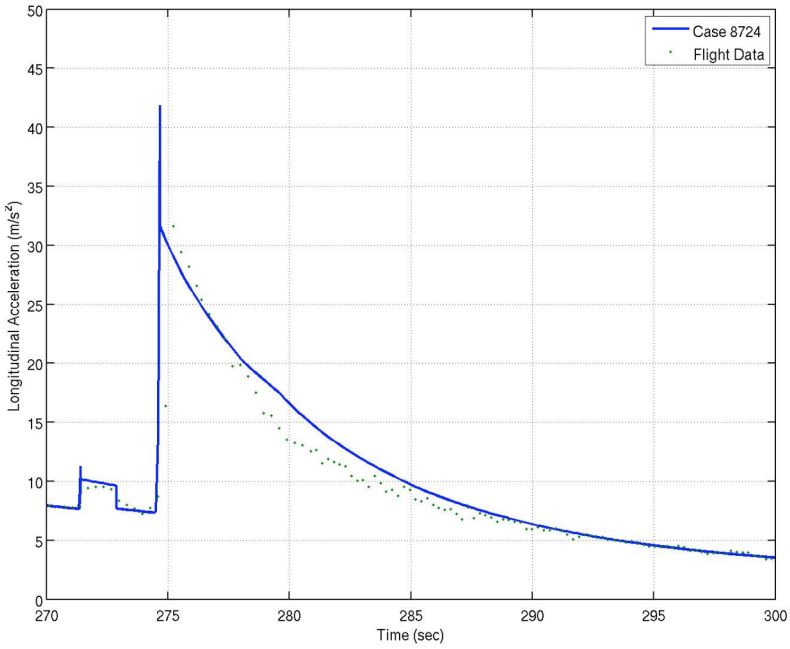

Figure 5-5. Huygens Flight Data Compared to Simulation Run Only – Main Parachute Deployment

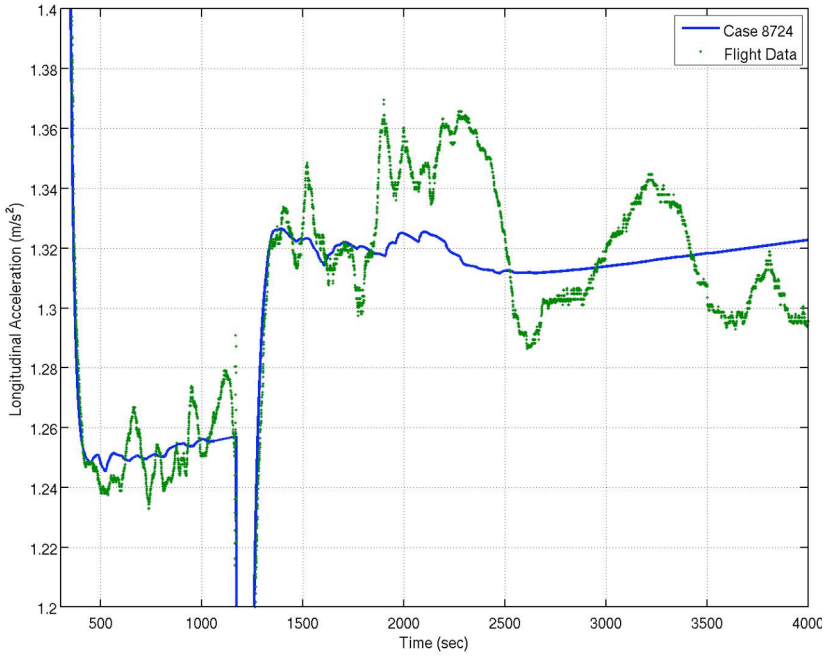

Figure 5-6. Huygens Flight Data Compared to Simulation Run Only – Main and Early Drogue Parachute Phases

Figure 5-7 shows accelerometer data from the flight and simulation during the Drogue parachute phase. Note that the variation in the flight data on the order of +/- 0.15 m/s^2 can be seen at the end of this plot. As shown in this figure, the mean of the accelerometer data is below the simulation accelerations by 1-2%. This data comparison is the first indication that the flight data and the POST2-based Huygens EDL simulation had a significant difference. Once the parachute was near terminal velocity and nearly vertical, the acceleration should match Titan's gravity. That is, ignoring transient updraft and downdrafts, steady state descent should result in an accelerometer reading of very nearly one Titan-g. Some definite variation in the simulation models would be necessary to match the flight data. This variation could be in the environment models (e.g., gravity, atmospheric density), the system models (parachute drag), or some other factor not necessarily captured in the simulation. These possibilities are examined further below.

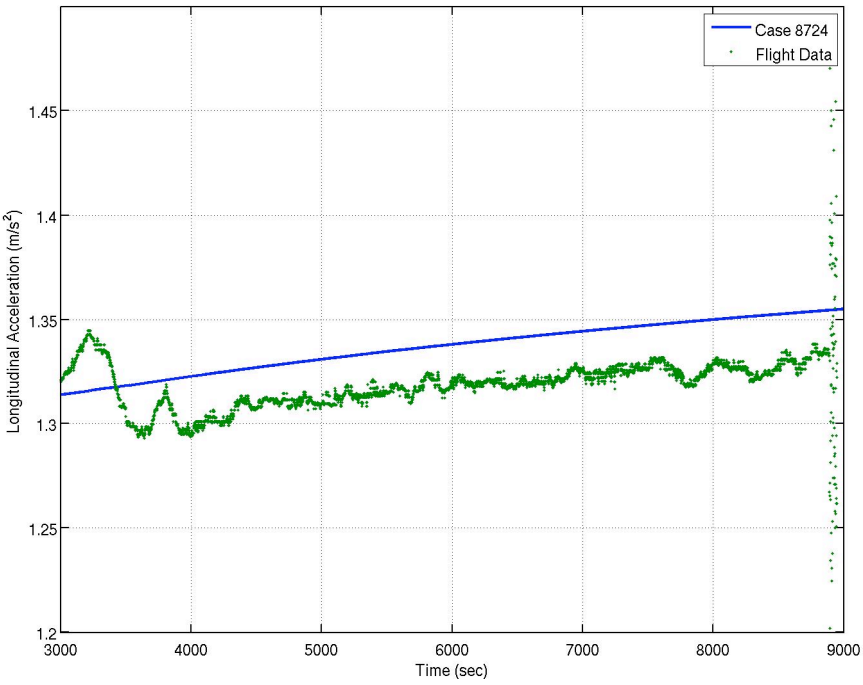

Figure 5-7. Huygens Flight Data Compared to Simulation Run Only – Drogue Parachute Phase

Altitude data from altimeter A is shown with the simulation results in Fig. 5-8. This plot shows that the simulated trajectory altitudes fall notably below the radar data. Before this analysis began, the Huygens DTWG generated altitude reconstruction did not match the radar measurements (it was also lower than the radar). This simulation altitude result appears to be in qualitative agreement with the DTWG result, however no reconstruction was done for this run. Further study of the altitude profile is given in the following reconstruction analyses.

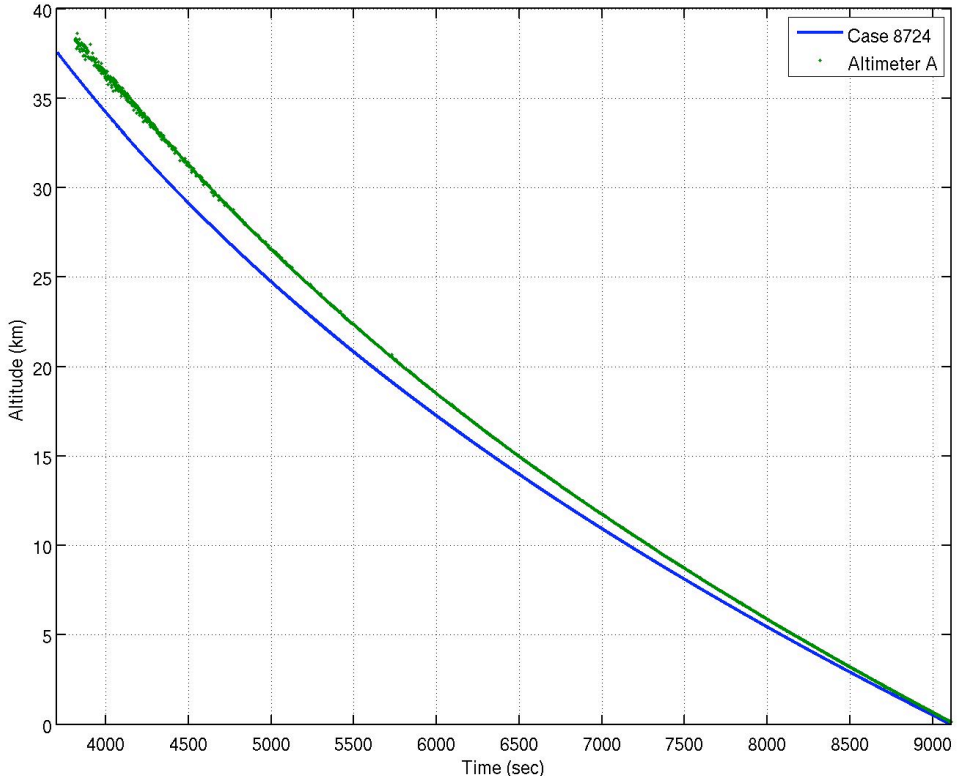

Figure 5-8. Huygens Flight Data Compared to Simulation Run Only – Radar Altimetry Comparison

5.2 PHASE ELEMENT RECONSTRUCTIONS

The trajectory reconstruction in this section focuses on evaluating the pre-flight models used in the main phases of the Huygens Titan EDL: entry aerodynamics, main parachute drag, and drogue parachute phase. Estimating the aerodynamics and environment (winds) for comparison with pre-flight models is the major consideration in these phases. However, rectifying differences in flight and reconstructed datasets is also an objective. The results from the evaluation of the pre-flight models using the Huygens flight data were discussed with the groups responsible for the model development.

5.2.1 Entry Capsule Aerodynamics

The focus of this section is to use the flight data to validate the entry aerodynamics model from the pre-entry simulation. For this portion of the analysis, the Titan-GRAM atmosphere model is assumed correct and all of the error in the measured accelerations is due to errors in the aerodynamics model. The POST2-based Huygens EDL simulation includes aerodynamic uncertainties for Monte Carlo simulations done prior to probe arrival at Titan. The aerodynamic database includes the uncertainty amount for the free molecular, hypersonic and supersonic flight regimes. For the reconstruction analyses, the uncertainty in axial force coefficient was estimated since only the axial accelerations were measured. Since this uncertainty effectively increases (or decreases) the axial force coefficient, this approach is similar to applying a multiplier to the nominally calculated axial force coefficient. Note that these were entry phase runs only, hence no reconstructed trajectory data is generated beyond the Pilot parachute mortar-firing event (aka T0 event) at about 270 sec.

As noted previously, the Kalman filter implementation includes system noise covariance input. Through the state covariance, this noise covariance can be used to increase the reconstructed state response to the measurements. The peak deceleration

region during entry is shown for the reconstruction case with the noise covariance set for a rapid filter response to the measurements in Fig. 5-9 and set for a slow response of the estimated state to measurements in Fig. 5-10. Note that the same flight data points appear in both Figs. 5-9 and 5-10. The solution generated using the "Low Noise" (or LN) setting (Fig. 5-9) allows an assessment of the entry aerodynamic model used prior to Huygens probe entry at Titan by assuming that all of the error during the entry is from errors in the aerodynamic predictions; whereas a "High Noise" (or HN) setting (Fig. 5-10) does not allow the filter to change the estimate as rapidly. As seen in Fig. 5-9, the acceleration for the LN case matched acceleration points closely as desired. The maximum error during this peak deceleration period was +/- 0.6 m/s^2 or less than 0.5%; most of the error in this region was less than 0.2 m/s^2 or 0.2%. As expected, the HN case did not match as well (see fig. 5-10).

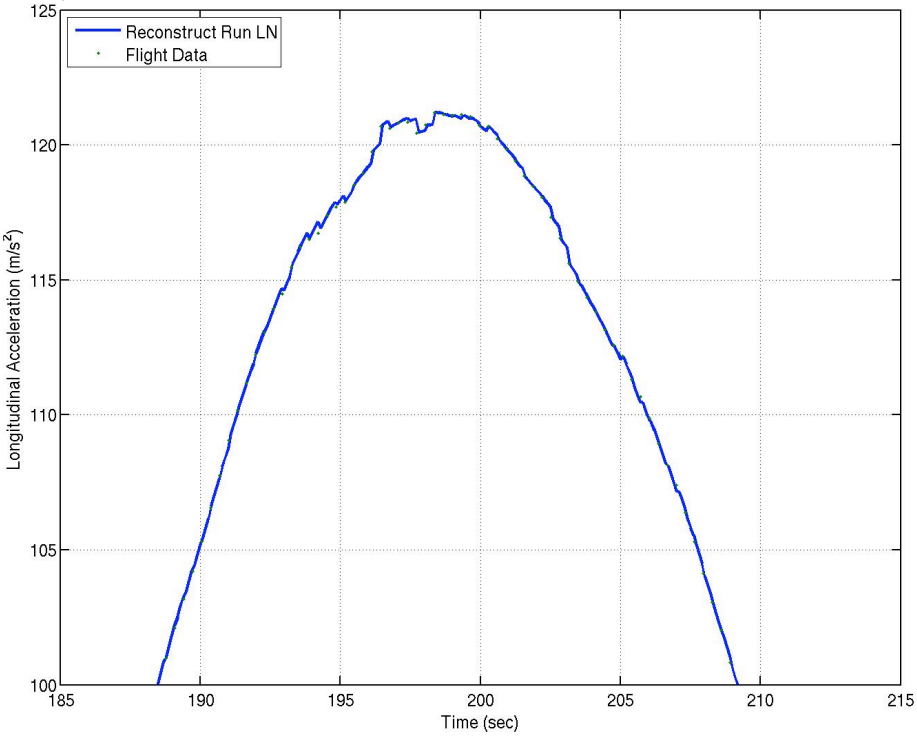

Figure 5-9. Comparison of Flight Data to Entry Aerodynamics Estimate Reconstruction Run – Peak Deceleration Region – Low Noise

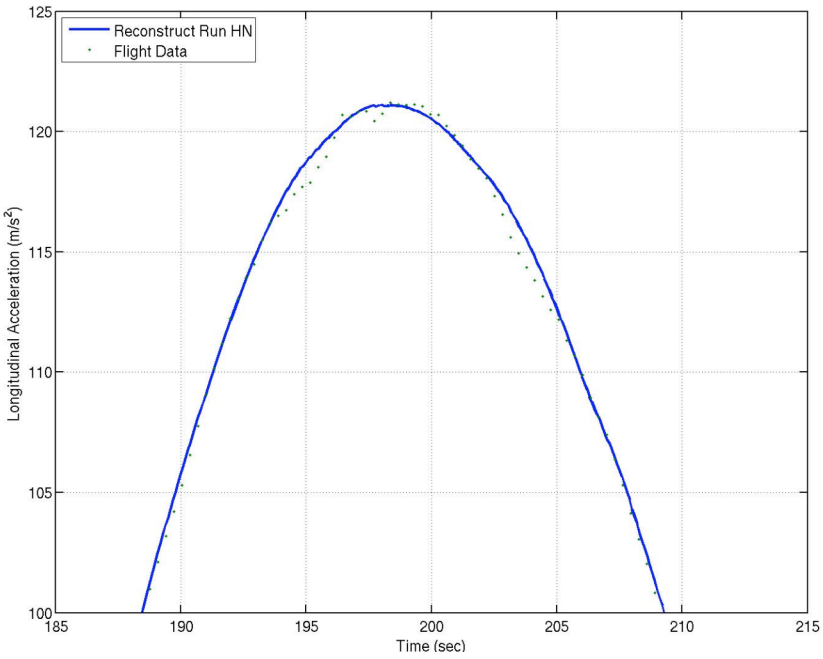

Figure 5-10. Comparison of Flight Data to Entry Aerodynamics Estimate Reconstruction Run – Peak Deceleration Region – High Noise

As can be seen from these two figures, the acceleration for the LN case matched more acceleration points than the HN case. The overall measurement error for these two cases is shown in Fig. 5-11. This figure also confirms the above observation that the LN case consistently matched the flight data better than the HN case. This result is especially true in the maximum deceleration region of the entry as indicated in Fig. 5-12. However, the HN case was an improvement in the residual error over the simulation only case as shown in Fig. 5-13. Whereas the simulation using the JPL state had a cumulative measurement error of near 170 m/s^2, case 8724 simulation run from the Monte Carlo analysis had 159 m/s^2, the HN case was around 110 m/s^2, and the LN case was the lowest at almost 30 m/s^2.(note that these cases ended slightly later than the Monte Carlo initial state runs, hence the plotted value for the simulation-only case is slightly higher than 159 m/s^2). Thus, the LN case captured the flight data quite well.

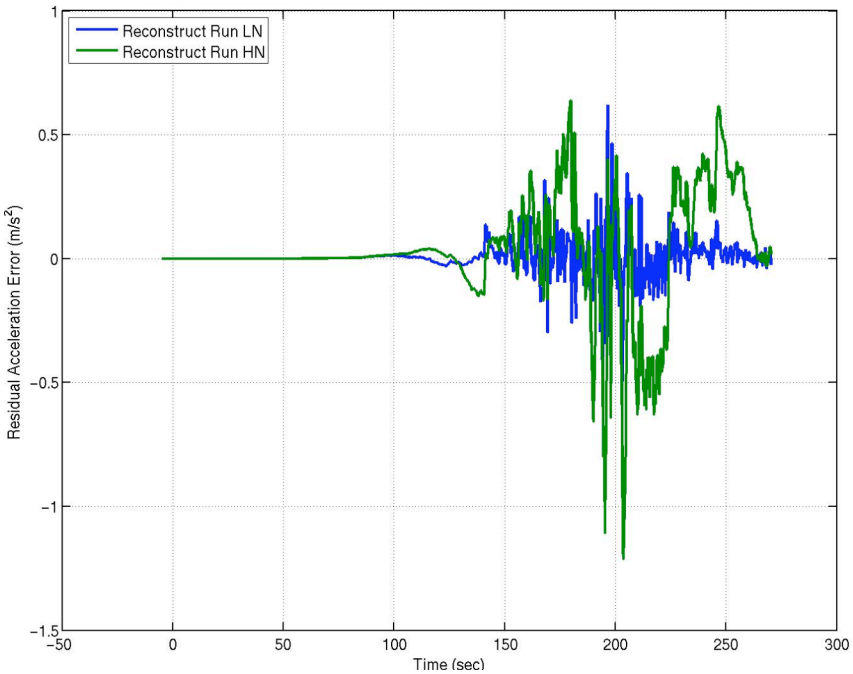

Figure 5-11. Comparison of Flight Data to Entry Aerodynamics Estimate Reconstruction Run – Residual Acceleration Error

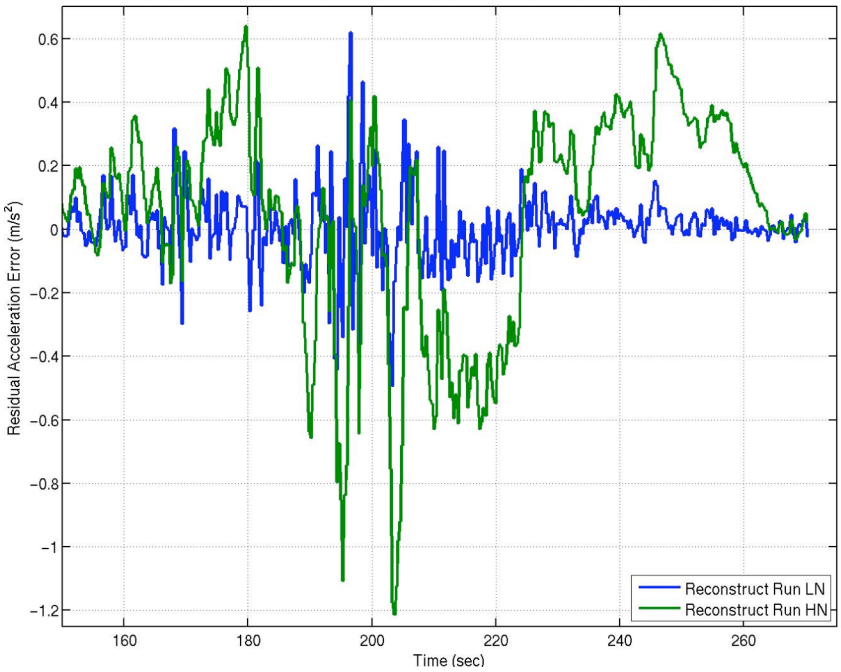

Figure 5-12. Comparison of Flight Data to Entry Aerodynamics Estimate Reconstruction Run – Residual Acceleration Error During Peak Deceleration

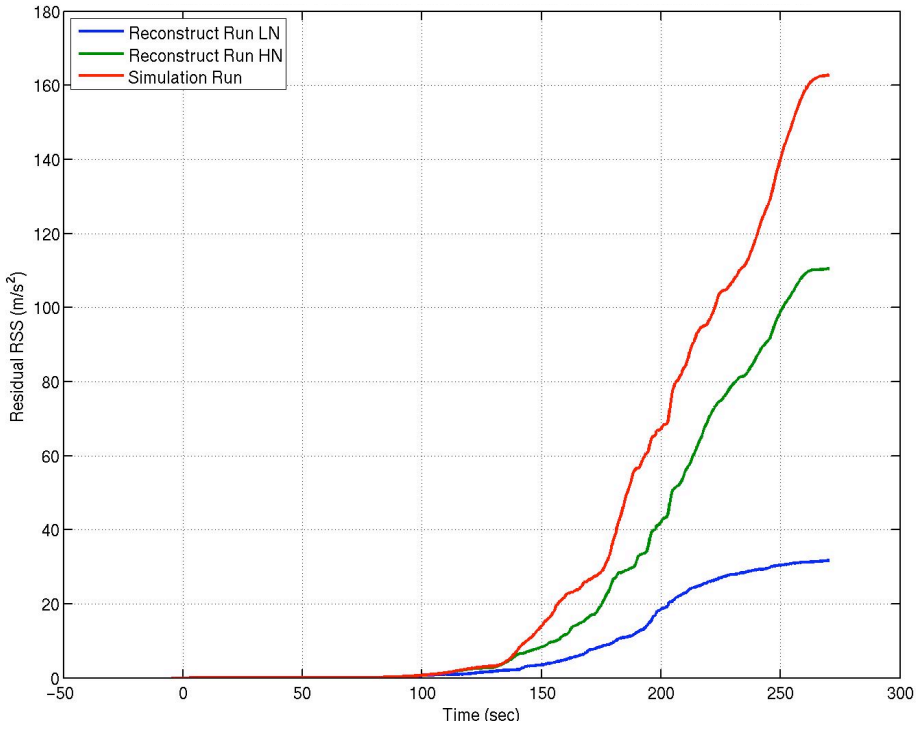

Figure 5-13. Comparison of Flight Data to Entry Aerodynamics Estimate Reconstruction Run – Residual Error Cumulative RSS

These reconstruction runs were estimating the adjustment from the nominal aerodynamics model necessary to meet the flight data. The actual states estimated were the aerodynamic dispersion parameters for C_A in each flight regime (free molecular, hypersonic and supersonic). These parameters applied the aerodynamicist-defined uncertainty to the coefficient in each regime; the 3-σ uncertainty value is used for an input of +1. For example, in the free molecular flight regime an uncertainty parameter of +1 corresponds to a 3-σ value for the C_A multiplier of 5% on as indicated in Table 4-1; that is, the nominal C_A was multiplied by 1.05 for an uncertainty parameter of +1 in the free molecular flight regime.

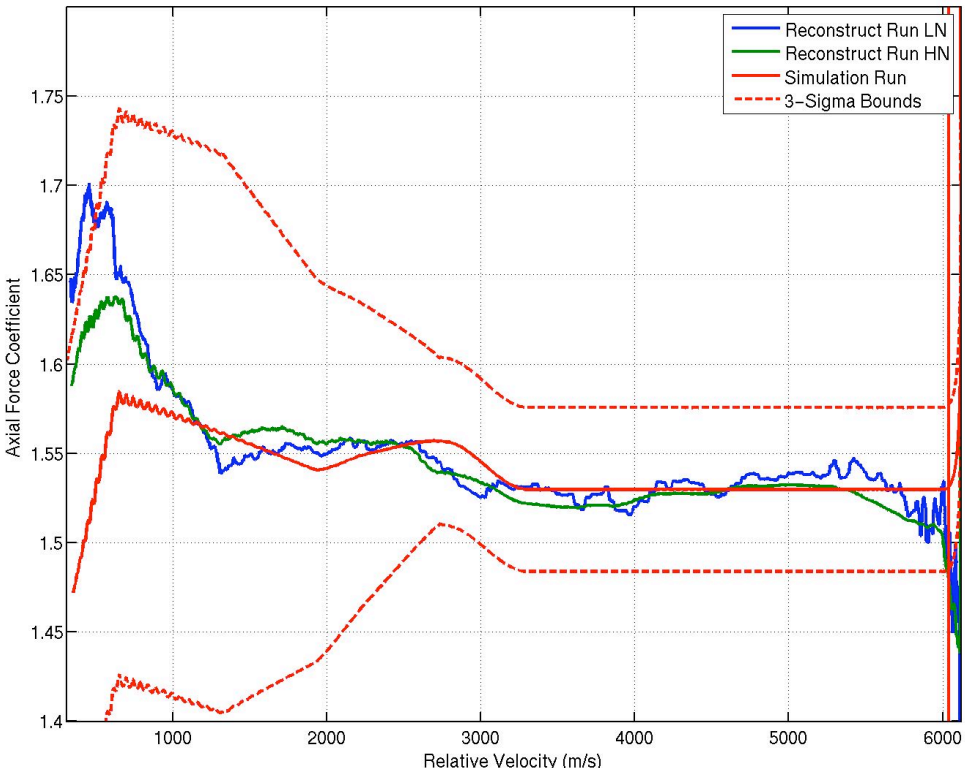

Figure 5-14. Estimated Entry Aerodynamic Axial Force Coefficient Values

Figure 5-14 shows the actual axial coefficient values corresponding to the estimated uncertainty parameters throughout entry for both the HN and LN versions of this reconstruction case as well as the simulation only case as a function of relative velocity. The 3-σ axial force coefficient uncertainty bounds established before probe entry are also shown in the figure. Note that the even in the extreme case of assuming all errors are in the aerodynamics (the LN case) the axial force coefficient is within the pre-entry boundaries throughout most of the entry, until about 400 m/s or Mach 1.5. As expected, the LN case has more variation in the axial coefficient than the HN case. Also, the HN result (which is closer to the nominal aerodynamics) are roughly the mean of the LN case as would also be expected since the HN case does not "chase" the measurement data points as rapidly as the LN case does. This reconstructed case shows that little

adjustment in C_A is required to be consistent with the flight data throughout most of the entry. This result indicates that the pre-entry aerodynamics predictions appear to have been accurate within the degree of uncertainty associated with the analysis.

5.2.2 Main Parachute Drag

After the entry aerodynamics necessary to match the measured accelerations had been established, attention focused on the Main parachute phase. During this phase, only the parachute drag was estimated; the atmospheric density was taken from the value reconstructed using the onboard measurements and the winds were taken from the Titan-GRAM model. To ensure that values stayed within reasonable limits, the actual estimated parameter was related to the drag multiplier by an S-type sigmoid curve shown in Fig. 5-15. This curve (essentially a hyperbolic tangent) allows the estimated state to have any value but maintain the drag coefficient multiplier between 0.6 and 1.6 (in the example shown in this figure). The limit curve helped keep the estimates from large variations during the region before the acceleration data was smoothed; without the limit curve, these variations could lead to unreasonable solutions, such as those that reach the surface several thousand seconds too soon, but still matched the acceleration profile while on the parachute.

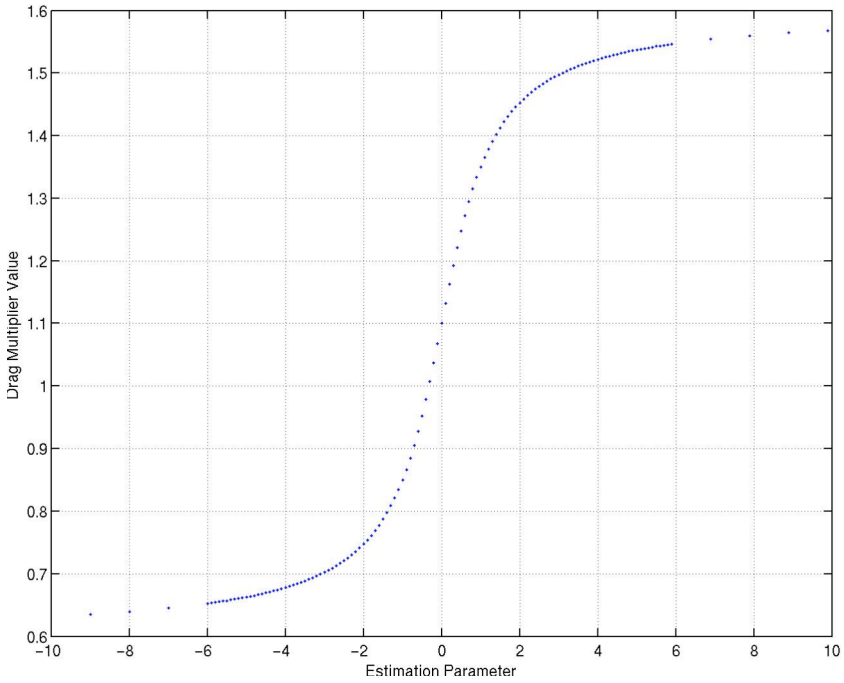

Figure 5-15. S-Curve to Limit Drag Multiplier Value Estimates

Results from the reconstructed trajectory are shown in Figs. 5-16 to 5-19. Figure 5-16 shows the axial acceleration at the very beginning before data smoothing is used. Figure 5-17 shows axial acceleration through most of the main parachute phase where nearly all of the data is smoothed. The figures indicate that good agreement with flight data is obtained by the reconstructed trajectory. The agreement is very good when the smoothed data is reached (at about 355 sec). This excellent agreement is also evident in the residual error in the longitudinal acceleration component shown in Fig. 5-18. After data smoothing begins, the error is less than +/- 0.002 m/s^2.

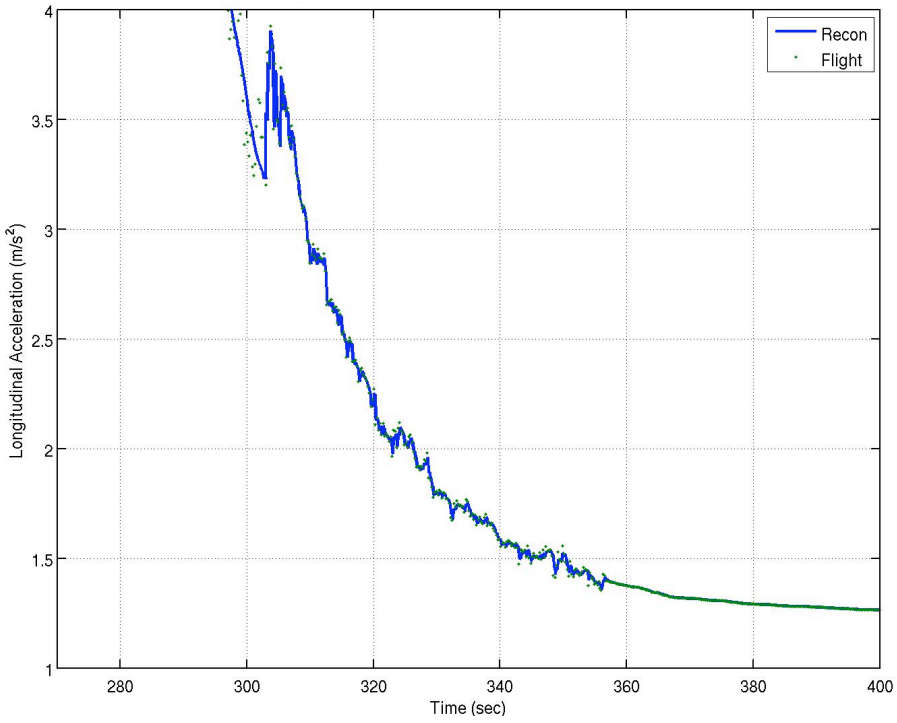

Figure 5-16. Axial Acceleration in Main Parachute Phase – Before Smoothed Data

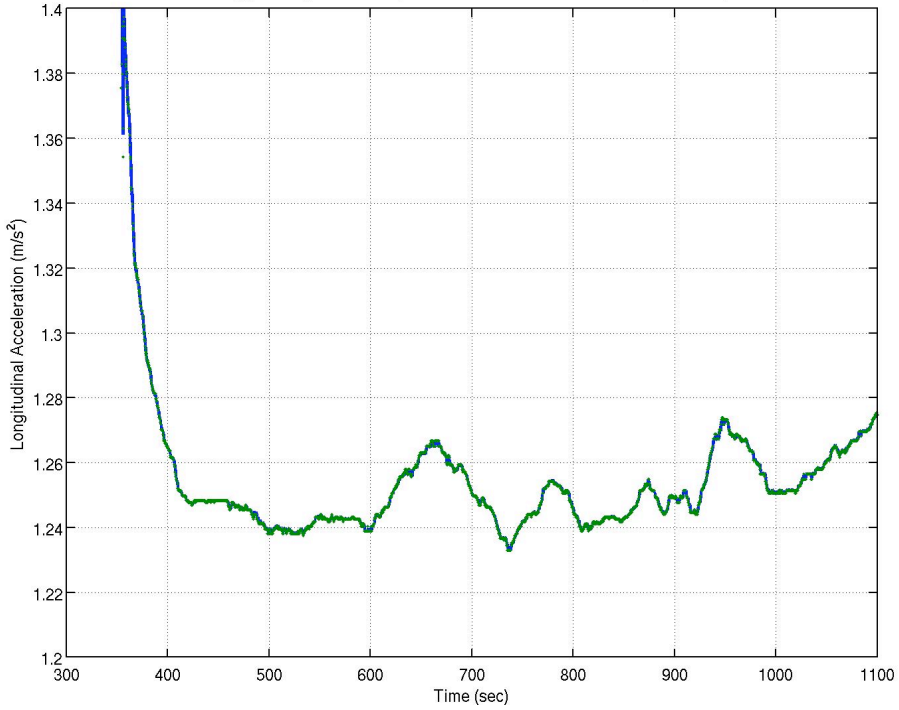

Figure 5-17. Axial Acceleration in Main Parachute Phase – In Smoothed Data

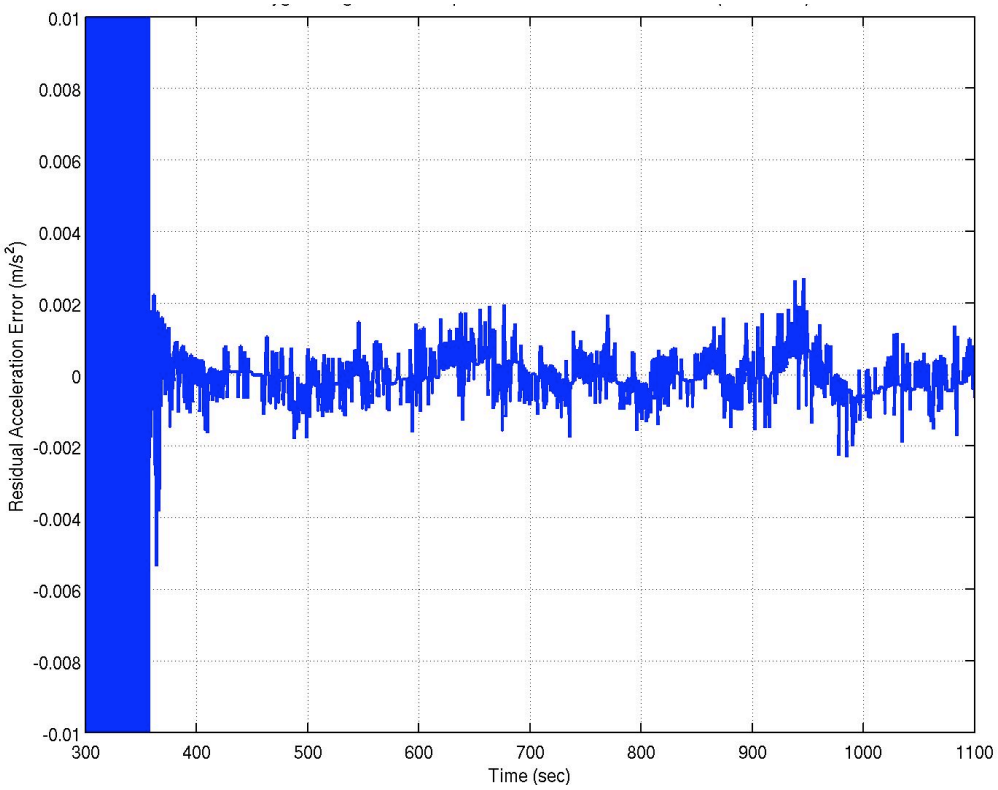

Figure 5-18. Axial Acceleration Residual in Main Parachute Phase Data

The parachute drag multiplier necessary to obtain this good agreement with the flight data is shown in Fig. 5-19. After the initial parachute transients, the multiplier rises to about 19% higher than the pre-flight value. Over the remainder of the Main parachute phase (about 15 minutes), the multiplier gradually drops to around 9% above the pre-flight values. Note that this change is somewhat sinusoidal which could indicate a small variation in another quantity (such as horizontal wind) not considered in this phase. However, the multiplicative factor shown is near the 11% increase predicted by Juan Cruz of NASA before entry. That is, the pre-flight model used by NASA had a factor of 11% above the nominal values applied to the ESA parachute drag model. Thus, the difference between the reconstructed flight values and the NASA prediction was at most

about 7%, which is within the 10% uncertainty bound (this 3-σ bound is in addition to the 11% nominal increase set before flight).

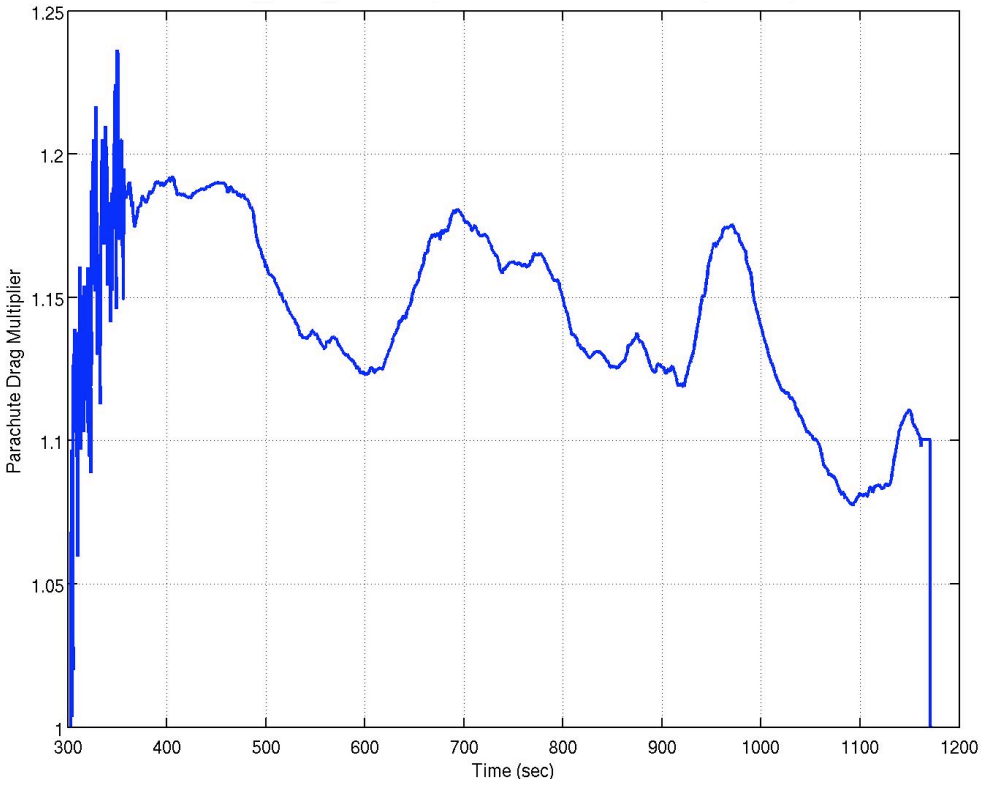

Figure 5-19. Main Parachute Drag Multiplier

5.2.3 Drogue Parachute Phase

For the entry and Main parachute phases, the dominant aerodynamic force acts in the direction of the one accelerometer (i.e., axially). The Drogue parachute phase was more difficult to reconstruct for several reasons. First, while the assumption was that the parachute was only influenced by drag, some side force would be created when the vehicle velocity (or parachute) is not aligned with the vehicle axis of revolution. Without lateral acceleration measurements, off nominal conditions (such as wind gusts or lifting

parachute) are difficult to verify. Also, there are multiple possible solutions that can match the axial acceleration, but not satisfy other measured constraints (such as total descent time) due to the unknown amount of lateral (and thus total) acceleration sensed by the system. Second, the probe spent more than two hours on the Drogue parachute at near terminal velocity (very little acceleration). Finally, the acceleration data collected had nearly +/- 0.1 m/s^2 of noise in the signal. Integrating the accelerations with this error directly would lead to numerical stability issues.

During the Drogue phase two significant observations can be made about the measured accelerometer data. First, some dynamic event appears to begin around 1800 sec and exists through about 4000 sec, with the dynamics smoothing out after about 2200 sec. This event is marked by a notable jerk (time derivative of acceleration) throughout. That is, something caused the acceleration rate to change unlike that expected from the nominal parachute. Second, the measured value of axial acceleration is inconsistent with a vertically hanging probe traveling at terminal velocity. That is, the expected axial acceleration value for that condition and probe orientation should be Titan's gravity. However, the measured accelerations are a couple percent too low. These two situations are discussed further below.

To reconstruct the Drogue parachute phase, the Drogue drag and atmospheric wind multipliers were estimated. The atmospheric density calculated from the measured pressure and temperature was used directly. As was noted earlier, due to the limited acceleration data (only the axial component is usable for reconstruction) several possible solutions can exist. The following result is a solution for the data available, but is not the only solution.

5.2.3.1 Early phase dynamic jerk event

Figure 5-20 shows the results of the reconstruction run and the flight data during the early part of the Drogue parachute phase. In the first 500 sec of the Drogue phase, the parachute is decelerating towards terminal velocity and showing variation in axial acceleration consistent with that in the Main parachute phase (on the order of 0.04 m/s^2 variation). The as yet unexplained event appears to begin around 1800 sec and exist through about 4000 sec, with the variations smoothing out after about 2200 sec. This unexpected jerk (acceleration derivative) in the profile can be noted in Fig. 5-21 where the time derivative of the air relative velocity is changing whereas a parachute approaching terminal velocity would be expected to exhibit smoother behavior as the velocity rate approaches zero as indicated in the simulation only case. This unexpected situation could have been caused by several possible events. These events could be horizontal wind shear, the parachute slipping into and out of a gliding mode, or the parachute characteristics changing due to environment (such as the parachute porosity reducing). None of these possibilities was confirmed in this analysis.

While the exact cause of this long event may never be known, the effect on the axial acceleration is clearly in the data. For this reconstruction, the variability in the acceleration is characterized by a changing parachute drag. While this representation may not be the actual reason, the resulting trajectory is consistent with the flight data. Figure 5-22 shows the drag multiplier on the Drogue parachute necessary to match the accelerometer data during this first event. Note that although the multiplier varied from nearly 40% to almost 220% these changes occurred over tens of minutes.

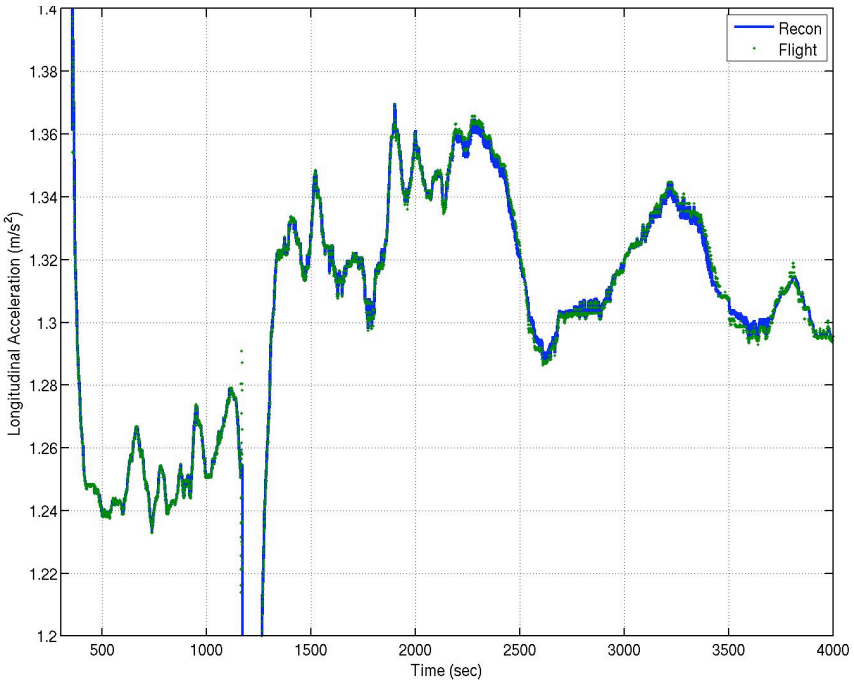

Figure 5-20. Early Drogue Parachute Phase Acceleration Comparison of Reconstructed Trajectory and Flight Data

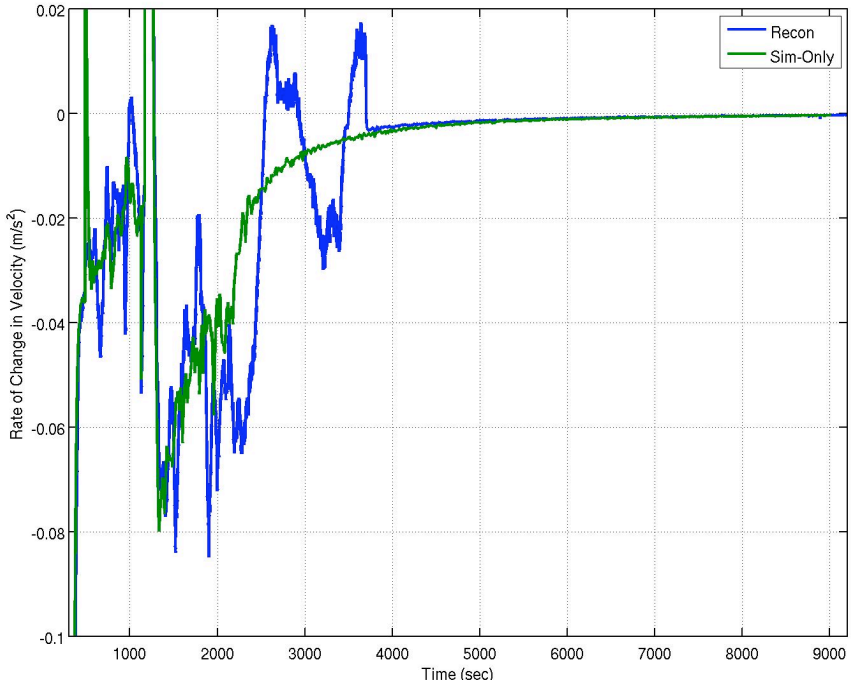

Figure 5-21. Profile of time derivative of relative velocity

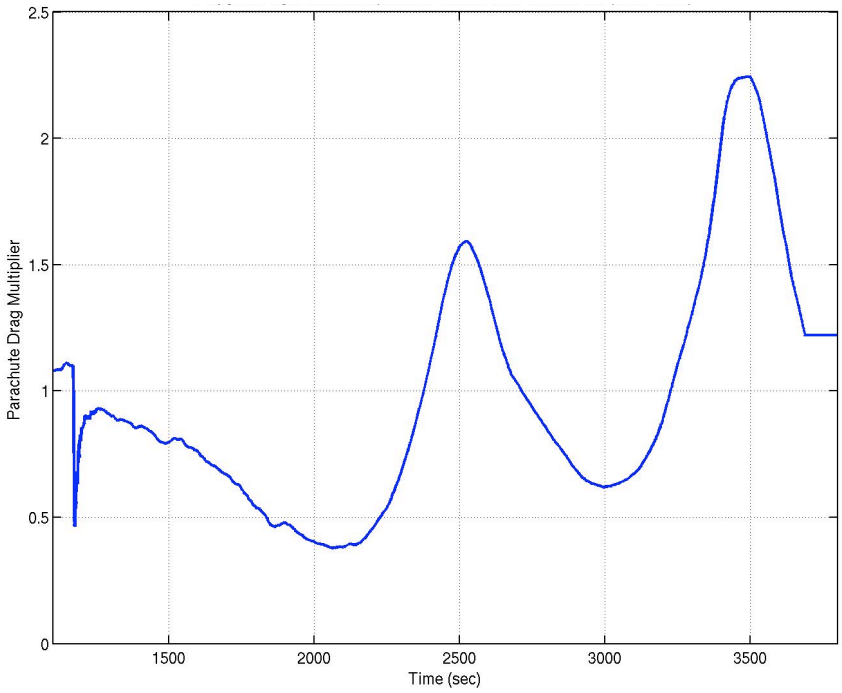

Figure 5-22 Reconstructed Parachute Drag Multiplier in First Part of Drogue phase

5.2.3.2 Late phase angle from vertical

During the last part of the probe descent on the Drogue parachute (after about 4000 sec), another interesting situation occurred. Figure 5-23 shows the comparison of accelerations from a simulation only run, accelerometer bias reconstruction, unbiased flight accelerometer data, and gravity acceleration during the drogue parachute phases. Since the parachute should be at or very near terminal velocity, the measured acceleration should equal the acceleration due to Titan's gravity if the probe was hanging vertically and the gravity vector was perpendicular to the local horizon (regardless of parachute drag values assumed). Note that the simulation-only run and gravity have nearly the same acceleration after about 4000 sec; whereas, the measured (unbiased) axial accelerations are notably below the gravity values. That is, since the final 90 minutes of the descent on

the drogue parachute was at or near terminal velocity, the measured accelerations should have been near the gravity of Titan and it was consistently lower by about 0.02 m/s^2 (or 1-2%).

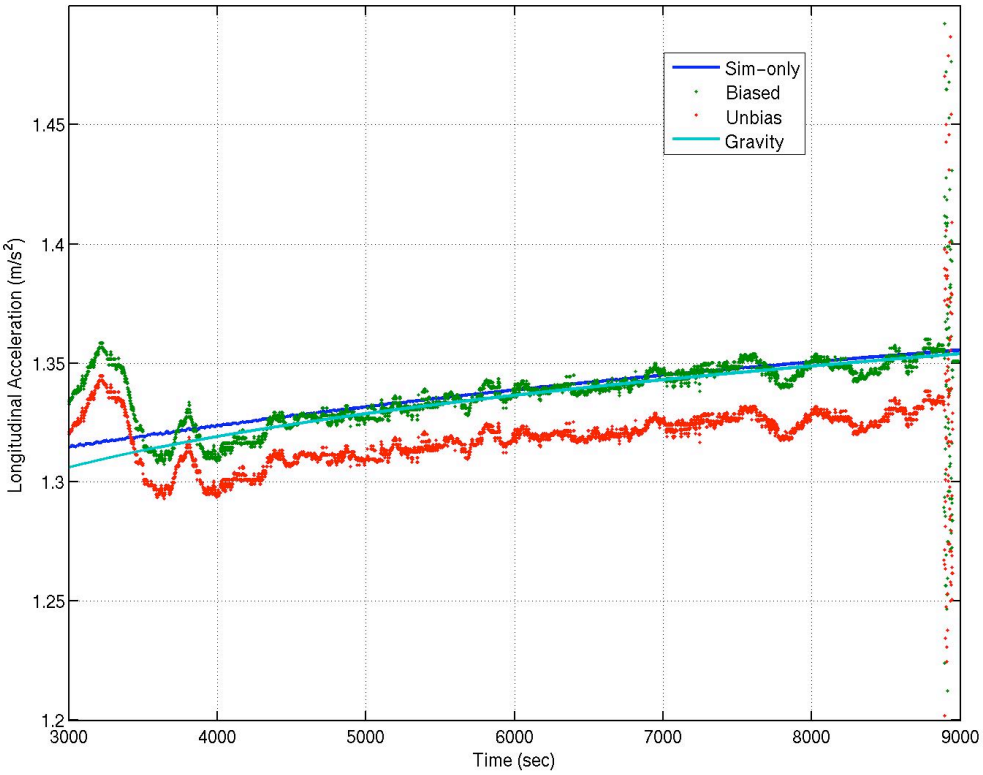

Figure 5-23 Accelerations and Accelerometer Data in Drogue Phase

Several different possibilities were considered to explain this situation: Titan mass concentration affecting the local gravity vector; unmodeled thrust from an instrument; bias or misalignment in the Servo axial accelerometer; and probe tilt resulting in an angle between the probe axial accelerometer and the gravity vector. In order to affect the gravity value in the region that the probe landed, a (negative) mass concentration that would produce about -0.02 m/s^2 (or -2000 mGal) acceleration change would be needed. When compared with the largest values of mass concentrations on the Earth's Moon (a body with the some of the highest mass concentration variations in the solar system)

which Konopliv indicates reaches around -500 mGal,[45] the -2000 mGal required at the Titan landing site appears to be too large (on the order of 4 times higher). A mass concentration of this size would affect Cassini's orbit as it passed Titan, and no indication of this effect has been reported. Thus, mass concentration seems an unlikely explanation. Another possibility involved unmodeled thrust acting along the axial direction. The Gas Chromatograph and Mass Spectrometer was considered since it expelled mass in the axial direction after analyzing a collected atmospheric sample, however the Principal Investigator indicated the force created by the expulsion process would be well below that require to produce the 0.02 m/s^2 acceleration sought.

Another possible explanation involved an accelerometer bias or misalignment. A reconstruction case was run to determine the bias required to bring the measured accelerations inline with the gravity. Figure 5-24 shows the bias solution determined from the reconstruction run. The biased accelerations are shown in Fig. 5-23. As expected, the accelerometer would have been biased about 0.022 m/s^2 during this long drogue parachute phase to bring the measurements into agreement with other factors (deceleration near the value of Titan's gravity, total flight time, etc). An accelerometer bias of this magnitude (about 2200 μ-g) is unusually large and not anticipated for a space quality instrument, particularly since just prior to atmosphere entry the bias was determined to be about 23 μ-g, as mentioned earlier. This change in bias by a factor of about 100 would mean that either the events occurring during the EDL, or the environment at Titan (i.e., minimum temperature during Drogue phase of 70 K) can substantially modify navigation sensors. As for accelerometer misalignment, for an error of about 0.022 m/s^2, an offset of around 10 degrees between the measurement direction and the actual acceleration vector would be required to match the acceleration

measurements. Although ten degrees is difficult to detect visually, an angular misalignment of that magnitude for a flight instrument is unlikely.

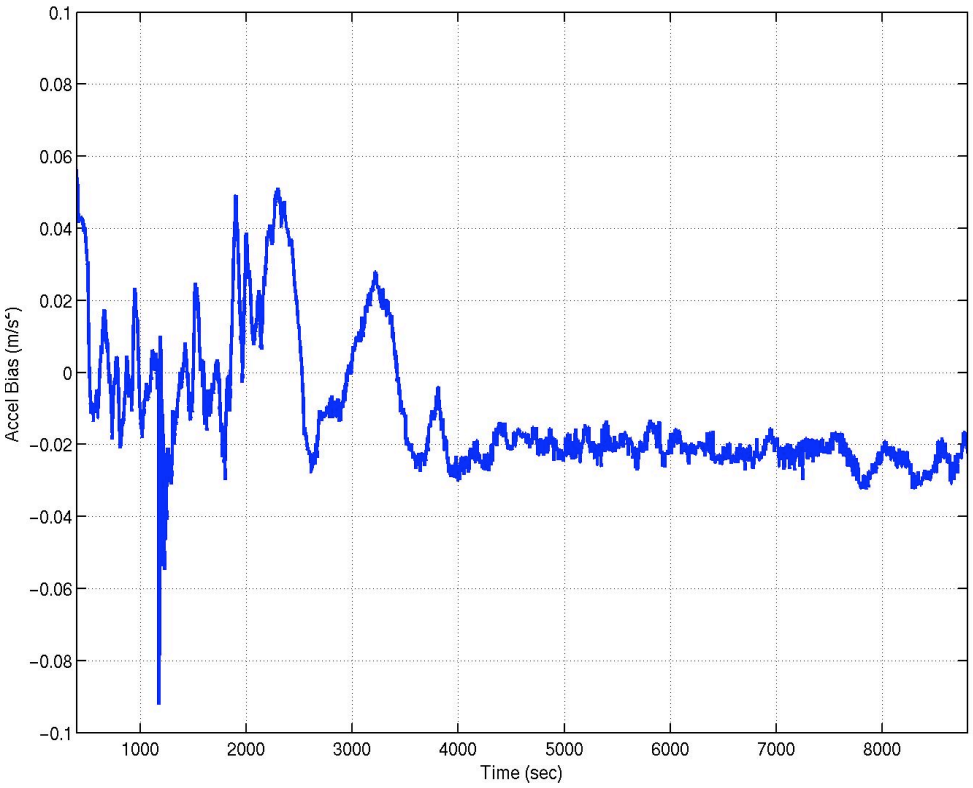

Figure 5-24 Estimated Bias to Measured Accelerometer Data

The last explanation considered in this analysis is a tilt angle on the probe. In this phase of the reconstruction, a constant parachute drag coefficient multiplier was chosen and the necessary probe tilt angle was estimated; choice of drag multiplier does not impact the issue of the axial accelerometer not matching Titan's gravity since any multiplier should eventually reach the steady state condition of terminal velocity. Since the NASA pre-flight estimate of Main parachute drag multiplier had good agreement with flight data (see section 7.4.2.3), the NASA pre-flight Drogue parachute multiplier of 22% was selected. Figure 5-25 shows the axial acceleration from the reconstructed trajectory

compared to the flight data. Figure 5-26 indicates an angle of around 10 degrees between the axially directed accelerometer and gravity was needed. As shown above, this off-vertical angle result agrees with flight data returned from an onboard tilt sensor (the SSP tilt sensor). That data indicated a mean value of tilt over the Drogue parachute phase around 8.7 deg. However, the Descent Imaging team maintains that the probe could be tilted no more than a couple of degrees based on analysis of images taken during descent.

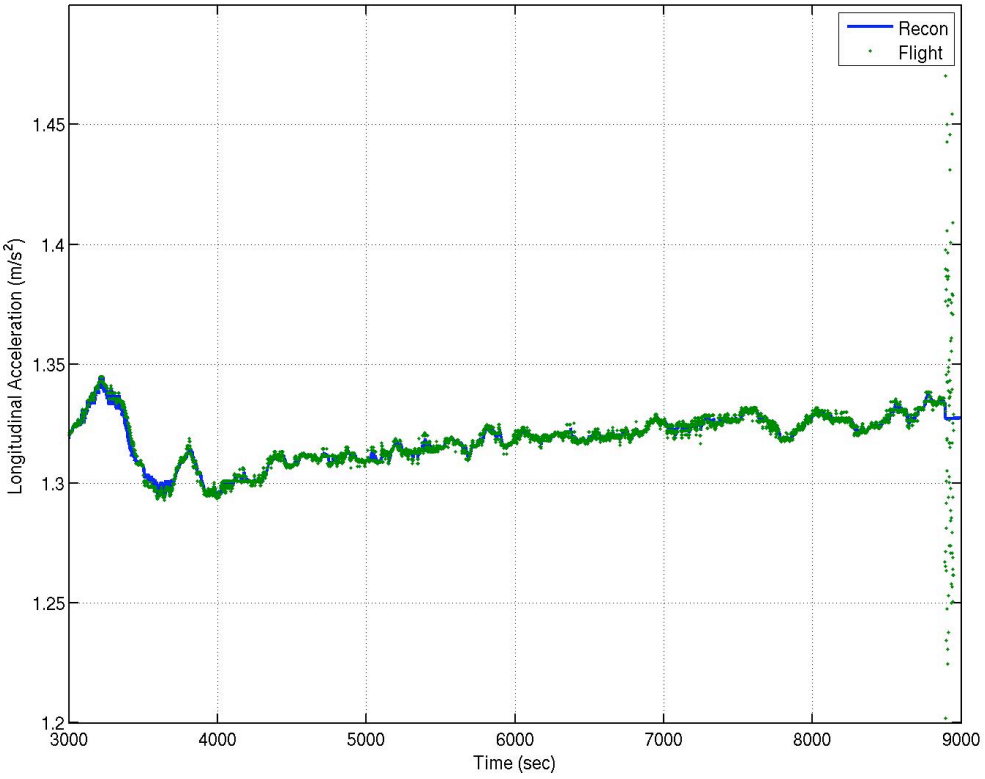

Figure 5-25 Tilt case reconstructed trajectory and flight axial accelerations.

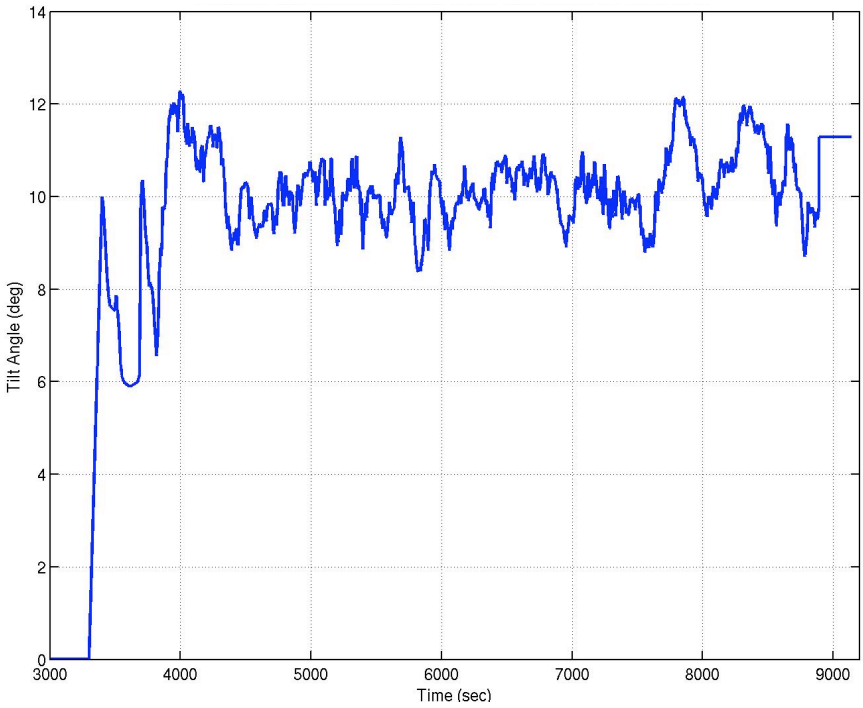

Figure 5-26 Estimated tilt angle required to match measured accelerations

5.2.3.3 Wind Velocity Estimates

Both the horizontal and vertical wind profiles were also estimated. Figure 5-27 shows the horizontal winds from this reconstruction, Titan-GRAM model winds, and the two wind profiles based on DWE generated data; note in this figure, the DWE#1 (cyan line) and DWE#2 (red line) are the same except for the 100 to 60 km region. At high altitudes, horizontal winds of about 50% higher than pre-flight Titan-GRAM and the post-flight value provided by the ESA project were estimated. Note that this result could be an artifact of matching the accelerations throughout the unexplained event mentioned above; the state estimation case given in the section below used the DWE#2 profile in Fig. 5-27. However, in the area of the tilt angle analysis, below about 50 km, the reconstructed trajectory winds were as much as 50% lower than the Titan-GRAM model,

but these reconstruction values were still higher than the ESA winds at these altitudes. Additionally, reduction in wind velocity at roughly 75 km (or 2000 sec from atmospheric interface) to nearly zero followed by an increase back to the original profile indicated by ESA was not confirmed by this analysis. However, a near 40 m/s departure, around 115 km altitude (or 1000 sec from atmospheric interface), just before drogue parachute deployment can be seen in Fig. 5-27. It should be noted that the wind profile provided by ESA used probe velocity from Earth-based radio telescope measurements from which winds were inferred.

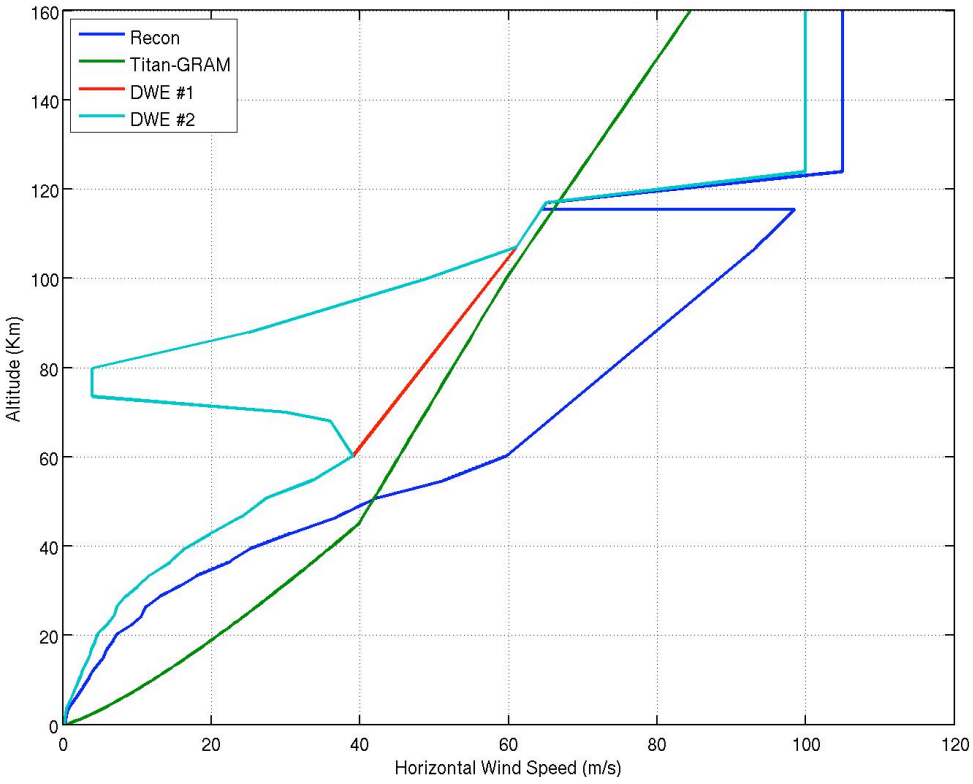

Figure 5-27 Comparison of horizontal wind speeds

The estimated vertical wind speed during the Drogue phase is shown in Fig. 5-28. As noted in the figure, the estimated vertical wind speed of around 0.5 m/s directed

upward (i.e., updraft) was determined. This case also assumed a probe tilt after 3800 sec. This vertical wind velocity was used to assure the final landing time constraint was met. The estimated altitude profile from this reconstructed trajectory is shown in Fig. 5-29.

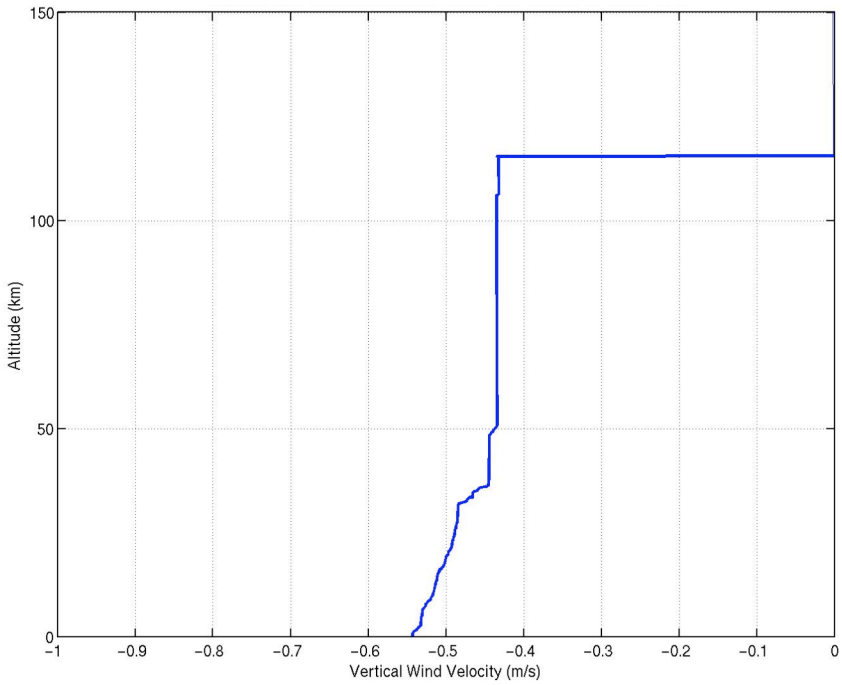

Figure 5-28 Estimated vertical wind velocity for reconstructed trajectory

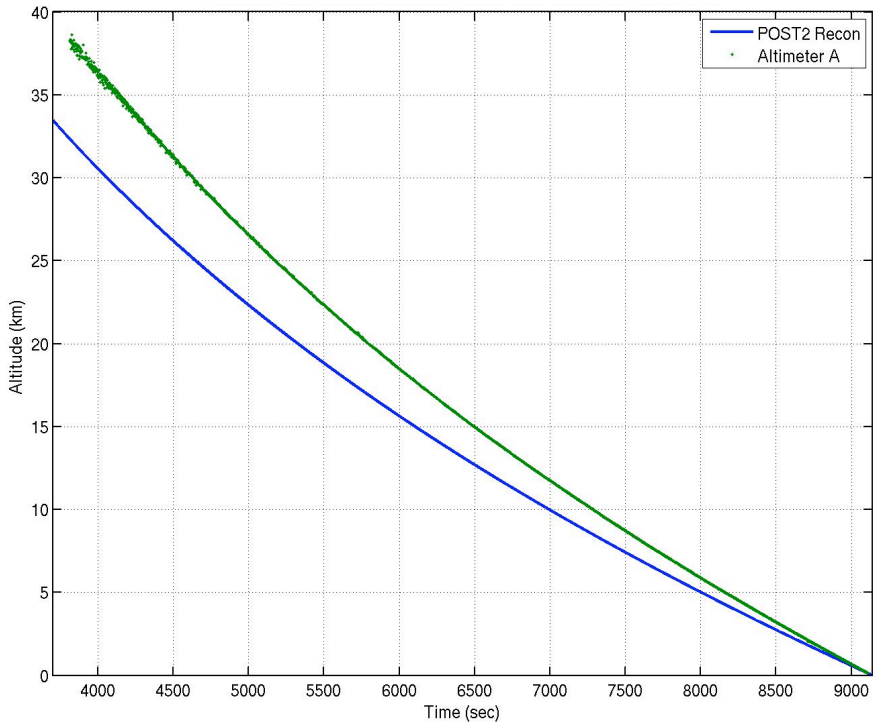

Figure 5-29 Altitude comparison between reconstructed trajectory and Radar

5.3 END-TO-END POSITION, VELOCITY ESTIMATION

The following trajectory reconstruction runs, focused on estimating the vehicle position and velocity throughout the entire EDL trajectory, were done using the initial state determined from the Monte Carlo analyses as indicated above. A ten degree tilt angle based on the result determined above was also applied to these cases. The density profile based on HASI instruments and the DWE wind profile (profile #1 in Fig. 5-27) were used. The deceleration pulse during entry for this reconstructed trajectory is shown in Fig. 5-30. The region of maximum deceleration in this figure shows that the reconstruction run captured the acceleration well; however it did not overly adjust the

state to meet the measurements. The region just after parachute deploy also shows good agreement between the flight and reconstructed accelerations.

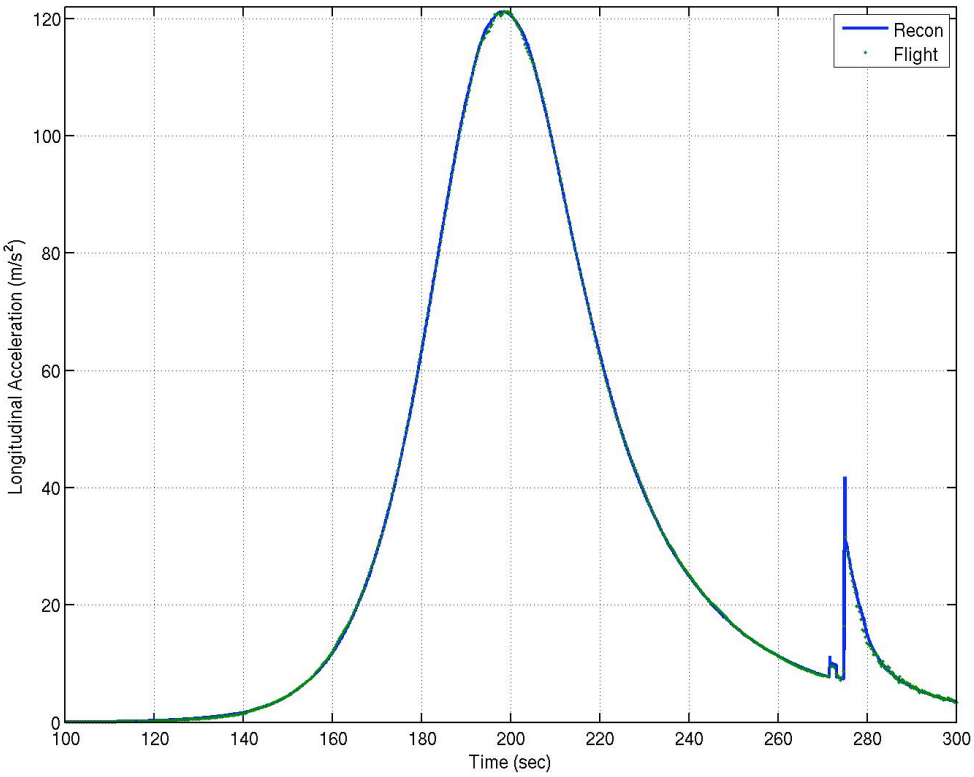

Figure 5-30. Huygens Flight Data Compared to State Estimate Reconstruction Run– Entry Phase

Figures 5-31 and 5-32 focus on the flight data comparison at the end of the Main parachute and throughout the Drogue parachute phases. These figures illustrate the agreement in axial acceleration between the flight data and those generated using the reconstructed trajectory. The reconstructed trajectory data matches well through the fifteen minute Main parachute phase and through most of the Drogue phase. The curves separate slightly between 2000 and 2500 sec, but return to agreement as time progresses.

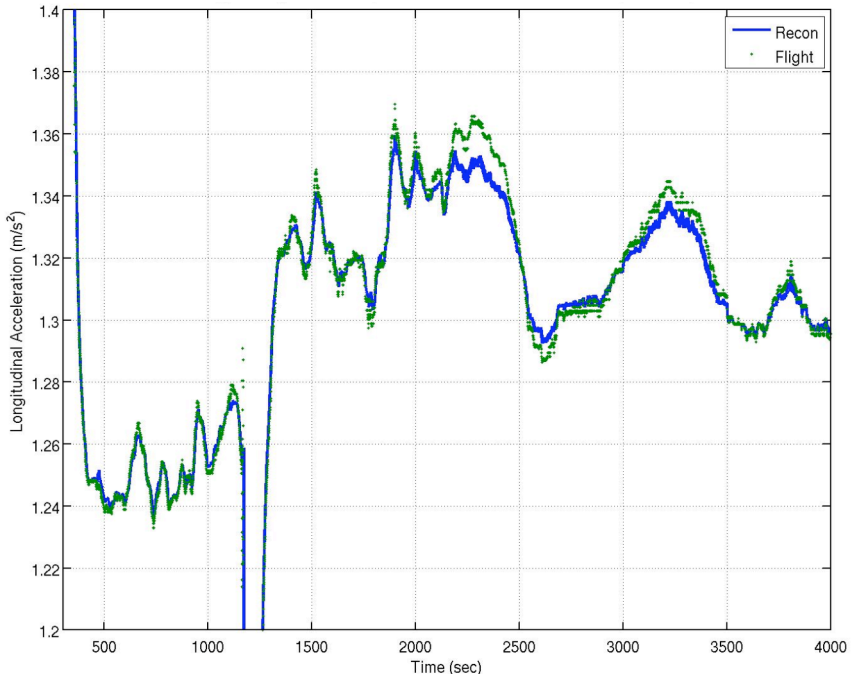

Figure 5-31. Comparison of Flight Data to State Estimate Reconstruction Run – Main and Drogue Parachute Phases

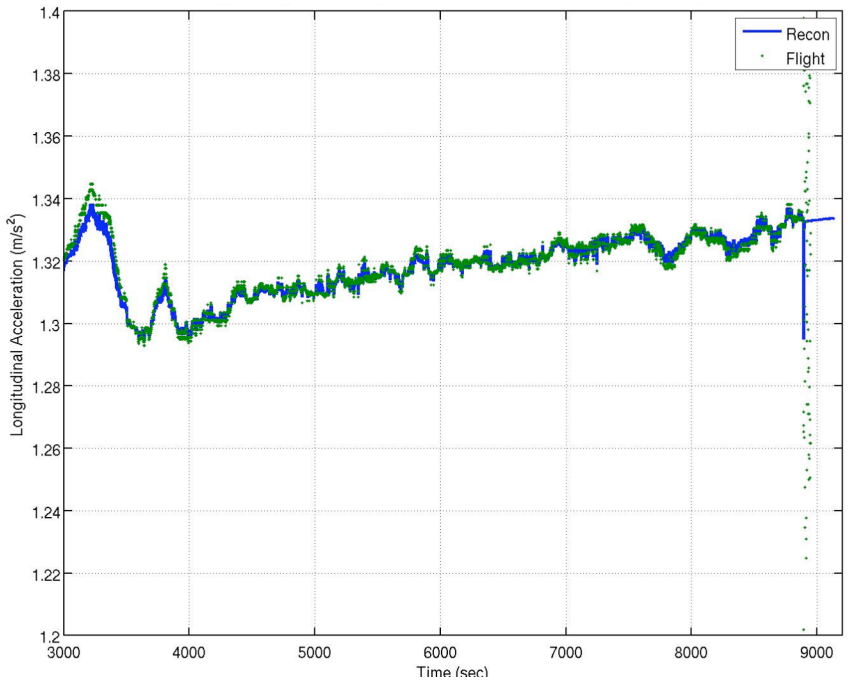

Figure 5-32. Comparison of Flight Data to State Estimate Reconstruction Run – Drogue Parachute Phase

Figure 5-33 shows another approach to measure how well the reconstructed trajectory matched the actual flight. This figure shows the difference between the accelerations compared in the figures above. The largest differences in the residual acceleration error are noted during the entry phase and the parachute deploy events. However, throughout most of the reconstructed trajectory, the acceleration error is near zero. A running sum of this error (absolute value) is shown in 5-34. As was noted above, the largest error occurs during entry and parachute deployment.

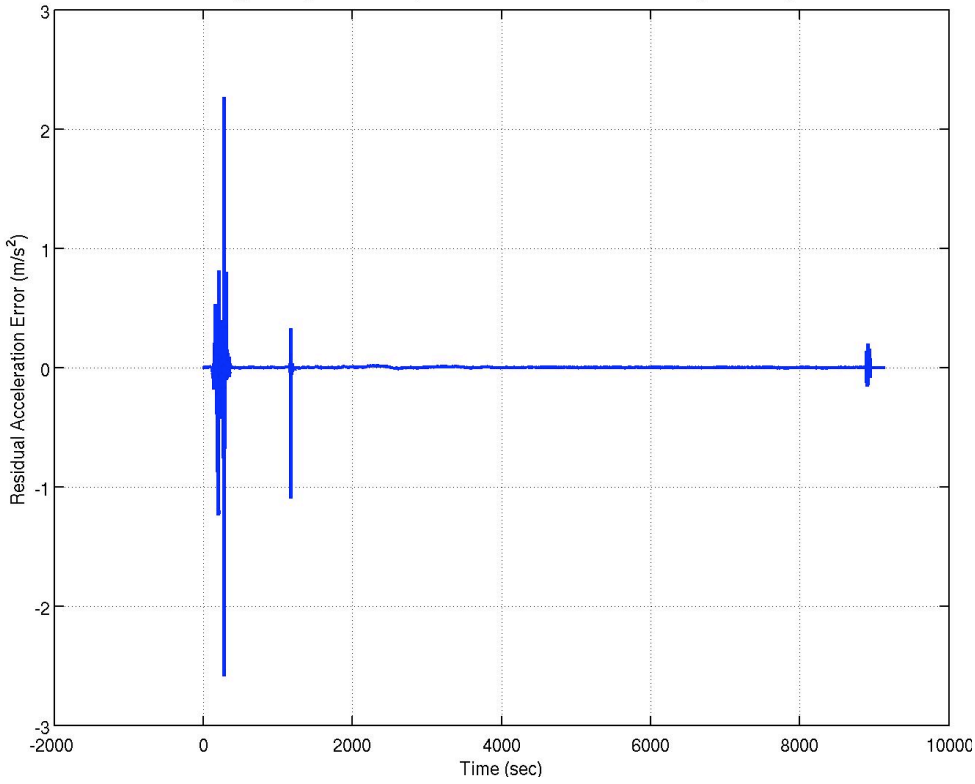

Figure 5-33. Residual acceleration error for reconstructed state case

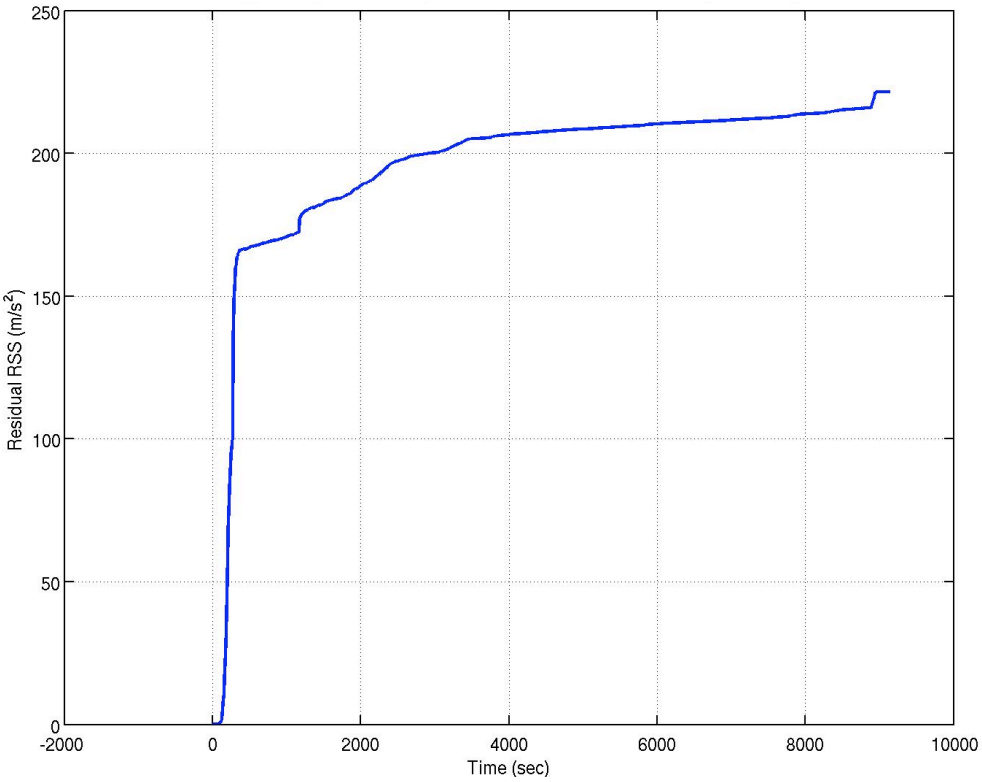

Figure 5-34. Running total of residual error for reconstructed state case

Figure 5-35 shows the altitude versus velocity profile for the reconstructed state. Even though the state is adjusted at each measurement point, a smooth profile is generated. The profile of the Main and Drogue parachute phases is shown in Fig. 5-36. The front shield release and Drogue parachute deployment events are noted at about 155 and 115 km, respectively. The front shield release event causes a change in probe aerodynamics and mass. Also note that the change in wind speed around 120 km altitude (from the DWE profile) affects the velocity change at that altitude. Table 5-2 gives key event data from the reconstructed trajectory. The total time is consistent (to within a few seconds) with that reported by Lebreton. [36]

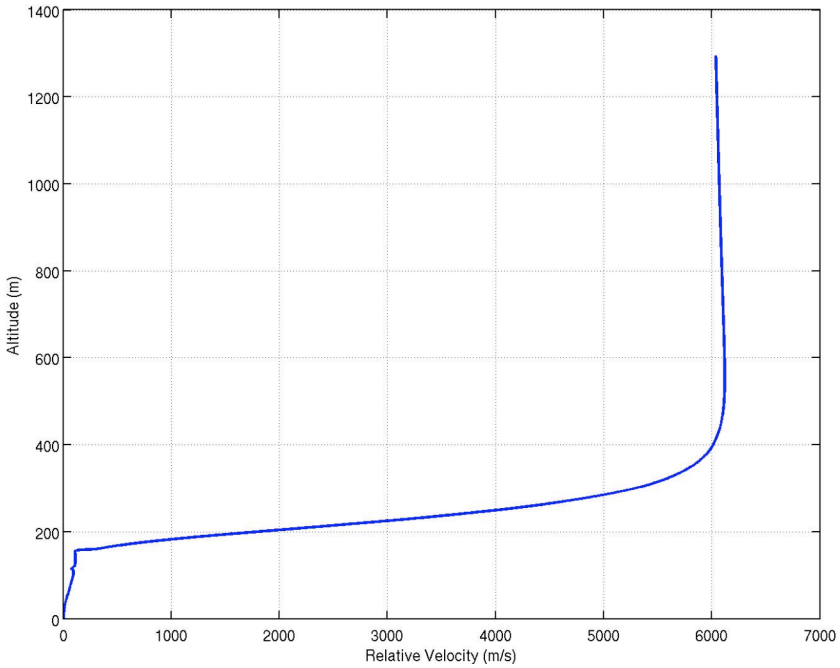

Figure 5-35. Altitude Velocity Profile for State Estimate of Case 8724

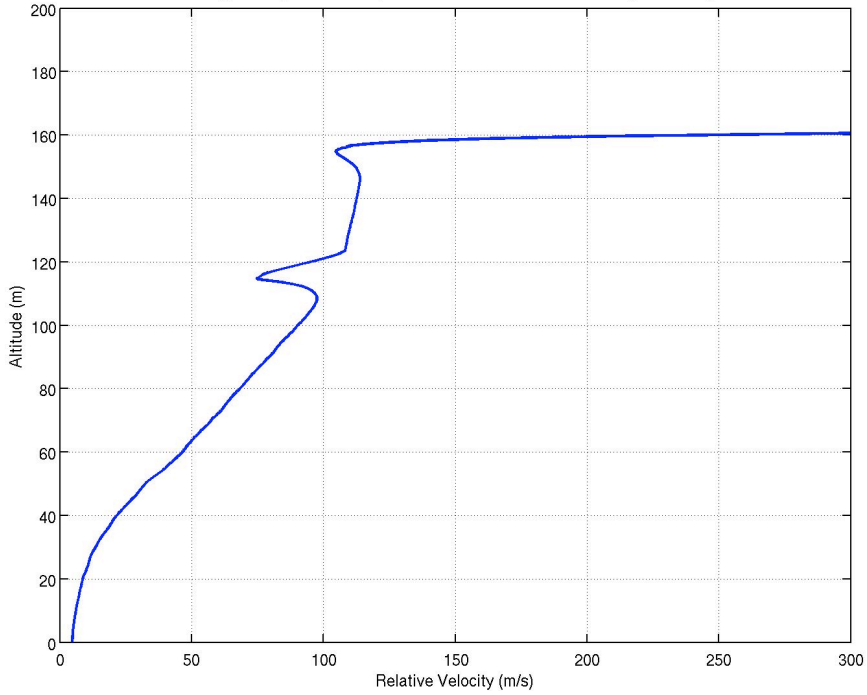

Figure 5-36. Altitude Velocity Profile for State Estimate of Case 8724 – Main and Drogue Parachute Phases

Table 5-2. Key Event Data From State Reconstructed Trajectory

	Time (sec)	Altitude (km)	Relative Velocity (m/s)	Mach Number	Dynamic Pressure (Pa)
Entry	0	1267	6039	21.2	0
Pilot Mortar Fire (T0)	271	162.4	349.6	1.42	298
Main Parachute Deploy	273	161.5	330.3	1.35	251
Front Shield Release	303	156.6	110.0	0.40	24.6
Main Parachute Release/ Drogue Chute Deploy	1171	114.6	74.5	0.14	9.3
Touchdown	9135	0	4.6	0.02	60.1

A comparison of the altitude versus time for the reconstruction case and the radar altimetry data for unit A is included in Fig 5-37. As noted in the figure, the reconstruction case is slightly below the radar altimetry, by about 5 km, at the highest altitude but then reduces to less than 100 m by touchdown. A comparison of several reconstruction cases is shown in Fig. 5-37. As noted in this figure, all of the cases show a similar comparison to the radar data. These altitude profiles are consistent with those determined by the DTWG, HASI, and another NASA group, but not the radar data taken by the probe. [39]

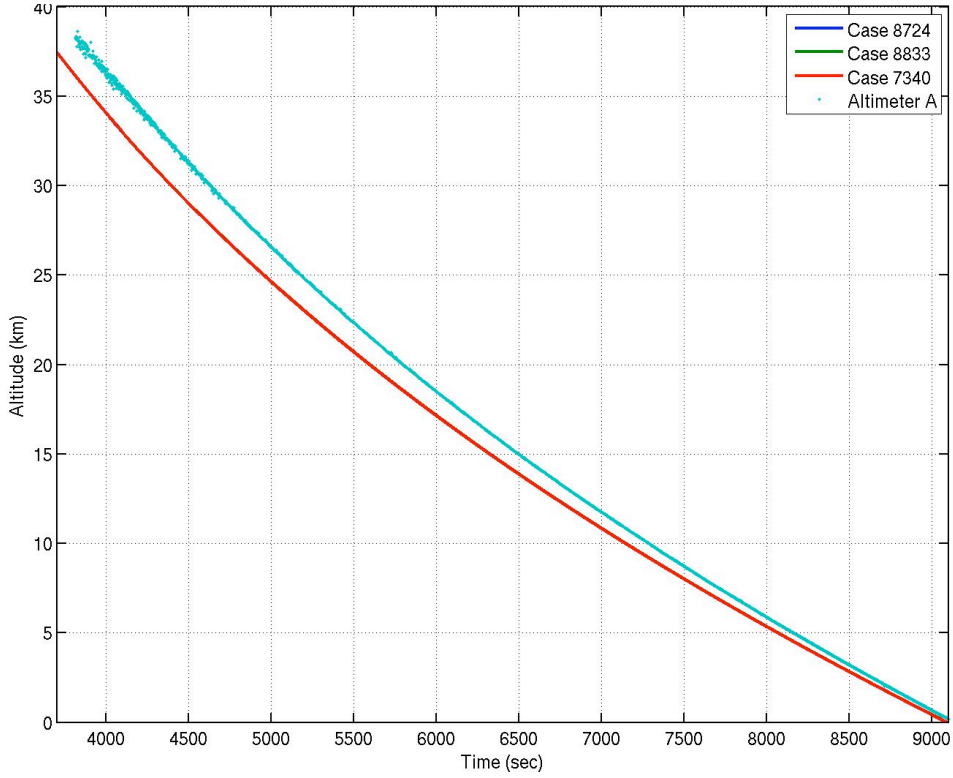

Figure 5-37. Altitude Profile for State Estimate of Several Cases –Radar Altimetry Comparison

5.4 HUYGENS RECONSTRUCTED TRAJECTORY OBSERVATIONS

An assessment of the reconstructed Huygens probe entry, descent, and landing trajectory yields several key points. The data for trajectory reconstruction was limited since no attitude rate or lateral acceleration data was available. Also, due to a ground command error, the wind profile determination was dependent on Earth-based observations. Multiple solutions exist that match the axial acceleration profile, but fail to meet total time of flight; for example, a lower drag coefficient estimate for the drogue parachute results in the probe being lower in the atmosphere faster (higher velocity and density) which produces the same axial acceleration as the measured profile until surface

impact several thousand seconds too soon. The use of a sigmoid curve to limit estimated parameter values to within expected ranges was very effective in preventing unreasonable trajectories such as the previous example. The entry axial aerodynamics and Main parachute drag were correctly predicted during the pre-flight analyses. A significant dynamic event occurred at the start of the Drogue parachute phase whose cause was not identified. Conflicting data and results with regards to probe tilt and altitude profile exist, with the conclusions of this analysis given below.

A comparison between the reconstruction calculated tilt and the tilt sensor value is given in Fig. 5-38. While the magnitudes are close (except the one spike at 5200 sec), similarity also exists in the character of the curves shown in this figure. Probe tilt angle as shown in this figure was generated from two independent datasets captured during flight – the axial acceleration and the tilt sensor. Note that any system moving vertically (atmosphere relative flight path angle at or near -90 deg) at terminal velocity must measure acceleration equal to gravity along that vertical direction. Since during this phase there is no indication of accelerating flight, atmospheric relative flight path angle of around -80 deg, or any reason that gravity would be directed 10 or so degrees from vertical, the current conclusion is that the probe axial direction was tilted about 10 deg from vertical. A 6.1% increase or decrease in the length of one riser would result in about a 10 deg tilt in the probe. Additional information from a lateral accelerometer would have helped clarify this disagreement, however as indicated above the laterally directed Piezo accelerometers were deemed not usable.

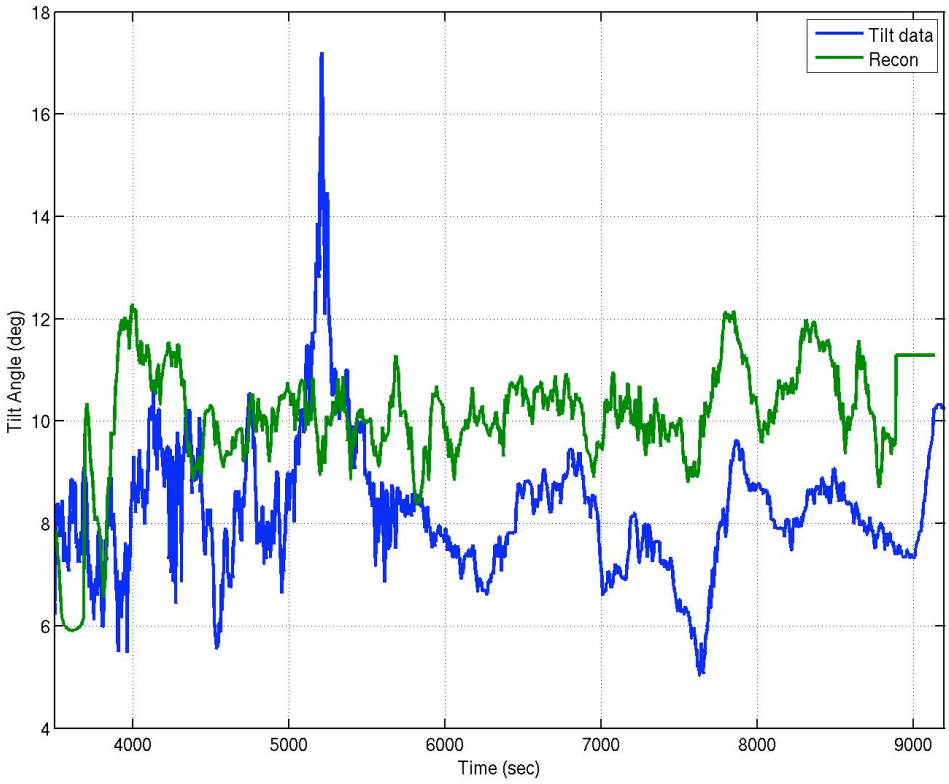

Figure 5-38 Tilt angle comparison between reconstructed and sensor data

Two independent sets of flight data, HASI Servo accelerometer and SSP Tilt sensor, provide results apparently in conflict with a third set, DISR images. The Descent Imager (DI) team has reported smaller tilt values as the probe descended to the surface (see Fig. 5-39). That is, the DI results indicate tilt angles as high as 10 degrees only above about 80 km (about ten minutes after Drogue deploy); whereas, probe tilt at lower altitudes (like 20 km, or about 70 min in the Drogue phase) are less than five degrees with only two degree tilt seen as the probe approached the surface. The assessment of the current research concurs with results from the tilt sensor, not the DI team assessment.

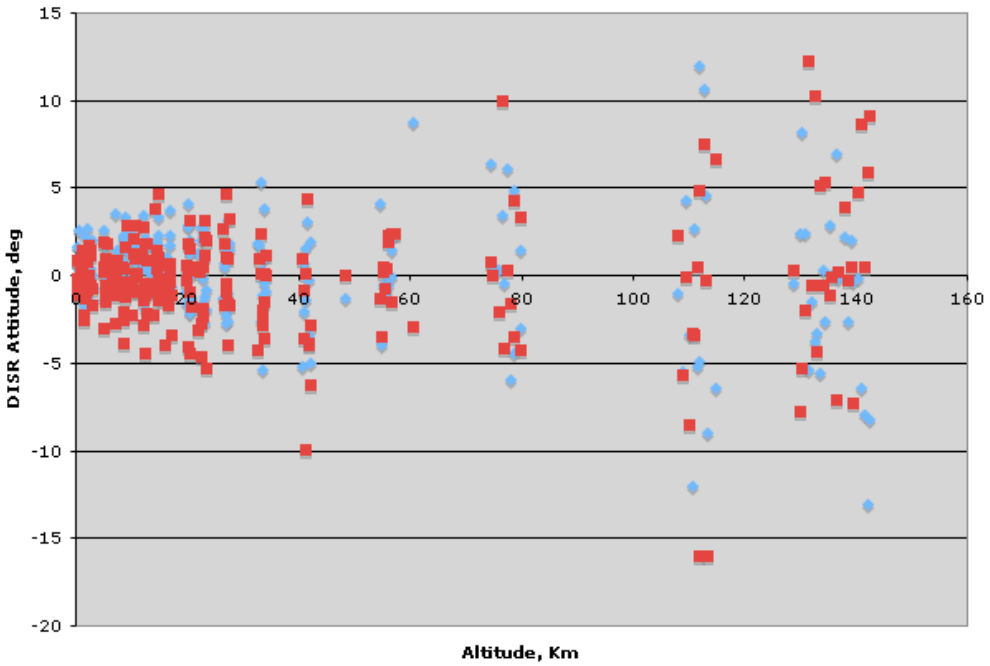

Figure 5-39. Huygens probe attitude as reported from DISR analysis [46]

The reconstructed trajectory altitudes are consistent with the DTWG profile that is in conflict with the radar data. However, a scale factor applied to the radar data could rectify this difference. Figure 5-40 shows the effect of a 0.93 scale factor on the radar data when compared to the same cases as shown in Fig. 5-37. This very good agreement between adjusted flight data and multiple reconstructed trajectories suggests that an adjustment of the radar data may be required. Alternatively, other possibilities exist that would also affect the radar measurements, namely radar electronics temperature sensitivity.

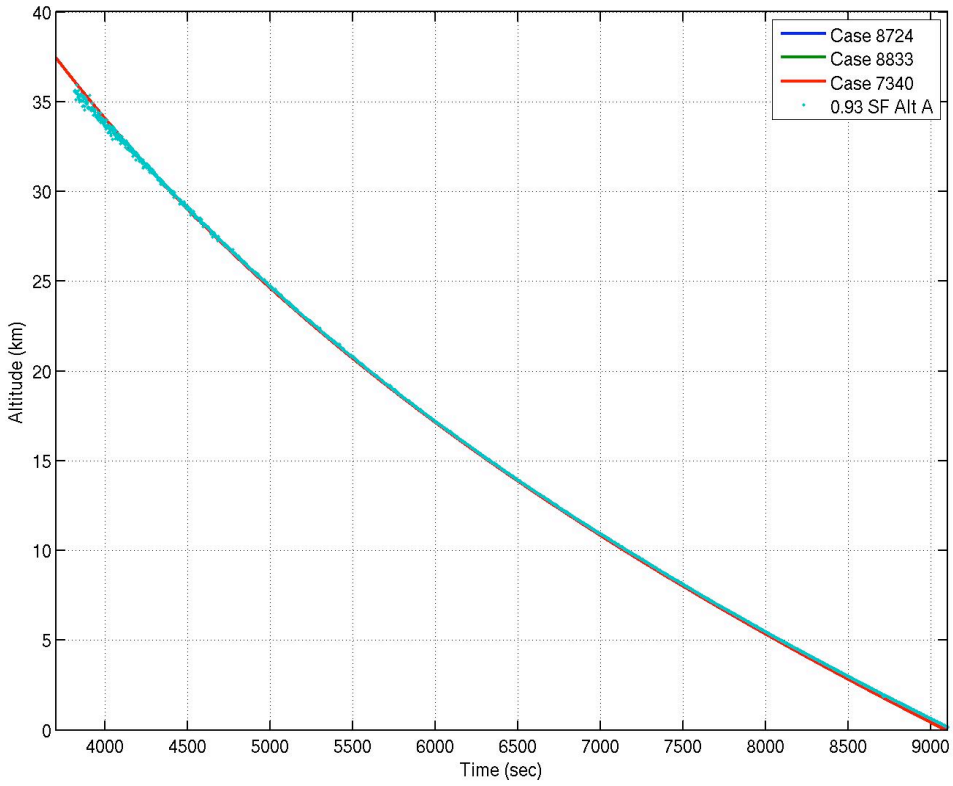

Figure 5-40. Altitude Profile for State Estimate of Several Cases–Radar Altimetry Scale Factor

Chapter 6: Summary, Conclusions, and Future Work

6.1 SUMMARY

6.1.1 Objectives and Background

The objectives of this research were to develop an Extended Kalman filter-based reconstruction capability using the Program to Optimize Simulated Trajectories II (POST2), apply this capability to reconstruct the Huygens Titan probe entry, descent, and landing (EDL) trajectory, evaluate the newly developed POST2 reconstruction module, analyze the reconstructed trajectory, and assess the pre-flight simulation models used for Huygens EDL simulation. On January 14, 2005, the European Space Agency (ESA) Huygens probe separated from NASA's Cassini spacecraft, entered the Titan atmosphere and landed on its surface. NASA was involved in the pre-entry EDL analyses of the probe. A POST2-based trajectory simulation was developed that included models of the probe aerodynamics, parachute trigger logic and drag models for the pilot, main, and drogue parachutes. The POST2 reconstruction module, developed as part of this research, was used in conjunction with the previously developed simulation to estimate the Huygens trajectory and assess pre-flight models.

As part of an agreement with ESA, NASA obtained the flight data from the probe so that trajectory reconstruction could be done and simulation models assessed. Trajectory reconstruction of the Huygens entry probe at Titan was accomplished using a simulation based method that was developed into POST2. Although the primary objective of the trajectory reconstruction portion of this research was to evaluate models used in the NASA pre-entry trajectory simulation, the resulting reconstructed trajectory was also

assessed against the Huygens project generated trajectory to provide an independent evaluation of the ESA result.

6.1.2 POST2 Reconstruction Module

The Program to Optimize Simulated Trajectories II is a generalized point mass, discrete parameter targeting and optimization trajectory simulation program. An extended Kalman filter (EKF) module was developed for POST2 as part of the current research to enable trajectory reconstruction and was integrated into POST2 in a similar fashion as the general optimization, constraints, and controls. This capability was developed to facilitate trajectory reconstruction using POST2-based mission specific simulations. The general nature of POST2 architecture was retained for this module; any POST2 input quantity can be a part of the estimated state and any POST2 outputs can be the observations. Separate files of observations and their associated weightings versus simulation time are required for use with this module. The utility of integrating this function into POST2 is to allow more rapid setup and execution of trajectory reconstruction runs using the same simulation that has been tested and validated for that particular mission. Note that the NASA Langley procedures for quality assurance testing were followed during the development process for this reconstruction module.

Several validation test cases were executed using the POST2 module for reconstruction. These cases ranged from a single, constant parameter estimate to multivariable estimation cases similar to an actual mission flight. The more complex cases were run from multiple starting conditions to measure how well the method produced the “truth” trajectory used to generate the test data. Based on test case output, the state estimation, observation weight and system noise covariance as well as general POST2 input functionality for reconstruction trajectory problems were confirmed to work

as desired. Results of these tests provided confidence that the reconstruction module in POST2 was functioning well and was ready for application to an actual flight trajectory reconstruction.

6.1.3 Huygens Titan Probe Trajectory Reconstruction

The main emphasis of the Huygens probe EDL trajectory reconstruction was to evaluate the simulation models used prior to probe entry on January 14, 2005 and to compare results with actual flight data. Another objective of the Huygens reconstruction was to compare the POST2-solved trajectory and the ESA determined altitude profile. The ESA Huygens probe science teams provided several sets of flight data from the Titan entry including vehicle accelerometer data (only one axis was usable), atmospheric pressure and density data (after probe heat shield separation around 160 km altitude), and radar altimetry data (below about 40 km altitude). This reconstruction uses accelerometer measurements to adjust an estimated state (e.g., position, velocity, and/or parachute drag, etc.) using a POST2-based simulation developed prior to entry to support EDL analyses and design.

A summary of conclusions and findings for the Huygens trajectory reconstruction identified from this assessment included the following:

1. Disagreement existed regarding the altitude profile of the Huygens probe below about 40 km when data from the onboard radars was compared to the profile reconstructed by ESA using measured atmospheric pressure and temperature. Another profile generated by Carlo Bettanini of the Huygens Atmospheric Structure Instrument (HASI) team using a different approach agreed with ESA's Descent Trajectory Working Group (DTWG). A NASA Engineering

Safety Center (NESC) analysis also agreed with DTWG altitude profile result by independently using the same reconstruction method and verifying that the DTWG analysis was sound. The POST2-based reconstruction using the accelerometer set of measurement data to estimate the probe position and velocity also agreed with altitude profiles from DTWG, HASI, and NESC results. However, none of these agreed with the measured radar data. A scale factor of approximately 0.93 on the radar data would bring it into agreement with all these results.

2. An assessment of the entry aerodynamics database model generated prior to entry showed that the variation from the nominal pre-flight values throughout the trajectory was within the 3-sigma bounds established by the aerodynamicists throughout most of the entry (above Mach 1.5). Due to limitations in the available data, only the axial component of the vehicle drag was assessed.

3. Based on the measured accelerations and reconstructed trajectory, the Main parachute had higher drag than was predicted using the ESA parachute model by 9% to 19%. NASA assumed an 11% higher drag value than the ESA model for the Main Parachute for analyses prior to entry, and the difference between reconstructed flight values and the NASA prediction was at worst about 7%.

4. The drogue parachute phase (which began after the Main parachute was jettisoned) was much longer (about 2 hours long) than that of the Main parachute. During this phase, a dynamical event occurs lasting roughly 30 minutes starting

about 15 minutes into the drogue phase. While this event is as yet unexplained, the dynamics are captured in the reconstruction by drogue parachute drag variations that range from about 40% to near 240% of the predicted values. The event is characterized by fluctuating acceleration rates not expected while on a parachute for hundreds of seconds; thus, the parachute drag was continually adjusted to mimic this notable jerk in the flight. That is, in order to follow the accelerometer measurements, large drag variations are required. Factors contributing to this event could be the extreme low temperatures (as low as 70 K) changing the parachute characteristics (such as material porosity), wind turbulence or horizontal wind shear. None of these conditions were confirmed by the current analysis.

5. The final 90 minutes of the descent on the drogue parachute had measured accelerations notably less than expected; since the parachute was at or near terminal velocity, the measured accelerations should have been near the gravity of Titan (assuming the probe was vertical) and it was about 1-2% lower than expected. Several options were explored to explain this situation: A Titan mass concentration, accelerometer bias, unmodeled thrust, and probe tilt. The solution that seems most likely from the data is that a probe tilt angle of roughly 10-12 degrees existed between the gravity direction and the axial accelerometer that was providing the only usable acceleration measurements. The tilt assumption matches flight data provided by an independent tilt sensor, but is in conflict with results determined from descent photographic images. It is noted that the probe measured external temperatures as low as 70 K and the effect of very low temperatures on these accelerometers may not preclude a large bias.

6. During the drogue phase, this analysis found nominal horizontal winds of about 50% greater than pre-flight Titan-GRAM predictions and the post-flight value provided by the ESA project. This result may be an artifact of the method selected to address the unexplained event outlined in element 5 above. Below about 50 km the reconstructed winds were as much as 50% less than those predicted by the Titan-GRAM model, however these reconstruction values were still greater than the ESA estimated winds at these altitudes. Additionally, a wind shear indicated by ESA after post-flight analysis was not confirmed by the current analysis. However, the reconstruction reported here did have a near 40 m/s departure from 100 m/s wind velocity around 1000 sec or just before drogue parachute deployment (around 115 km altitude).

6.2 CONCLUSIONS

The utility of the POST2 reconstruction model was successfully demonstrated for the Huygens trajectory reconstruction. The general nature of the POST2 architecture allowed this problem to be addressed using the usual POST2 methodology of problem setup and execution. While demonstrated for an EDL trajectory, application of the reconstruction module to other trajectory types (such as ascent and orbital only) is expected to be viable as they are within the normal capability of the POST2 software and the architecture of POST2 was preserved during the development of the reconstruction capability.

From the Huygens trajectory reconstruction, based on the tilt sensor and accelerometer data, the probe was tilted about 10 degrees during the drogue parachute phase; this conclusion is disputed by the Descent Imager team who concluded the probe

could not be tilted more than two degrees. Also, the altitude profile returned from the radar altimetry appears to need a scale factor of about 0.93 in order to be consistent with results generated using accelerometer, atmospheric pressure and temperature data. Pre-entry models for vehicle axial aerodynamics and main parachute drag were well predicted. As part of the NASA-ESA agreement, the results generated in the Huygens reconstruction trajectory analysis part of this research have been provided to ESA.

Based on the analysis from this research, one recommendation to improve the entry, descent, and landing trajectory reconstruction for future missions like Huygens is to include measurements from additional sensors such as angular rates, spacecraft acceleration along lateral axes, wind measurement data, and information about parachute performance such as force data on bridle support lines and images of parachute during descent. Some of these data were planned for the Huygens mission but not obtained; the suggestion here is to include additional sensors to preclude a single point sensor failure from causing loss of critical data.

6.3 FUTURE WORK

Several areas of future work are planned. First, POST2 will be translated into ANSI-C language for all modules, thus the reconstruction module routines need to be converted. Next, the reconstruction routines and function need to be completely separated from the optimization module routines to allow reconstruction and optimization/targeting to be used concurrently within POST2. Further investigation of using the reconstruction enabled POST2 with a Monte Carlo assessment is needed. Combining the computer cluster compute power with this new capability for reconstruction could lead to even faster, more robust reconstruction solutions. Finally, near term use of this POST2-based

capability is planned for Phoenix and Mars Science Laboratory EDL trajectory reconstructions.

Appendix POST2 Reconstruction Module Inputs/Outputs

For the reconstruction capability in POST2, the inputs and outputs are given below. Additionally, a file containing the measurements as a function of time (with time being in the first column) are assumed to be in a file named FORT.25 with the associated weight for each measurement given in a file named FORT.26. The tables below are given in standard POST2 manual format. The inputs are given in Table A-1 whereas the outputs are shown in Table A-2.

Table A-1. POST2 Reconstruction Module Input Variables

Input Symbol	Type/ Units	Stored Value	Definition
COVj, j=1,100	real*8		The initial value of the covariance matrix.
INITIAL_RECON_ STATEj, j=1,100	real*8		The initial value of the state being reconstructed (as identified by RECON_STATE).
INITRECON	integer	0	Initialize reconstruction quantities (set to 1 after initialization).
MEAS_NOISEj, j=1,100	real*8	0	Measurement noise matrix.
NOBS	integer	0	Number of observation quantities.
NSTATES	integer	0	Number of states to be reconstructed.
RECON_OBSERVj , j=1,100	character		The name of the output variable that is measured for reconstruction.
RECON_PERTS	same as the variable specified by RECON_ STATE	1.0E-4	The perturbation (increment) to be added to the reconstruction state variable, RECON_STATE(i) whose value is currently CURRENT_RECON_STATEi. Used to determine the sensitivity of the state derivative wrt time (RECON_STATE_DERIVj) and calculated observation (RECON_OBSERVj) to the reconstruction state (RECON_STATEj).
RECON_STATEj, J=1,100	character		The character name of the j-th state variable used for the reconstruction process.
RECON_STATE_ DERIVj, J=1,100	character		The character name of the j-th state variable's derivative wrt time used for the reconstruction process.
SRCHM	integer	0	POST2 control flag. =99 indicates reconstruction run.
SYS_NOISEj, j=1,100	real*8	0	System noise matrix.

Table A-2. POST2 Reconstruction Module Output Variables

Output Symbol	Type/ Units	Definition
COVj, j=1,100	real*8	The current value of the covariance matrix.
COVDOTj, j=1,100	real*8	The current value of the covariance matrix derivative wrt time.
CURRENT_ RECON_ST ATEj, j=1,100	same as the variable specified by RECON_ STATE	The current value of the reconstruction state identified in RECON_STATE.
OBSNUM	integer	The number of the current observation being used in the reconstruction process.
RECONSTA TEj, j=1,100	same as the variable specified by RECON_ STATE	The current value of the reconstruction state identified in RECON_STATE.

Bibliography

1 Braun, R.D., and Manning, R.M., "Mars Exploration Entry, Descent, and Landing Challenges," Journal of Spacecraft and Rockets, Vol. 44, No. 2, Mar.-Apr. 2007, pp. 310-323.[doi:10.2514/1.25116]

2 Mitcheltree, R.A., Steltzner, A.D., Chen, A., SanMartin, A.M., Rivellini, T.P., "Mars Science Laboratory Entry Descent and Landing System Verification and Validation Program," IEEE Paper 2.1309, March 2006. [hdl:2014/39158]

3 Gnoffo, P.A., Braun, R.D., Weilmuenster, K.J., Mitcheltree, R.A., Engelund, W.C., and Powell, R.W., "Prediction and Validation of Mars Pathfinder Hypersonic Aerodynamic Database," Journal of Spacecraft and Rockets, Vol. 36, No. 3, May-June 1999, pp. 367-373.

4 Euler, E.A., Adams, G.L., and Hopper, F.W., "Design and Reconstruction of Viking Lander Descent Trajectories," Journal of Guidance and Control, Vol. 1, No. 5, Sept.-Oct. 1978, pp. 372-378.

5 Witkowski, A., Kandis, M., Bruno, R., and Cruz, J.R., "Mars Exploration Rover Parachute System Performance," AIAA Paper 2005-1605, May 2005.

6 Spencer, D.A. and Braun, R.D., "Mars Pathfinder Atmospheric Entry: Trajectory Design and Dispersion Analysis," Journal of Spacecraft and Rockets, Vol. 33, No. 5, Sept.-Oct. 1996, pp. 670-676.

7 Braun, R.D., Powell, R.W., Engelund, W.C., Gnoffo, P.A., Weilmuenster, K.J., and Mitcheltree, R.A., "Mars Pathfinder Six-Degree-of-Freedom Entry Analysis," Journal of Spacecraft and Rockets, Vol. 32, No. 6, Nov.-Dec. 1995, pp 993-1000.

8 Queen, E.M., Cheatwood, F.M., Powell, R.W., Braun, R.D., and Edquist, C.T.," Mars Polar Lander Aerothermodynamic and Entry Dispersion Analysis," Journal of Spacecraft and Rockets, Vol. 36, No. 3, May-June 1999, pp 421-428.

9 Tartabini, P.V., Munk, M.M., and Powell, R.W., "The Development and Evaluation of an Operational Aerobraking Strategy for the Mars 2001 Odyssey Orbiter," AIAA Paper 2002-4537, Aug. 2002.

10 Hanna, J.L., Chavis, Z.Q., and Wilmoth, R.G., "Modeling Reaction Control System Effects on Mars Odyssey," AIAA Paper 2002-4934, Aug. 2002.

11 Striepe, S. A., Queen, E.M., Powell, R.W., Braun, R.D., Cheatwood, F.M., Aguirre, J.T., Sachi, L.A., and Lyons, D.T., "An Atmospheric Guidance Algorithm Testbed for the Mars Surveyor Program 2001 Orbiter and Lander," AIAA Paper 98-4569, Aug. 1998.

12 Powell, R.W., "Numerical Roll Reversal Predictor-Corrector Aerocapture and Precision landing Guidance Algorithms for the Mars Surveyor Program 2001 Missions." AIAA Paper 98-4574, Aug. 1998.

13 Desai, P.N., Schoenenberger, M., and Cheatwood, F.M., "Mars Exploration Rover Six-Degree-of-Freedom Entry Trajectory Analysis," Journal of Spacecraft and Rockets, Vol. 43, No. 5, Sept.-Oct. 2006, pp 1019-1025, [doi:10.2514/1.6008].

14 Desai, P.N., and Cheatwood, F.M., "Entry Dispersion Analysis for the Genesis Sample Return Capsule," Journal of Spacecraft and Rockets, Vol. 38, No. 3, May-June 2001, pp 345-350.

15 Desai, P.N., Mitcheltree, R.A., and Cheatwood, F.M., "Entry Dispersion Analysis for the Stardust Comet Sample Return Capsule," Journal of Spacecraft and Rockets, Vol. 36, No. 3, May-June 1999, pp 463-469.

16 NASA Engineering and Safety Center, "Assessment of the Cassini/Huygens Probe Entry, Descent and Landing (EDL) at Titan," NESC-RP-05-67, May 2005.

17 Hollis, B.R., Striepe, S.A., Wright, M.J., Bose, D., Sutton, K., and Takashima, N., "Prediction of the Aerothermodynamic Environment of the Huygens Probe," AIAA Paper 2005-4816, June 2005.

18 Broome, J.M., and Prince, J.L., "Potential Entry Guidance Modifications to Improve Landing Accuracy for the 2007 Phoenix Mars Mission," AAS Paper 05-061, February 2005.

19 Striepe, S.A., Way, D.W., Dwyer, A.M., and Balaram, J., "Mars Smart Lander Simulations for Entry, Descent, and Landing," Journal of Spacecraft and Rockets, Vol. 43, No. 2, March-April 2006, pp 311-323.

20 Fisher, J.L., and Striepe, S.A., "POST2 End-to-End Descent and Landing Simulation for the Autonomous Landing and Hazard Avoidance Technology Project," AAS Paper 07-119, January 2007.

21 Bauer, G.L., Cornick, D.E., and Stevenson, R., "Capabilities and Applications of the Program to Optimize Simulated Trajectories (POST)," NASA CR-2770, Feb. 1977.

22 Striepe, S.A., et al.: "Program to Optimize Simulated Trajectories (POST II), Vol. II Utilization Manual." Version 1.1.6.G, January 2004, NASA Langley Research Center, Hampton, VA.

23 Desai, P.N., Braun, R.D., Powell, R.W., Engelund, W.C., and Tartabini, P.V., "Six-Degree-of-Freedom Entry Dispersion Analysis for the METEOR Recovery Module" Journal of Spacecraft and Rockets, Vol. 34, No. 3, May-June 1997, pp 334-340.

24 Braun, R.D., Mitcheltree, R.A., and Cheatwood, F.M., "Mars Microprobe Entry-to-Impact Analysis," Journal of Spacecraft and Rockets, Vol. 36, No. 3, May-June 1999, pp 412-420.

25 Lockwood, M.K., Powell, R.W., Graves, C.A., and Carman, G.L., "Entry Configurations and Performance Comparisons for the Mars Smart Lander," Journal of Spacecraft and Rockets, Vol. 43, No. 2, March-April 2006, pp 258-269.

26 Fraysse, H., Powell, R.; Rousseau, and Striepe, S., "CNES-NASA Studies of the Mars Sample Return Orbiter Aerocapture Phase." IAF-00-A.6.05. Presented at the 51st International Astronautical Congress, Rio de Janeiro, Brazil Oct 2-6, 2000.

27 Ro, T., and Queen, E., "Study of Martian Aerocapture Terminal Point Guidance," AIAA Paper 98-4571, Aug. 1998.

28 Queen, E.M., Striepe, S.A., and Powell, R.W., "An Approach to Simulation of Extreme Conditions for a Planetary Lander" NASA TM -2001-211246, Nov. 2001.

29 Spencer, D.A., Blanchard, R.C., Braun, R.D., Kallemeyn, P.H., and Thurman, S.W., "Mars Pathfinder Entry, Descent, and Landing Reconstruction," Journal of Spacecraft and Rockets, Vol.36, No. 3, May-June 1999, pp. 357-366.

30 Prince, J.L., and Striepe, S.A., "Mars Reconnaissance Orbiter Operational Aerobraking Phase Assessment," AAS Paper 07-244, Jan. 2007.

31 Euler, E.A., Adams, G.L., and Hopper, F.W., "Design and Reconstruction of the Viking Lander Descent Trajectories," Journal of Guidance and Control, Vol. 1, No. 5, 1978, pp 372-378.

32 Compton, H.R., Blanchard, R.C., and Findlay, J.T., "Shuttle Entry Trajectory Reconstruction Using Inflight Accelerometer and Gyro Measurements," AIAA 79-0257, Jan. 1979.

33 Gelb, A. (ed), Applied Optimal Estimation, MIT Press, Cambridge, MA, 1974.

34 Brown, R.G., and Hwang, P.Y.C., Introduction to Random Signals and Applied Kalman Filtering, 2nd ed., John Wiley and Sons, Inc., New York, NY, 1983.

35 Matson, D.L., Spilker, L.J., Lebreton, J.-P., "The Cassini/Huygens Mission to the Saturnian System," Space Science Reviews, Vol. 104, 2002, pp. 1-58.

36 Lebreton, J.-P., et al., "An overview of the descent and landing of the Huygens probe on Titan", Nature, Vol 438, 8 Dec 2005, pp 758-764.

37 Lebreton, J.-P., and D. L. Matson (1997), "The Huygens Probe: Science, payload and mission overview", Space Science Reviews, Vol. 104, 2002, pp. 59-100.

38 Kazeminejad, B., et al., "Huygens' Entry and Descent through Titan's Atmosphere – Methodology and Results of the Trajectory Reconstruction", Planetary and Space Science, in Press, 2007.

39 NASA Engineering and Safety Center, "Assessment of the Cassini/Huygens Probe Entry, Descent and Landing (EDL) at Titan – Phase 2 Huygens Probe Reconstruction," NESC-RP-07 (in press), August 2007.

40 Justus, C. G., Duvall, A., and Keller, V. W., "Engineering-Level Model Atmospheres for Titan and Mars", Proceedings of the International Workshop on Planetary Probe Atmospheric Entry and Descent Trajectory Analysis and Science, Lisbon, Portugal, 6-9 October, 2003, ESA SP-544, February, 2004.

41 Ferri, F., and Lion, P., "HASI ACC Data Processing and Calibration Report," HASI-RP-UPD-106, ESTEC, Netherlands, 2005.

42 Sarlette A., Characterization of the spin and attitude of the ESA Huygens Probe during its descent onto Titan using the engineering dataset. Graduation Thesis, Liege University, Belgium, 2005.

43 Lorenz, R.D., et al., "Descent motions of the Huygens probe as measured by the Surface Science Package (SSP) : Turbulent evidence for a cloud layer", *Planetary and Space Science*, in Press, 2007.

44 Folkner, W. M., et al., "Winds on Titan from ground-based tracking of the Huygens probe," Journal of Geophysical Research, 111, 2006, E07S02. [doi:10.1029/2005JE002649]

45 Konopliv, A.S., Asmar, S.W., Carranza, E., Sjogren, W.L., and Yuan, D.N., "Recent Gravity Models as a Result of the Lunar Prospector Mission", Icarus, 2001, no. 150, pp. 1-18.

46 Karkoschka, et al., "DISR imaging and the geometry of the descent of the Huygens probe within Titan's atmosphere", Planetary and Space Sciences, in press, 2007.

Vita

Scott Striepe began working at NASA's Langley Research Center soon after his graduation from Auburn University. Scott, who was also a co-operative education student with NASA-Langley, earned his Bachelor of Aerospace Engineering degree in August 1988. In May 1991, he received a Master of Science in Engineering degree from the University of Texas at Austin under the direction of Dr. Wallace Fowler through the NASA Graduate Study Program. During his tenure at NASA, he has worked on the Pegasus XL Return-to-Flight team, the X-33 Phase-1 program, 2001 Mars Odyssey Orbiter mission, 2003 Mars Exploration Rover Lander mission, Genesis EDL simulation team, 2005 Mars Reconnaissance Orbiter mission, NESC Cassini/Huygens probe independent technical assessment, Mars Science Laboratory mission, Lunar Lander technology, as well as human and robotic mission planning and development. He is the author or co-author of over 40 technical papers. His capabilities include trajectory simulation development as well as design, development and analysis of Mars and Earth atmospheric entry systems. Scott is the program manager for the Program to Optimize Simulated Trajectories II (2006 NASA Software of the Year Runner-Up). In 2007, Scott was awarded NASA's Exceptional Achievement Medal for his leadership of the NASA Langley technical team responsible for the evaluation, design, development, operation, and engineering simulation of the aerobraking phase of the Mars 2005 Reconnaissance Orbiter mission. Scott currently leads the NASA reconstruction team for the NESC Cassini/Huygens probe independent technical assessment. He also leads the NASA and industry team developing the

Autonomous precision Landing and Hazard Avoidance (ALHAT) lunar landing simulation.

Permanent address: 110 Atoka Turn, Yorktown, VA 23693

This dissertation was typed by the author.